UNIVERSITY OF COPENHAGEN

Active Layer Modelling and Flocculation Processes in the Disko Area, West Greenland

Field and Methods Course – Greenland 2014
Block 4 and block 1

Jeppe Dalskov Frederiksen
Andreas Elmelund Hass
Andreas Hvam Hoffmann
Paulina Karkauskaite
Britt Gadsbølle Larsen
Tue Mariager
Ellen Lindholt Nissen
Marta Merino Ramos

Contents

Foreword

The Department of Geoscience and Natural Resource Management and the Faculty of Sciences at University of Copenhagen continue to emphasize the importance of conducting a field course in Arctic Physical Geography at Arctic Station, Qeqertarsuaq (Godhavn), Disko Island, West Greenland. Hence, every fourth year this course enables a selected group of students enrolled at University of Copenhagen to perform their own research projects in close collaboration with a supervisor. The projects are carefully prepared and the planning started five months in advance to the beginning of the field course. The field course provides for the first time the possibility to experience the Arctic environment in a three-dimensional space. Furthermore, the practical projects deliver a significant hands-on experience that not even the best textbook will be able to encompass. With the persistent national and international interest in the Arctic environment and the numerous ongoing studies addressing the effects of global warming on the Arctic climate it is of outmost importance that students for years to come are given the opportunity to do research and learn about the Arctic in general.

The Field Course in Physical Geography 2014 took place between 1-15 of August at Disko in West Greenland. In total 8 students participated in the course and have now completed the different parts: Preparations i.e., fine-tuning of projects, packing of equipment and the actual field course in Greenland. This report represents the final part for the course. The course was organized and lead by Birger Ulf Hansen and Thor Markussen.

The aim of the Field Course in Physical Geography 2014 was to investigate:

1) Flocculation processes in the Disko Fjord area and cloudburst effects on the flocculation.
2) Edaphic Factor of Soils in Blæsedalen, Disko Island - A Pedological Study of the Abiotic Factors Controlling the Edaphic Factor.
3) Nt-factor for Disko Island based on NDVI.
4) Estimating Degree Days of Thaw for Disko Island using satellite imagery.
5) Potential Radiation Index for Disko Island.
6) Modelling of Active Layer Thickness of Disko Island.

The combination of these six parts can provide new insight with respect to the current and future sediment transport and permafrost thawing within the study area taken current and future climate trends into account. The southern part of "Blæsedalen" was chosen as the study area due to that the landscape is fairly well-described and due to the presence of all landscape types representative for the Arctic environment.

Part of the course has been directly linked to CENPERM – a centre of excellence, which will integrate hypothesis-based studies of biogeochemical and physical processes in a "climate-vegetation-soil-microorganism-permafrost" context. Therefore, several other people took part in the field work at Disko this summer including Anders Michelsen, Cecilie Skov Nielsen, Daan Blok, Frida Lindwall, Jens Gammeltoft and Kent Pørksen, Kerstin Elise Krøier Rasmussen.

Thanks to 8 enthusiastic students, the CENPERM Center, Arctic Station (including Ole Stecher, Gitte Henriksen, Kjeld Akaaraq Mølgaard, Erik, Søren and Otto) as well as Faculty of Science, University of Copenhagen for financial supporting this Field Course in Physical Geography.

October 2014 Birger Hansen
(Course responsible)

Back row: Birger Ulf Hansen, Jeppe Dalskov Frederiksen, Andreas Hvam Hoffmann, Andreas Elmelund Hass, Tue Mariager and Thor Markussen

Front row: Kjeld Akaaraq Mølgaard, Britt Gadsbølle Larsen, Marta Merino Ramos, Kerstin Elise Krøier Rasmussen, Ellen Lindholt Nissen, Paulina Karkauskaite

Climate change in the arctic regions

The occurrence of increase in surface air temperatures is evident globally (IPCC, 2013). However, the intensity of climate forcing is highest in the Arctic Region, where temperature rise is exceeding the tendencies of the rest of Northern Hemisphere and the global average (Figure 1) (Serreze et. al, 2006). This phenomenon of accelerated warming in the high latitudes of the Northern Hemisphere is acknowledged as Arctic Amplification and is mainly caused by positive feedbacks occurring in the cryosphere, comprised of snow, river and lake ice, sea ice, glaciers, ice shelves, ice sheets, and frozen ground (Miller et al, 2010; IPCC, 2013). According to various climate change models, amplified warming will continue in the Arctic region and substantially exceed the global average over the coming century (Miller et. al, 2010). One of the most significant positive feedbacks to the rising temperatures is melting of the sea and inland ice, which leads to sea level rise and glacial runoff (Ibid.). These changes result in decreased surface albedo, owing to increased air temperature and thawing of the frozen ground areas that further induce temperature rise (Ibid.) In order to account for the mentioned impacts, it is important to investigate the processes occurring within the cryosphere's components of the high latitudes (Miller et al, 2010).

This report will therefore focus on the Arctic region, more precisely Disko Island in West Greenland, in order to investigate processes and components of permafrost and glacial runoff.

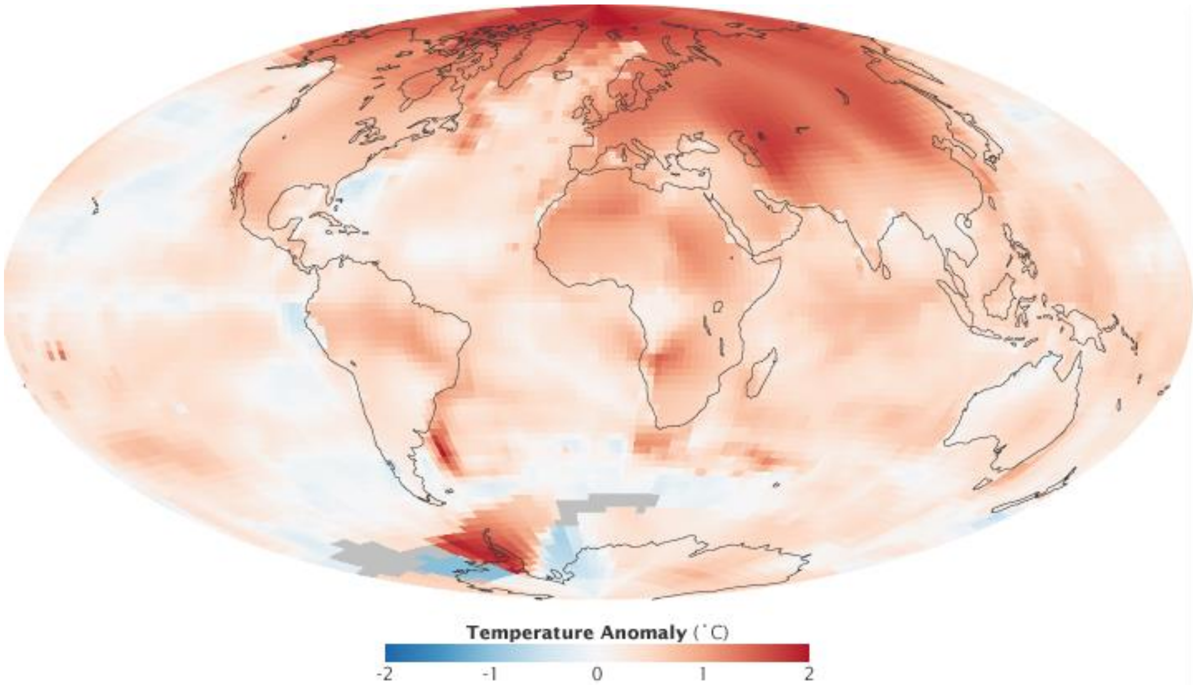

Figure 1 – Global temperature anomalies acquired for the period of January 1, 2000 - December 31, 2009. A twice so fast increase is apparent within the high latitudes of the Northern Hemisphere. Source: NASA Earth Observatory

Permafrost investigation

Frozen ground, also known as permafrost is a perennially frozen ground that remained at the temperatures below 0˚ for at least two constitutive years. (Riseborough et. al, 2008) Permafrost is considered to play an important role in the climate change research due to its inherent sensitivity to changes in surface temperatures and snow cover, as well as influence on energy exchanges, hydrological processes, natural hazards and carbon budgets of the global climate system. (Riseborough et. al, 2008) It is particularly essential to ascertain permafrost trends and characteristics in the Arctic region, where surface air temperature warming is the most significant and permafrost degradation would further enhance the increases of temperatures (Hollesen et al, 2011; IPCC, 2013). Near surface permafrost thawing is considered to be one of the most substantial positive feedbacks that induce the amplification in the high latitudes (Lawrence et al, 2008). Thawing of the permafrost results in increase of the thickness of the active layer that leads to mineralization of organic matter that was previously frozen and release of carbon dioxide (CO_2) and methane gases (CH_4), which is a roughly 20 times stronger heat absorbing greenhouse gas than carbon dioxide (CO_2) (IPCC, 2013; Hollesen et al., 2011). In addition to that, decomposition of organic carbon in soils may also be responsible for subsurface heat production which can act as a positive feedback on soil temperatures contributing to further ground thaw. (Hollesen et al, 2011). It is estimated, that permafrost covers around one fourth of the Northern Hemisphere area, and it contains approximately 1672 Pg of organic carbon that accounts for 50% of estimated global belowground organic carbon pool (Lawrence et al., 2008). If released, it would result in vast amounts of greenhouse gas concentrations in the atmosphere that would further contribute to the temperature increases and result in a positive feedback mechanism causing profound ecological changes (Walvoord et al., 2012). Some of the changes, such as shift in bioclimatic zones are already taking effect due to more than 24% increase in summer warmth index (SWI; sum of the monthly-mean temperatures above freezing), and increases in vegetation cover expressed through Normalized Difference Vegetation Index (NDVI; indication of the greenness of the vegetation cover) over the Arctic region (Bhatt et. al, 2010).

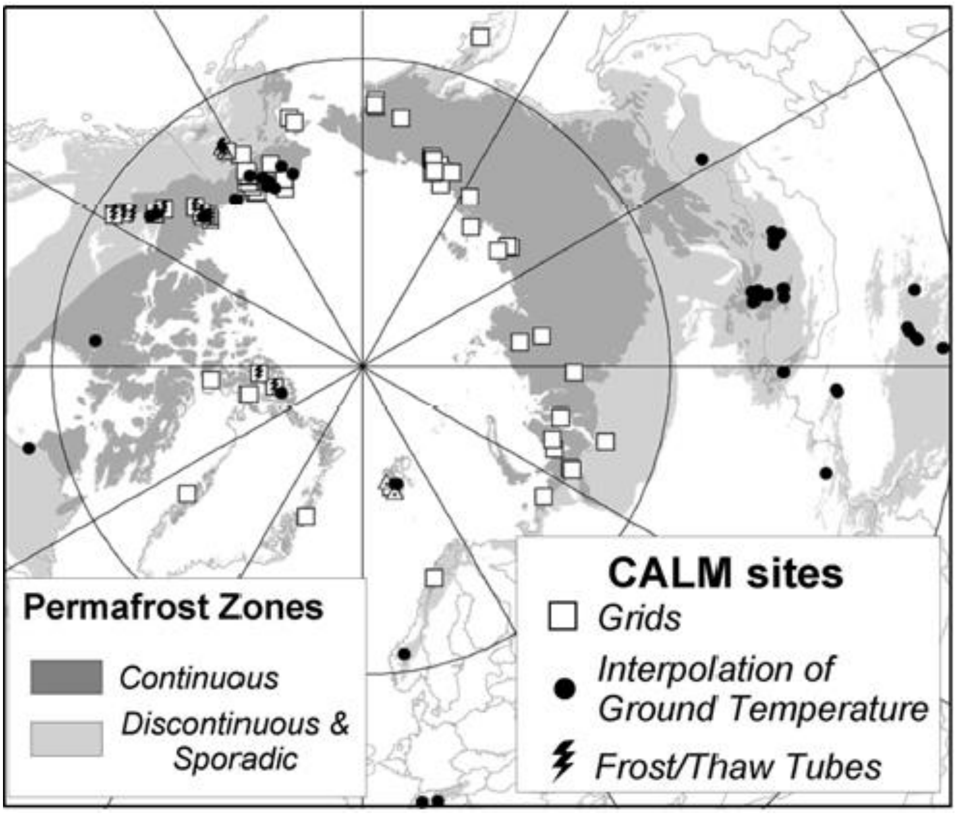

Figure 2 - Permafrost variability and Circumpolar Active Layer Monitoring (CALM) in the Arctic region (Shiklomanov et al. 2008).

As already mentioned, a key parameter indicating trends in thawing progress in near-surface permafrost is the active-layer thickness. Active-layer is the uppermost layer of the ground, which is subject to summer thawing and winter freezing where permafrost is present (Christiansen, 1999). It is considered to be an important indicator of climatic change, since it is strongly controlled by summer temperatures and precipitation (Ibid.). Active layer monitoring started in the 1990 through the establishment of International Permafrost Association (IPA) Circumpolar Active Layer Monitoring (CALM) program (Shiklomanov, 2008). The monitoring network consists of 168 active sites within 15 participating countries, where thickness of active layer is observed periodically (see Figure 2). Greenland is part of this program with one grid site at Zackenberg in NE Greenland,74 °N and another in Disko Island in W Greenland, 69 °N, where active layer has been investigated since 1996 and 1997, respectively (Christiansen, 1999). According to the observations, increases in active layer thickness in Greenland has accelerated since late 1990's, particularly at the Disko Island site, where active layer has been recorded to reach 71cm thickness in mid-August in 1998 and 91cm in September, 2013 (Christiansen, 2010; IPCC, 2013, Permafrost sonderinger 2007-2014). This tendency is supported by the trendline in Figure 3.

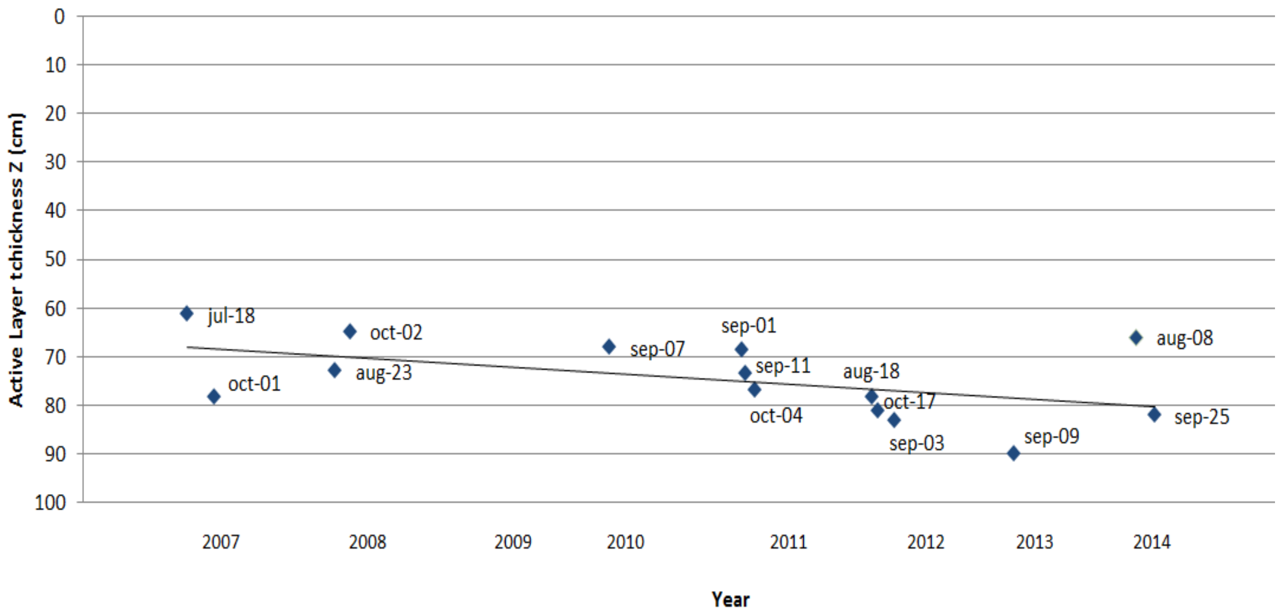

Figure 3 – Active layer monitoring at the DISKOCALMI (DCI) from 2007-2014.

Active layer investigation based on Stefans solution

This study focuses on the Disko Island site and aims to estimate and map the active layer thickness over the entire island through applying GIS (Geographic Information Systems) that incorporates remotely sensed data acquired from MODIS and Landsat satellite databases. The remotely sensed data has been processed according to the approach method named Stefans Solution.

Stefans solution, based on numerical model of Stefan problem, is widely used method for predicting the depth of thawing in soils, hereby estimating spatial active layer thickness characterization (Nelson et. al, 1997). It has been used to map the active layer in the Kurparak River basin, Alaska in high-resolution (Nelson, et al., 1997), to do Circumpolar Active Layer Monitoring in northern Alaska (Hinkel, et al., 2003) and to investigate the Russian arctic drainage basin (Zhang et. al, 2005).

Stefans problem approaches the phase change in matter and can be explained though an example of an infinite column of ice that is kept at 0°C. The column is enclosed by non-conducting walls and by time temperature changes at one end of the column. Stefans problem finds the interface between ice and water caused by the influence of temperature and the distance to the heat source (Østerby, 1974). It is a free-boundary –and phase change problem that when modified can be applied for determining the thawing depth of permafrost. Stefans solution is often used in large scale permafrost investigations since it only needs a small amount of site specific data, compared to other models (Nelson, et al., 1997). Furthermore EASE-grid has used Stefans solution to calculate thawing depth for the northern hemisphere, which makes the determined values comparable with EASE-grid (Zhang, et al., 2012). The Stefan solution consists of the parameters as follows:

Equation 1.1

$$Z = E\sqrt{nt * PRI * DDT}$$

Where Z is the thawing depth, E is edaphic factor, nt is a vegetation parameter, PRI is potential radiation index and DDT is the thawing index.

Stefans solution is central for this study since it is used to model the active layer at Disko Island and each article concerning permafrost is therefore structured to deal with one of the parameters in Stefans solution.

In order to support and validate the results derived from remotely sensed data, certain field work procedures within the representative locations, including CALM site, were conducted. Ground-based measurements involved probing into the ground in order to acquire permafrost depth, taking soil samples from different depths and measuring edaphic parameters, measuring NDVI and logging climatic data from portable climate stations established at the site in order to obtain summer air temperature records.

Glacial Runoff investigation

Due to the evidence of increasing temperatures in the arctic regions, glaciers in many regions are withdrawing from their previous positions (IPCC, 2013).

Sorg et al., (2012) stated that the increasing temperatures and thus the disturbance in the glacial movements has not yet resulted in huge changes in the annual glacial runoff, but predicted an impact later in this century in the Tien Shan region in central Asia. However, in the arctic regions, an increase in the runoff from the Greenlandic Ice sheet (GRIS) has already been detected (Hanna et al., 2007).

Inevitably, an increase in glacial runoff will result in an increase in the sediment discharge from the glaciers too, hence making the transport of nutrients from the glacial river systems towards the sea bigger (Tranter, et al., 1993). The change in the glacial runoff hereby has an effect on the primary production in the fjord systems. However, if the nutrient and iron rich sediments from the glacial systems flocculate, and hereby becomes heavier and then settle, the nutrient addition does not have any influence on the primary production, hence creating a negative feedback with regards of the amount of CO_2 in the atmosphere.

The field campaign in the Disko Fjord investigates the flocculation processes and their effect on the redistribution of nutrients in the area. Furthermore investigations of the availability of particles on the flocculation are carried out.

In the Red River near the Arctic station, the effect of precipitation on the river system is up-scaled, so that the results can be used to describe the influence of climate change on the river system in the Disko Fjord.

Hereby the climatic parameters most important to the glacial runoff are the temperature and the precipitation. Furthermore the geology of the surrounding rocks is important with regards to nutrient –iron- availability.

Study Area description

The fieldwork for the studies took place at Disko Island, which is located in Baffin Bay, on the coast of Central West Greenland (69°45′N 53°30′W). The island covers an area of 8,578 km^2 with a length of around 160km and highest elevation of 1,919 m. Fieldwork procedures were conducted in two main areas. One in Blæsedalen near Arctic research station (69º15'N, 53º31'W) in the South part of Disko Island, and one in the Disko Fjord area, further north in the Island, see Figure 4 and Figure 5. The following sections will provide detailed information of the study area and the important parameters to the investigation. The sections will describe *climatic characteristics, geology, pedology and vegetation*.

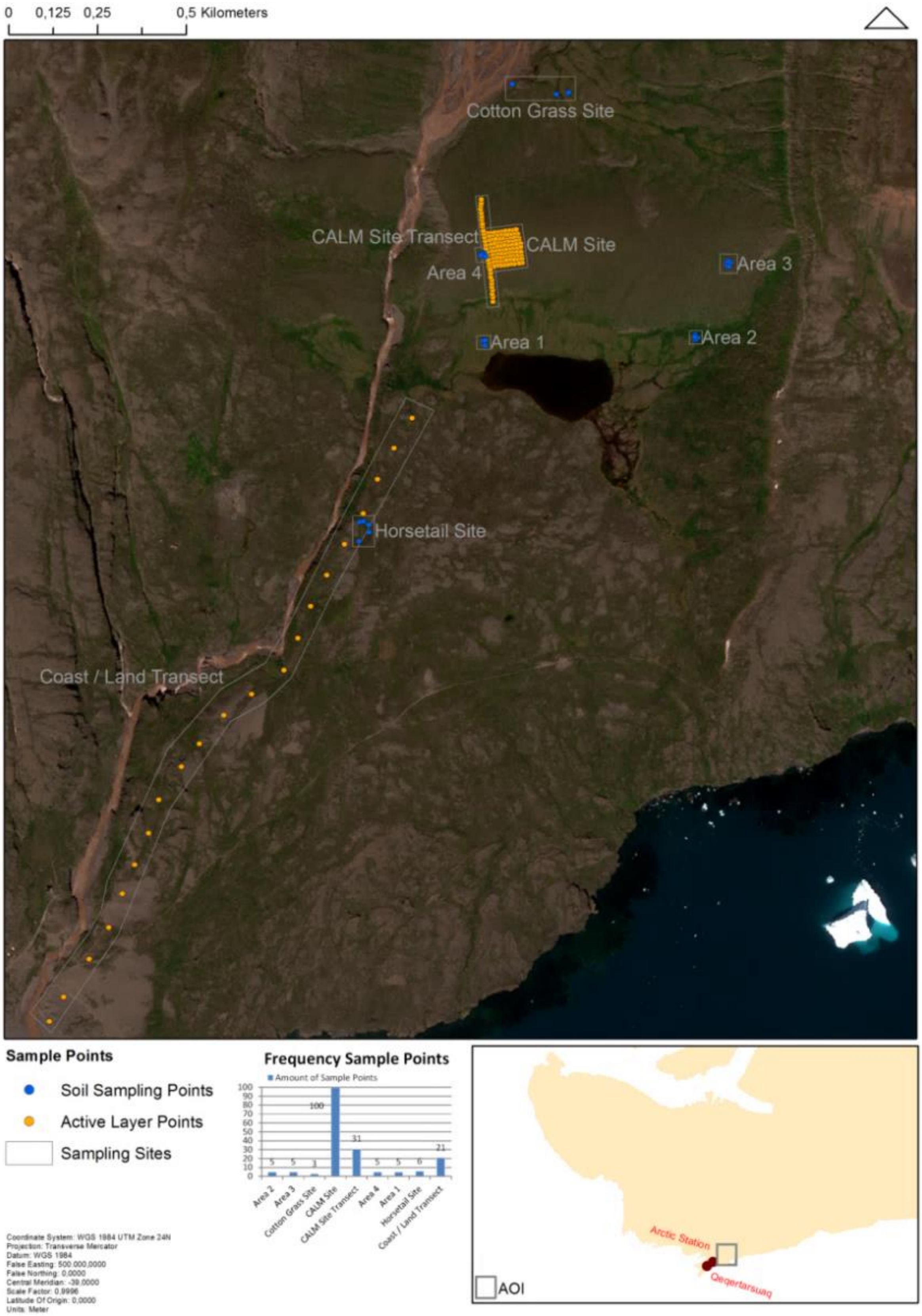

Figure 4 - Spatial distribution of field sites and sample points for the active layer modeling.

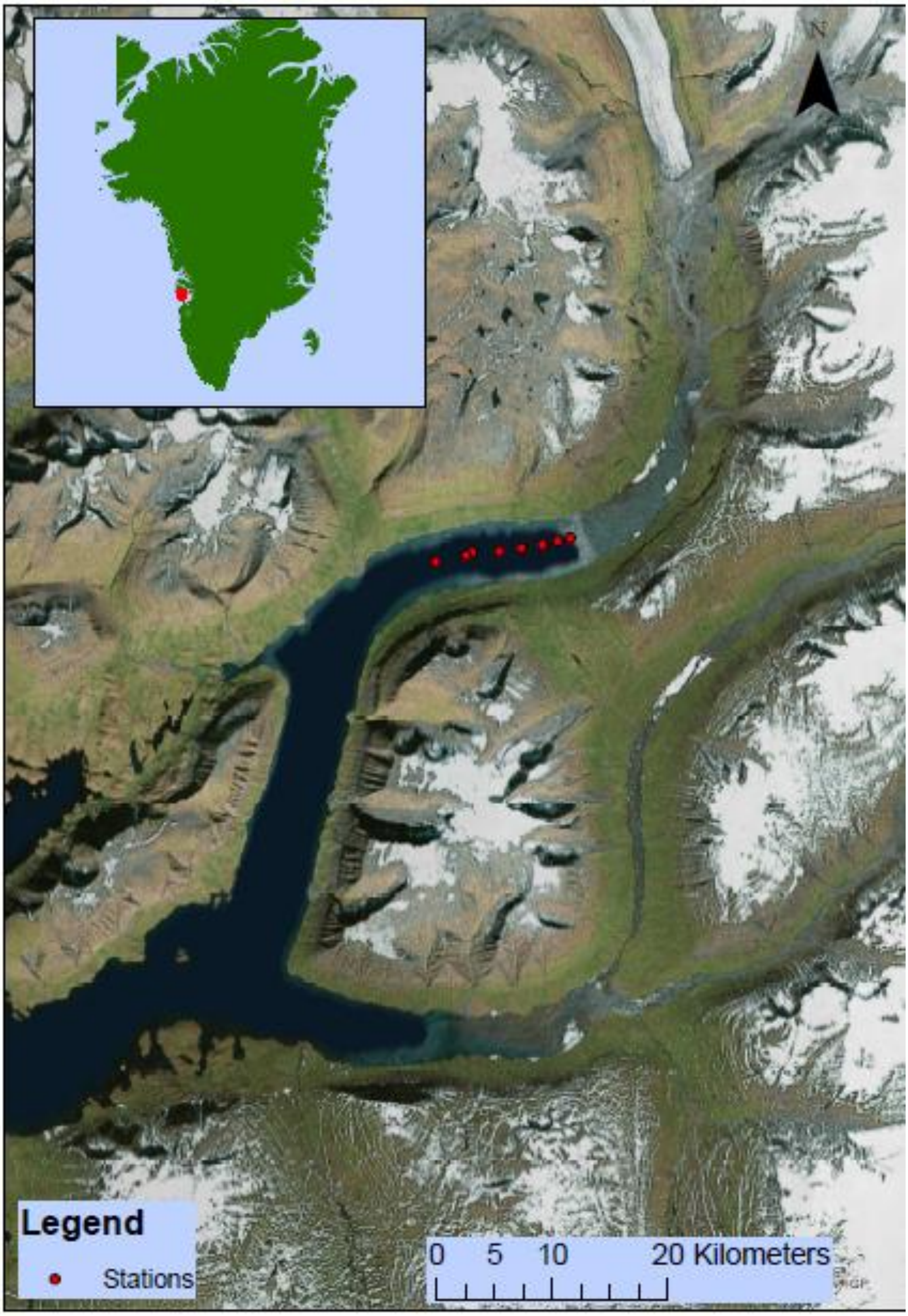

Figure 5 – Spatial distribution of the field measurements in Disko Fjord.

Climatology of Disko Island

The climate of Greenland is mainly regulated by the inland ice sheet that covers around 80% of the total Greenland area, and interaction between cold and warm winds coming from Northwest/North and South. (Hansen et. al, 2006) Disko Island climate, however, is influenced by additional factors such as summer and winter extension of sea ice and warm and cold ocean currents coming from the Cumberland Strait (See Figure 6) (Hansen, 2014).

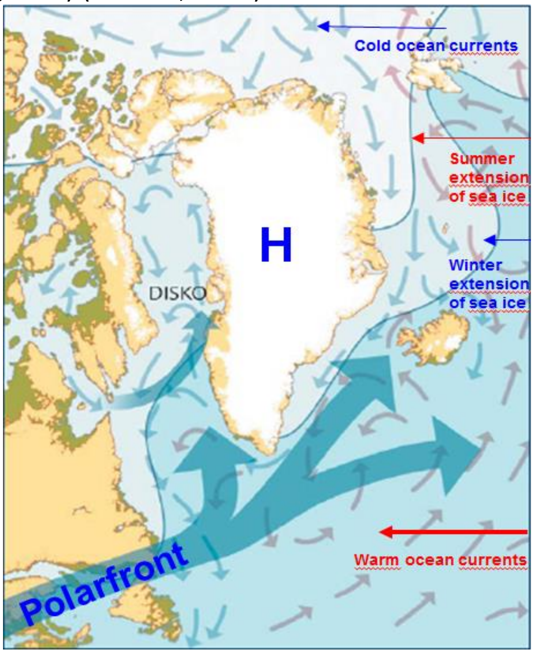

Figure 6 - Climatic conditions around Greenland.

Cold water masses are flowing out from the polar ocean and move south along the eastern part of Greenland, whilst warmer water masses are flowing north along the south western coast of Greenland. The cold air masses are streaming out from the mainland from Canada and Siberia, and when these meet the warmer and moister air masses originating from the Atlantic region, low-pressure zones are created. The relations between these two air masses are called the polar front. The position of the polar front along with the movement of the water masses is the main controller of the weather in Greenland (Hansen et al., 2006).

Solar radiation and albedo

Because of the low sun angle in the Arctic regions, the general heat supply to the region is quite low. Together with the very alternating cloud cover, the changing sun angle causes large variations in the incoming- and outgoing radiation. Furthermore the albedo changes a lot from year to year. In general the incoming radiation is highest in the summer-months and non-existent in the winter-months. The albedo on the other hand is highest in the winter-months and lowest in the summer months because of the sparse snow cover during the summer (See Figure 7).

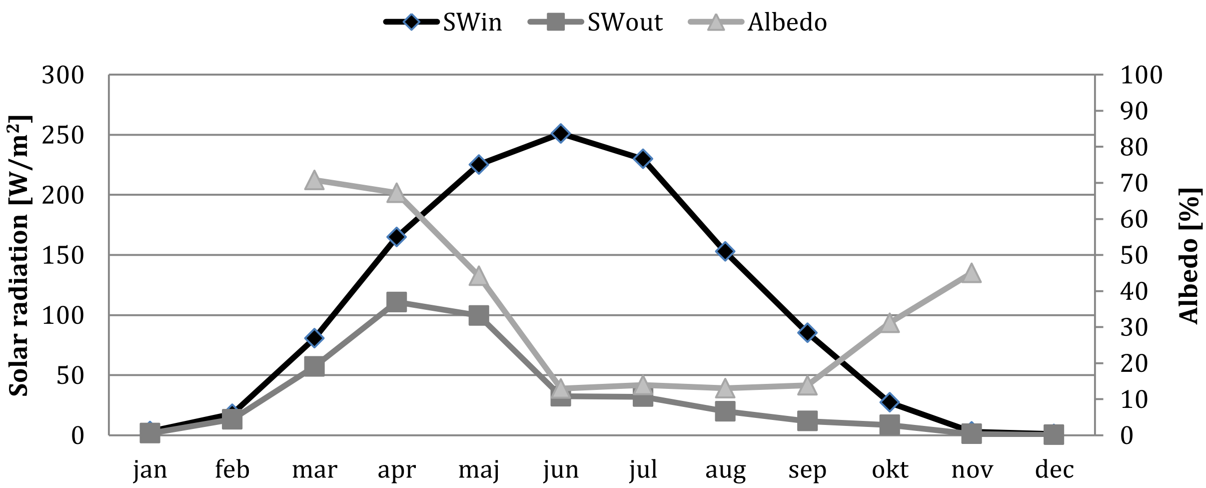

Figure 7 - Short wave- in and out going radiation and albedo at the scientific leaders house next to Artic Station from 1991-2014

Temperature and precipitation

Artic climate is strongly dependent on the temperature regime, particularly summer temperatures. For the period 1991 to 2013, the yearly average temperatures have increased from around -5 degrees Celsius to almost 0 degrees Celsius (See Figure 8). The maximum and minimum temperatures during the years also seem to increase during this period, though these vary quite a lot.

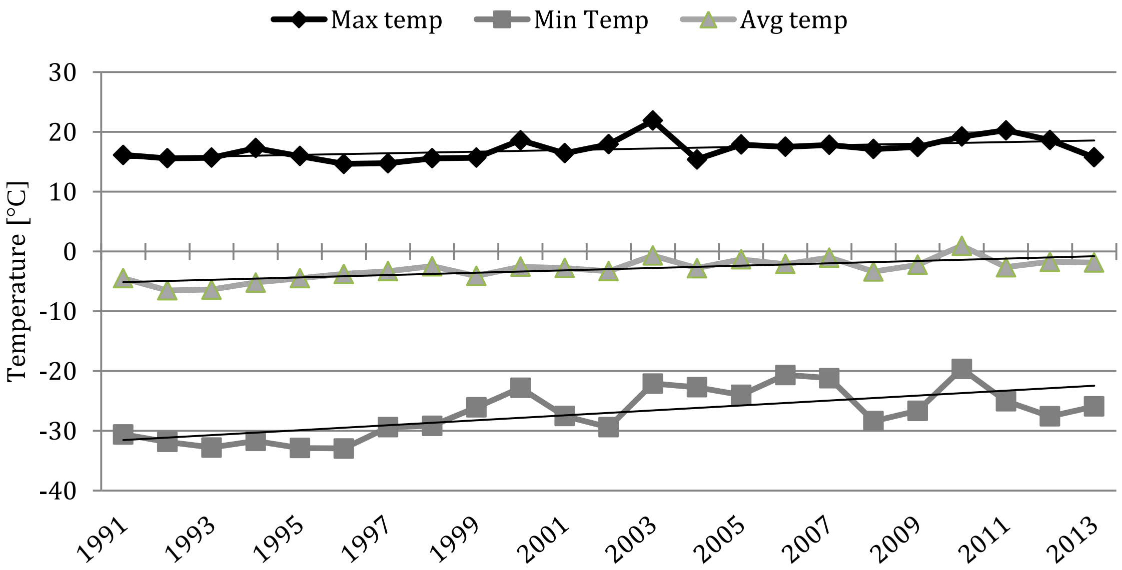

Figure 8 - Average, maximum and minimum air temperatures from the scientific leaders house for 1991-2013.

The main part of the precipitation in Greenland is associated with the low-pressure fronts. Therefore the southern part of Greenland, where the polar front is quite manifesting, receives more precipitation than the northern part. The low-pressure zones are especially dominating the area around the Arctic Station during the summer and autumn, and therefore half of the annual precipitation around Arctic Station is falling during this part of the year. The yearly mean precipitation is 585 millimetres at the station. Of these 585 millimetres, 42% is snow. In Figure 9, the variation in snow cover at the Arctic Station for the period 1991 to 2013 can be seen:

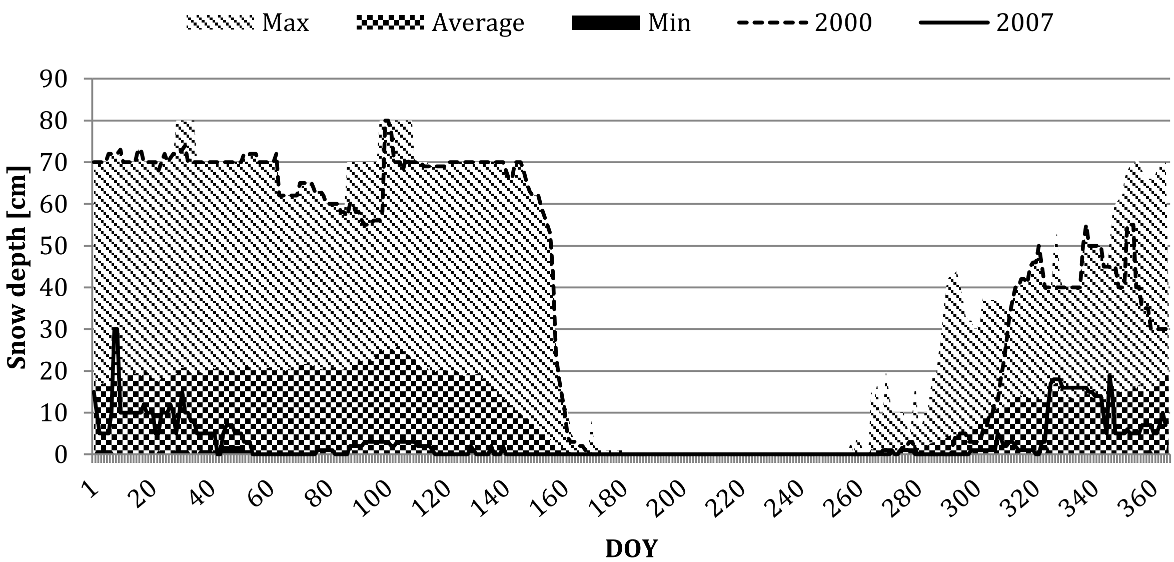

Figure 9 - Average, maximum and minimum snow depth at Arctic Station (1991-2013).

The snow cover varies very much from year to year. In 1994, which was a year with little snow, the snow cover reached 40 centimetres in height, while during winter in 1999, which was a year with a lot of snow, it reached 70 centimetres. The snow cover in 1999 was present for almost 6 months, 50 days more than in 1994 (Hansen et al., 2006).
However, no particular pattern in the amount of snow over the period of time can be detected as opposed to the sea ice, where a clear tendency with less sea ice over time can be detected.

Sea ice
The sea ice around the Disko Island is called the Western ice. This ice is created during the winter when the temperatures are low. The dissemination of this ice has however changed during the last two decades. In the beginning of the 90's the western ice could be found in the Disko bay for almost 5 months of the year whilst it in the later period has been covering the bay for lesser time spans. In Figure 10 the dissemination of the sea ice in the Disko bay for the period 1991 to 2014 can be seen.

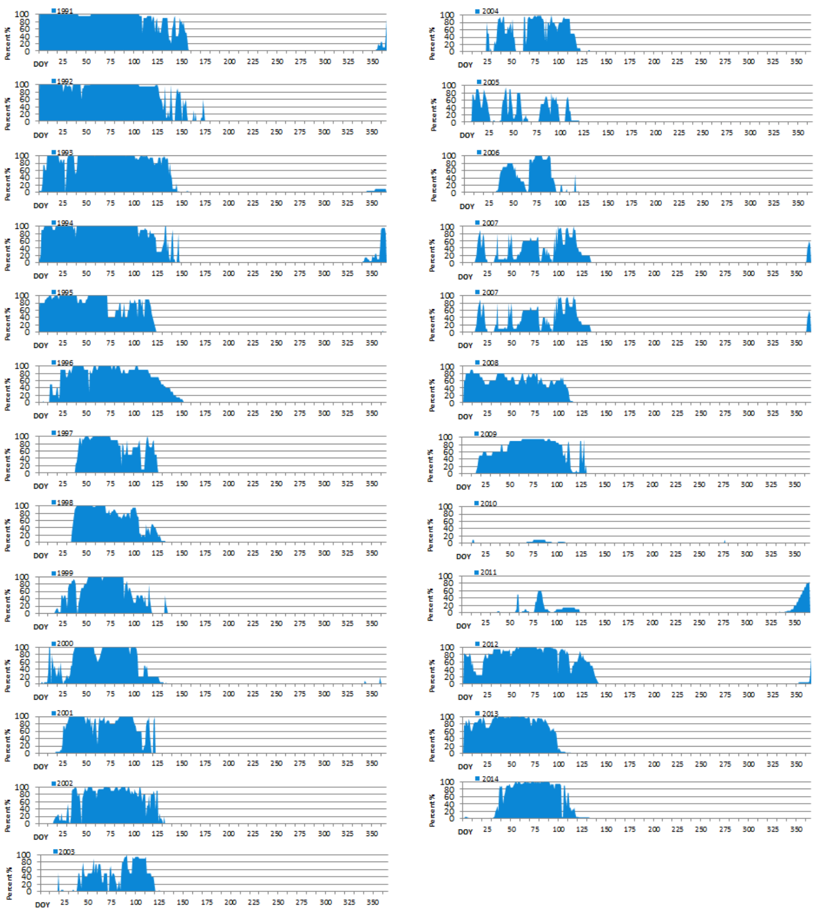

Figure 10 - Dissemination of sea ice in the Disko bay from 1991 to 2014, based on climatic data from Arctic Station (x-axis: DOY, y-axis: Dissemination (%).

The occurrence of sea ice is closely related to the air pressure. This is because the sea ice reflects a significant amount of the incoming radiation, which leads to a cooling of the atmospheric layers near the surface, and in this way the air pressure near the surface increases. This means that sea ice corresponds to a relative stable high-pressure situation whilst no sea ice makes the air parcels unstable (Hansen et al., 2006).

Bioclimatic zones of Disko Island

Air with a low temperature holds less water vapour than air with higher temperatures. Therefore the most important climate factor in the Arctic regions is the air temperature. The Arctic climate zones (illustrated in Figure 11) are in this way characterized by the warmest month having a lower mean temperature than 10 degrees Celsius.

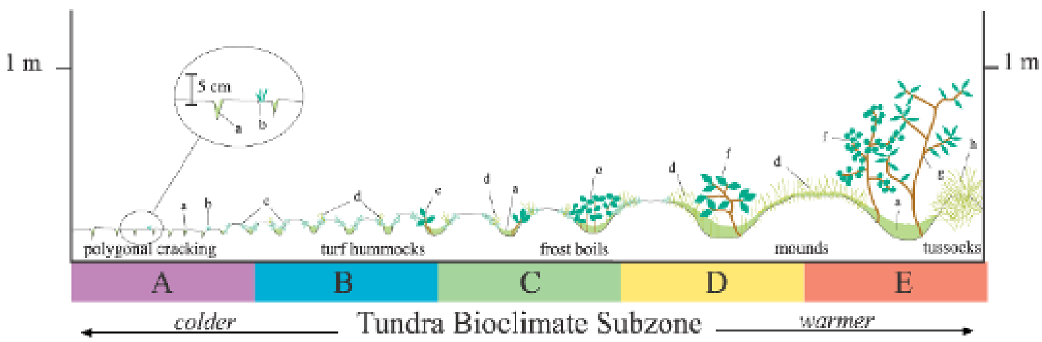

Figure 11 - Graphic illustration of the 5 bioclimatic subzones.

The Arctic climate zone extends more than 2700 kilometres from north to south, and therefore a subdivision of the bioclimatic zones within the Arctic has been implemented. The High Arctic zone is defined by the warmest month having a mean temperature below 5 ˚C and the Low Arctic zone is defined by the warmest month having a mean temperature between 5˚ and 10˚ (W.A. GOULD et al. 2002) Both subdivisions can be divided into a moist coastal zone and a dryer continental zone. Because the division between the High Arctic and the Low Arctic zone lies at 70˚ North, Disko Island is covered by both high and low arctic zones (Hansen et al., 2006).

Subzone	Definition	SWI	$Ta_{mean,}$ July, °C
A	Arctic Polar Desert	<6	0 – 3
B	Northern Arctic Tundra	6-9	3 – 5
C	Middle Arctic Tundra	9-12	7 – 9
D	Southern Arctic Tundra	12-20	9 – 11
E	Arctic Shrub Tundra	20-35	11 – 13

Table 1 - Definition of the 5 bioclimatic subzones.

Vegetation

Disko is located in the transition zone between High Arctic and Low Arctic which means that compared to other locations at the same latitude the vegetation at Disko is more diverse. More than 70 % of the species in West Greenland and more than 50 % of all species in Greenland are found at Disko (Mølgaard et al., 2006). The northern part of Disko is the southern frontier of High Arctic species and the southern part of Disko is the northern frontier of Low Arctic species.

Hot springs at the southern coast of Disko enable growth of four orchid species: Small White Orchid, Northern Green Orchid, Coralroot and Lesser Twayblade (Mølgaard et al., 2006). Because of the hot spring, Kuannit, located by Disko Fjord this is the northern frontier of linnaea borealis which is normally found hundreds of kilometers further south.

A change in dissemination of species can be an indication of climate change. Species that have its northern frontier at the southern part of Disko can spread to the more northern part of the island and species that have its southern frontier at the northern part of Disko can be eradicated from the island.

Because of the low temperatures and short growing season the vegetation at Disko is low and dominated by dwarf shrubs, mosses, and herbs. In wet areas gray willow is dominating and more dry areas are dominated by heath vegetation such as the widespread mountain avens. In areas where the ground is covered by snow for long periods a special kind of vegetation will occur characterized by dwarf willow.

At higher elevation polygonal soil patterns can occur at hill slopes where the top layer is unfrozen and permafrost is beneath. The top layer of soil will slide on top of the permafrost and create soil polygons of wet soil without vegetation.

In the area around Arctic Station the mountain tops reach elevations of 800-900 meters and the vegetation here is very sparse. The vegetation at the mountains is dominated by arctic willow, arctic poppy, and saxifrage (Mølgaard et al., 2006).

Closest to the water, salt marches characterize the area from the high water level to one meter above the high water level. Salt marches have a large content of water, chloride and sodium. Further up the salt march the content of sodium is decreasing and the content of calcium is increasing.

Warmer summers and reduced seasonal duration of snow cover lead to a vegetation response. As summers warm, and the growing season lengthens, dark shrub tundra advances poleward, replacing low-growing tundra that, compared to the shrub vegetation, is more easily covered by high-albedo snow. This leads to an albedo feedback that furthers the warming (Fig. 2; Chapin et al., 2005; Sturm et al., 2005; Goetz et al., 2007). The albedo difference between shrub- and low-tundra is most effective in spring, when the solar radiation flux is strong and snow cover is still extensive. The feedback is even more pronounced if warming allows evergreen boreal forest with its dark foliage to advance northward and replace tundra or shrub vegetation. In the case of boreal forest migration, the warming feedback would tend to be partially balanced for a period of time by sequestration of carbon in forest ecosystems, which have more above-ground carbon than shrub ecosystems (Denman et al., 2007). The situation may be different farther south, where the winter solar flux is still substantial. If warming is sufficient to allow deciduous forest replacement of evergreen boreal forest, then there is an increase in the wintertime surface albedo, acting as a negative (cooling) feedback (Bonan et al., 1992; Rivers and Lynch, 2004).

Crowberry was very common. It is a plant that grows in heaths and bogs especially in coastal areas. In west Greenland it is seen northwards to 79°N.

Dwarf birch was also very common and is a dominating plant at heaths and fell-field areas. It was 15-20 cm tall and was creeping across the surface.

Salix - Northern willow was also a common vegetation type in Blæsedalen and it grows all over Greenland. The plant was up until one meter tall in Blæsedalen and was hereby the tallest vegetation type in the area.

Clubmosses is common at heaths and fell-field sites. It is a perennial plant that is 3-30 cm tall.

Bog bilberry is a dwarf-schrub plant that grows on low nutrient soil in heaths and marches. The plant is not seen north of 79°N

Cotton grass was seen on peaty, marchy ground. It is a perennial plant that grows on wet clay or sand all over Greenland.

Horsetail was seen in wet areas as well. It is a plant with a very simple plant structure and it grows on moist and clayey ground in all of Greenland.

Large-flowered wintergreen was also seen in the area and is common on quit dry soil in dwarf-shrub heaths and copses. It grows northwards to 79°N in western Greenland.

Angelica is the largest perennial herb in Greenland and is also seen in Blæsedalen. It is common on moist herb-slopes, in willow shrub, at river banks and it grows northwards to Disko.

Narrow leaved Labrador-tea was also seen at several spots in Blæsedalen. It is a dwarf-shrub and very common on acid, nutrient poor soil. The plant grows in mossy heaths, shrubs and bogs, especially in gneiss areas and only in west Greenland from 62°N to 72°N.

Common butterwort was also seen in Blæsedalen. It is a perennial herb that is Common in Greenland until 71°N.

Box 1 – Main Characteristics of the common vegetation in Blæsedalen, Disko Island.

Vegetation and its response to bioclimatic zones shift

Vegetation has an isolating effect on permafrost, but the vegetation in the Arctic and hereby Disko is limited by a short growing season, low nutrient content, cryoturbation and climatic conditions (Cherov, 1985). The vegetation is short (5-30 cm), but in some places arctic willow shrubs were found to be one meter. The precipitation at Disko is high compared to other Arctic environments due to the coastal location (Henriksen, 2014). When precipitation saturates the soil bogs and ponds are formed, a moisture environment for vegetation is created (Chernov, 1985). Furthermore, permafrost limits drainage in the system which remains ponds and bogs in lowland areas. Landscapes like this are often dominated by cotton grass and field horse tail.

The vegetation achieves nutrients from the organic matter in the soils but there is no deep root system due to cryoturbation processes throughout the frost and thawing seasons. The vegetation has adapted into these condition where strong winds are also a factor that the plants need to resist. The vegetation groups together to survive and the perennial species as cotton grass, angelica and common butterwort are protected by the snow during winter.

The absent of solar radiation during polar night and the twilight period before and after polar nights result in a short growing season which means plants are more likely to reproduce by budding and division than flowering. However

the growing season is very intense due to the midnight sun. At the Arctic Station the midnight sun is present from the 20th May until the 24th July.
Furthermore the arctic vegetation is able to do photosynthesis at low temperatures and dark conditions (Chernov, 1985).

Geology of Disko Island

In the area around the Disko Fjord, four major geological formations can be seen. The oldest of these formations are the bedrock formations, which are more than 1.6 billion years old. Furthermore tertiary formations from cretaceous and Paleogene can be seen. These are approximately 60 to 100 million years old. In these deposits some distinguished formations formed in the late Paleogene period can be observed, these are volcanic rocks formed approximately 54 to 60 million years ago. The youngest deposits in the area are from the quaternary period, which are around 100.000 years old (Pedersen et al., 2006). In Figure 12 the different depositions for the area can be seen, however the quaternary deposits cover most of the area, and therefore these are not shown on the figure.

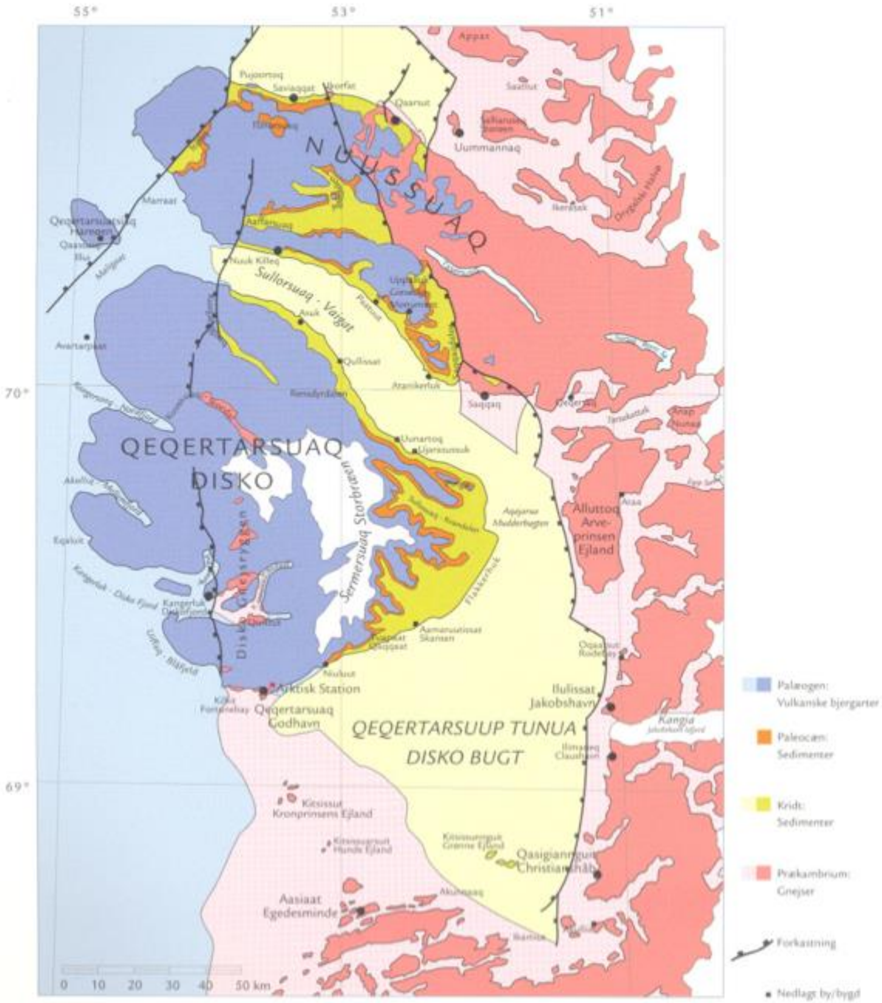

Figure 12 - Geology of the study area. Yellow/green marks the deposits from cretaceous, blue marks the volcanic deposits from paleogene and shifting dark and light red marks the bedrock deposits (Pedersen et al., 2006).

The depositions from cretaceous are formed in a large depositional basin called the Nuussuaq-basin. However in late cretaceous and early Paleogene the basin was affected by large tectonical activity, which resulted in a breakup of the stratified depositions, such that some of them are tilting more than 10 degrees.

From the formation of the bedrock approximately 1600 mio years ago up until the deposits in late cretaceous, no geological layers are detected. This means that no geological depositions can be found for this period of time in the area.

After the depositions in the Nuussuaq-basin and breakup of these, the Disko area was affected by volcanism. The volcanic rocks formed approximately 60 million years ago are a result of this intense volcanism. The volcanic activity was a result of large tectonical activities that affected the whole northern Atlantic region. Through this period, two major depositions of volcanic rocks were formed at the Disko Island. The oldest is the Vaigat formation, which dominates the northern part of the Disko Island, and the youngest is the Maligât formation, which dominates the central and southern part of the Disko Island. Approximately 6 million years later, the volcanic activity was at a high at the Disko Island again. This resulted in a large plateau created in the western part of the island. Today, the landscape at the Disko Island can be characterized as a large cenozoic plateau traversed by rivers and fjords (Pedersen et al., 2006). The geological history is a base for the pedology in the area and this will be the focus in the next section.

Pedology of Disko Island

According to JRC[1] soil atlas of the Northern Circumpolar Region, there are 5 dominating soil types in Greenland (See Figure 13).

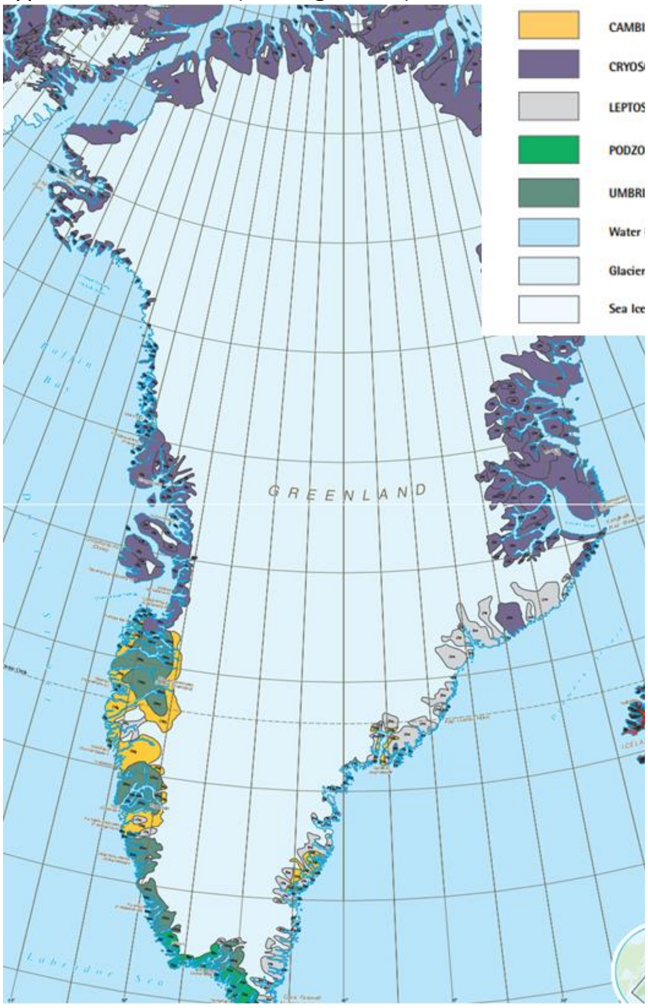

Figure 13 - Dominating **soil types of Greenland (Jones, et al., 2009).**

The southeastern part is dominated by Leptosols, the southern part is dominated by Podzols, the southwestern part is dominated by Cambisols, and Umbrisols and the northern part is dominated by Cryosols (for definitions see Box 2).

Leptosols: Shallow soils over hard rock that are mainly found in mountainous regions.
Podzols: Acid soils with a bleached horizon underlain by an accumulation of organic matter, aluminum and iron (Podsolization).
Cambisols: Poorly developed soil due to limited age or rejuvenation of the soil material.
Umbrisols: Soil with a dark and acid surface horizon rich in organic matter.
Cryosols: Soils with permafrost within a depth of 1 meter from the surface, or within 2 meters if accompanied by features of cryoturbation.

Box 2 - Definition of the dominating Greenlandic soil types.

Disko is located at latitude 69°N, on the boundary between continuous- and discontinuous permafrost and belongs to the temperature regimes hypergelic and pergelic (Jones, et al., 2009), see Figure 15. This classifies the soil type at Disko to be a crysol. A Cryosol is defined by the presence of permafrost in the upper 1 meter of the profile or in the upper 2 meters accompanied by features of cryoturbation. Cryoturbation is a process where soil is mixed through the horizons to the bedrock of a profile as a result of freeze and thawing (Kimble, 2004). As a result the spatial distribution of Cryosols is very much related to climatic conditions and soil temperature regimes. Due to climatic change it can be argued that the temperature regime will change through time.
The cryosol at Disko has been subdivided into four goups; Haplic Cryosols (CRha), Leptic Cryosols (CRle) and Turbic Cryosols (CRtu) (see Figure 14).

[1] Joint Research Center under EU Comission.

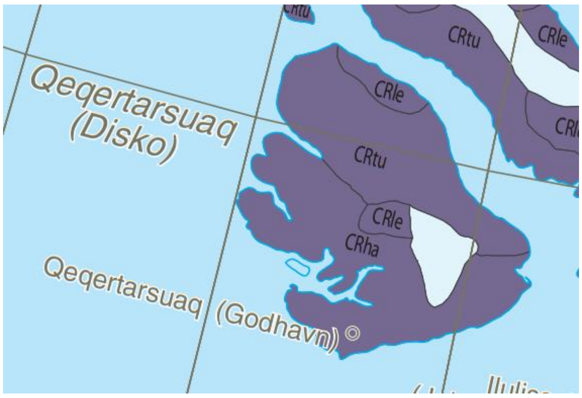

Figure 14 - Soil types of Disko (Jones, et al., 2009).

The Haplic Cryosol is defined as a Cryosol without indications of cryoturbation, but still affected by permafrost. Though, as shown in Image 1, this classification is not 100 percent valid for Blæsedalen. Cryoturbation have resulted in both freeze-thaw circles and steps op slopes in the area (Jones, et al., 2009).

The climatic conditions, with long cold winters and short cold summers, cause the land cover to be dominated by Grass- and Shrubland. Furthermore an accumulation of organic matter, takes place as a result of reduced decomposition by microbes and fungi (Kimble, 2004).

At the northern part of the Disko Island the soil type is classified to be a leptic cryosol, which is classified to be cryoturbated permafrost covering hard rock. The last type that is representing at Disko Island is Turbic cryosol, which is a cryotubated permafrost soil.


Image 1 – Steps formed by cryoturbation.

DDT & DDF

Figure 15 shows the distribution of continuous, discontinuous, sporadic and no permafrost in Greenland according to the frost number. The Frost number is defined as:

$$F = \frac{DDF^{1/2}}{DDF^{1/2} + DDT^{1/2}}$$

Where, DDF is degree days of freezing and DDT is degree days of thawing (Nelson, 1986).

The frost number predicts the absence or present of permafrost as a function of air and freezing influences. Permafrost is expected when the depth of winter freezing overdoes summer thaw or when the accumulated freezing degree days are greater than accumulated thawing degree days. It is seen of Figure 15 that western part of Disko is classified to have continuous permafrost and that discontinuous permafrost is found in the southern and eastern part of the Island.

Figure 15 - Distribution of permafrost with the frost number. Where Dark blue is Continuous permafrost, light blue is discontinuous permafrost, yellow is sporadic permafrost and green is no permafrost.

References

Andresen, C. S., Schmidt, S., Seidenkrantzc, M., Straneo, F., Grycel, A., Hass, C., Kjær, K. H., Nørgaard-Pedersen, N., Dyke, L. M., , Olsen, J., Kuijpers, A. (2014): *A 100-year record of changes in water renewal rate in Sermilik fjord and its influence on calving of Helheim glacier, southeast Greenland.* Continental Shelf Research, Vol. 85, pp. 21-29.

Auslander, M., Nevo, E., Inbar, M. (2002): *The effects of slope orientation on plant growth, developmental instability and susceptibility to herbivores*. Journal of Arid Environments 55 (2003) 405-416.

Bhatia, M. P., Kujawinski, E. B., Das, S. B., Breier, C. F., Henderson, P. B., Charette, M. A. (2013): *Greenland meltwater as a significant and potentially bioavailable source of iron to the ocean*. Nature Geoscience, Vol. 6, Issue 4, pp. 274-278.

Christiansen, H. H. (1999): *Active layer monitoring in two Greenlandic permafrost areas: Zackenberg and Disko Island*. Geografisk Tidsskrift, Bind 99 (1999), p. 117.

IPCC, Cubasch, U., D. Wuebbles, D. Chen, M.C. Facchini, D. Frame, N. Mahowald, and J.-G. Winther, 2013: Introduction. In: *Climate Change 2013: The Physical Science Basis. Contribution of Working Group I to the Fifth Assessment Report of the Intergovernmental Panel on Climate Change* [Stocker, T.F., D. Qin, G.-K. Plattner, M. Tignor, S.K. Allen, J. Boschung, A. Nauels, Y. Xia, V. Bex and P.M. Midgley (eds.)]. Cambridge University Press, Cambridge, United Kingdom and New York, NY, USA.

Gilbert, R. (2000): *Environmental assessment from the sedimentary record of high-latitude fiords*. Geomorphology, Vol. 32, Issue 3-4, pp. 295–314.

Gilbert, R., Nielsen, N., Møller, H., Desloges, J. R., Rasch, M. (2002): *Glacimarine sedimentation in Kangerdluk (Disko Fjord), West Greenland, in response to a surging glacier*. Marine Geology, Vol 191, p 1-18.

Hanna, E. Huybrechts, P., Cappelsen, K. J., Shuman, H. R., Irvine-Flynn, C. T., Wise, S., Griffiths, M. (2007): *American Meteorological Society*. Journal of Climate.

Hansen, B. U. (2014): *Godhavn/Disko Climate*. Power Point presentation, 29.04.14.

Hansen, B.U., Elberling, B., Hollesen, J. and Nielsen N. (2006): *Vejret og klimaet*. Pp. 44-57 in: Bruun, L., Kristensen, R. M., Nielsen, N., Pedersen, G. K. and Pedersen, P. M. (eds.): *Arktisk Station 1906-2006*. København, Forlaget Rhodos.

Hinkel, K. M., Nelson, F. E. (2003): *Spatial and temporal patterns of active layer thickness at Circumpolar Active Layer Monitoring (CALM) sites in northern Alaska, 1995-2000*. Journal of Geophysical Research: Atmospheres, pp. 9-13.

Hollesen, J., Elberling, B., Jansson, P. E. (2011): *Future active layer dynamics and carbon dioxide production from thawing permafrost layers in Northeast Greenland.* Global Change Biology (2011) 17, 911-926.

Jones, A., Stolbovov, V., Tarnocai, C., Broll, G., Spaargaren, O., Montanarella, L. (2009): *JRC Northern Circumpolar Soil Map*. EU Comission.

Kimble, J. (2004): *Cryosols, Permafrost-Affected soils.* New York: Springer

Lawrence, D. M., Slater, A. G., Romanosky, V. E., Nicolsky, D. J. (2008): *Sensitivity of a model projection of near-surface permafrost degradation to soil column depth and representation of soil organic matter*. Journal of Geophysical Research-Earth Surface, Vol. 113, Issue F2, Article number F02011.

Markussen, T. N., Andersen, T. J. (2014): *Flocculation and floc break-up related to tidally induced turbulent shear in a low-turbidity, microtidal estuary*. Journal of Sea Research, Vol. 89, pp. 1–11.

Mølgaard, P., Kristiansen, P., and Pedersen, P. M.(2006): *Plantelivet*. Pp. 70-83 in: Bruun, L., Kristensen, R. M., Nielsen, N., Pedersen, G. K. and Pedersen, P. M. (eds.): *Arktisk Station 1906-2006*. København, Rhodos.

Møller. H. S, Christiansen, C., Nielsen, N., Rasch, M. (2001): *Investigation of a modern glacimarine sedimentary environment in the fjord Kuannersuit Sulluat, Disko, West Greenland*. Danish Journal of Geography, Vol. 101, pp. 1-10.

Nasa Earth Observatory: http://earthobservatory.nasa.gov/IOTD/view.php?id=81214, obtained 09.11.2014

Nelson, F. E. (1986): *Permafrost Distribution in Central Canada: Aplications of a climate-Based Predictive Mode*l. American Geographers, pp. 550-568.

Nelson. F. E., Shiklomanov, N. I., Mueller, G. R, Hinkel, K. M, Walker, D.A., Bockheim, J. G. (1997): *Estimating Active-Layer thickness over a large region: Kupurik River Basin, Alaska, U.S.A.* Arctic and Alpine Research, Vol. 29, No. 4, 1997, pp. 367-378.

Pedersen, K.A., Pedersen, G.K., and Larsen, L.M. (2006): *Geologien*. Pp. 17-32 in: Bruun, L., Kristensen, R. M., Nielsen, N., Pedersen, G. K. and Pedersen, P. M. (eds.): *Arktisk Station 1906-2006*. København, Forlaget Rhodos.

Rasch, M., Nielsen, N., Christiansen, C., Balstrøm, T., Gilbert, R., Desloges, J. (2003): *Role of landscape parameters in riverine run-off and sediment and organic matter yield on Disko Island, West Greenland*. Danish Journal of Geography, Vol. 103 (2), pp. 1-11.

Riseborough, D., Shiklomanov, N., Etzelmüller, B., Gruber, S., Marchenko, S. (2008): *Recent Advances in permafrost modelling*. Permafrost and Periglacial Processes. 19: 137-156 (2008).

Rune, F. (2011): *Wild Flowers of Greenland*. Gyldenlund Naturforlag.

Sorg, A., Bolch, T., Stoffel, M., Solomina, O., Beniston, M. (2012): *Climate change impacts on glaciers and runoff in Tien Shan (Central Asia)*. Nature Climate Change 2, pp. 725-731.

Tranter, M., Brown, G. H., Hodson, A., Gurnell, A. M., Sharp, M. J. (1993): *Variations in the nitrate concentration of glacial runoff in Alpine and sub-Polar environments*. Yokohama Symposia.

Zhang, T., McCreight, J., Barry, R. G. (2012): *Arctic EASE-Grid freeze and thaw depths, 1901-2002.* Boulder: Natonal Snow and Ice Data Center. http://nsidc.org/data/docs/fgdc/ggd651_frzthw_depth_efact/#5.

Østerby, O. (1974): *Analysis of nummerical solution of the stefan problem.* Århus: Institute of mathematics.

Appendix 1 - Field schedule and procedures

	Active layer group			Boat group
01-08-2014	**Arrival at Arctic Station**			**Arrival at Arctic Station**
02-08-2014	**Introduction to Blæsedalen and Arctic Station** Visiting the location of climate stations and CENPERM snow fence experiment. Introduction to CALM Site at Pettersons Moraine and sedimentary measurements at Røde Elv .			**Introduction to Blæsedalen and Arctic Station** Visiting the location of climate stations and CENPERM snow fence experiment. Introduction to CALM Site at Pettersons Moraine and sedimentary measurements at Red River.
03-08-2014	**CALM Site Measurements** Recovering of field site, plotting of GPS Points, NDVI, soil temperature, surface temperature, thermal conductivity, soil moisture and permafrost probing.			Leaving Arctic station with Porsild towards the Disko Fjord. Setting up divers in water and stationary camera on land. Pretesting measurements with different instruments.
04-08-2014	**CALM Site Transect Measurements** Establishing transect from south to north, plotting of GPS Points, NDVI, soil temperature, surface temperature, thermal conductivity, soil moisture and permafrost probing.			Measuring stationary profiles with water samples. During night time stationary measurements.
05-08-2014	**NDVI for Snow-fence Experiment Site** Establishing GPS coordinates of 96 plots and accessing NDVI values by using a NDVI converted camera.	**CALM Site Drone RGB** Capturing normal RGB photos via drone	**CALM Site Temperature mast** Setting up a portable climate station at the site for measuring surface temperature and air temperature at 2 meters height.	Stationary profiling with water samples and transect measurements with water samples. Filtration of water samples.
06-08-2014	**Horsetail Site** Taking soil samples from different depths, measuring soil temperature, moisture and thermal conductivity.	**CALM Site Drone NDVI** Capturing NDVI photos via drone		Hike towards the glacier. Placement of two divers, and measurements with castaway CTD.
07-08-2014	**Godhavn Site** *In situ* measurements and visual identification of training sites for classification in and around Godhavn	**Lab work** Drying, sorting and weighting of soil samples.		Hike back towards Porsild. Water samples taken on the way together with sediment samples. CTD measurements and collection of divers. Transect measurements with water samples in the evening.
08-08-2014	**Tue individual project** Taking soil samples and measuring different parameters from random plots around Pettersons Morane	**Cotton-grass Site** Permafrost probing, soil temperature, surface temperature, soil moisture and exploring active layer thickness via excavation.	**Østerlien** *In situ* measurements and visual identification of training sites for classification in and around Østerlien	Transect measurements with water samples. Bottom sediment samples taken with the Van Veen grab. Pick up of stationary camera on land and divers in water. Arrival at Arctic station in the evening.
09-08-2014	**Data processing** Tapping in the data collected in the field. Working with GIS data for Disko island.	**Lab work** Drying, sorting and weighting of soil samples. Measuring and estimating bulk density.		Filtration of water samples.
10-08-2014	**Data Processing** Tapping in the data collected in the field. Working with GIS data Disko island.	**Church/Football**		Filtration of water samples. Discharge measurements in the Red River.
11-08-2014	**Data Processing** Tapping in the data collected in the field. Working with GIS data Disko island.	**Coast temperature mast** Setting up a portable climate station close to the coast, that measures surface and air temperature(2m height)		Filtration of water samples. Discharge measurements in the Red River.
12-08-2014	**Coast to land transect** Making two 2km length 'Coast to land' transects with 100meters interval between the measurements. Measurements consisted of air temperature and air moisture at 2 meters height, surface temperature, soil temperature, soil moisture and thermal conductivity. In addition to that, information on land surface and vegetation type was collected for validation of???			Filtration of water samples. Discharge measurements in the Red River.
13-08-2014	**Data Processing** Tapping in the data collected in the field. Working with GIS data Disko island.			Filtration of water samples. Experiment with salinity and iron concentration.
14-08-2014	**Cotton-grass Site** Measuring thermal conductivity at the previously explored plots.			Filtration of water samples. Measurements in the Disko Bay with camera and CTD. Experiment with salinity and iron concentration.
15-08-2014	**Download of data from portable climate stations**	**Leaving Artic Station**		Filtration of water samples. Discharge measurements in the Red River. Packing and leaving the arctic station

Flocculation processes in the Disko Fjord area (Western Greenland) and cloudburst effects on the flocculation

Jeppe Dalskov Frederiksen, Britt Gadsbølle Larsen and Marta Merino

Abstract

Flocculation processes were studied in a large tidal influenced plume in the Disko Fjord in western Greenland through measurements with a partcamera. Furthermore measurements with CTDs, a LISST and water samples were used to complement the camera-measurements. The results of the LISST showed to be insufficient because of the high turbidity in the plume, and therefore these measurements are not shown in this paper. Through MATLAB scripts, the camera images were investigated, and the calculated number of particles and mean particle diameters were analyzed through Ocean Data View, together with the CTD measurements. The SPMC values showed to be important with regards to the flocculation, and the settling of the particles showed to be controlled largely by the current velocity, hence most of the settling happening during slack water. CTD measurements and water samples were also taken in the Red River near the Arctic Station in Qeqertarsuaq. SPMC values showed to be largely controlled by rainfall, and the cloudburst happening on the 9th of August 2014, had a huge impact on the concentration levels. The measurements from the Red River were used as indicator of general reactions to climate in the Glacial River system creating the plume, in the Disko Fjord.

Keywords: *Flocculation, Plume dynamics, SPMC, Disko Fjord, Cloudburst*

1. Introduction

Glacial runoff is an important parameter with regards to climate change. The volume of runoff can act as an indicator of glacial movements. The sediment discharge from glaciers is an important factor as well. Tranter et al., 1993, state that one of the major contributors of NO_3^- to the hydro glacial systems is snowmelt. Nutrients, such as nitrate, can influence the climate on local scales, and hereby act as a marker for possible large scale changes in the primary production in the Arctic (Dugdale, 1967).

Nutrients act as fertilizers for phytoplankton, and can in this way affect the exchange of CO_2 between the sea and the atmosphere. In this way glacial rivers transporting nutrient rich sediments, act as distributors of nutrients to the sea and the use of these nutrients affects primary production.

The importance of nutrients on primary production makes it important to study the precipitation of these nutrients throughout the water column. The process of flocculation hereby becomes important. Flocculation processes are controlled by the water properties and the particle properties (Markussen & Andersen, 2014). The level of turbidity is important for the flocculation processes, as it increases the probabilities of particles colliding (Markussen & Andersen, 2014). However Pejrup & Mikkelsen (2010) showed that when the Turbulent-shear forces become stronger than the cohesive forces, at a certain threshold value of turbidity, they cause a floc break up.

Sholkovitz (1978) showed that presence of iron increases flocculation, and therefore iron rich sediments influences the uptake of CO_2 from the atmosphere towards the sea in two ways; Both by enhancers of flocculation, but also as an important nutrient for phytoplankton (Raiswell, 2013).

The braided glacial river leading into the Disko Fjord transports iron rich sediments, and therefore the dynamics of the created plume are important to investigate. Furthermore glacial runoff and sediment discharge are highly dynamic processes that alter the river systems constantly. Hereby measurements of these parameters are important with regards to climate change, and the dynamics of the glacial river system.

Through this study the general dynamics of the Red River in Qeqertarsuaq, west Greenland, will be described, and the measurements will be up-scaled so that they can be used to describe the general dynamics in the braided glacial river leading into the Disko Fjord. Furthermore measurements of the general water properties and the flocculation processes in the fjord are carried out, and investigated.

2. Study site

2.1 Red River

Red River is situated in Blæsedalen near Qeqertarsuaq on the southern part of Disko Island. The river is flowing from north to south with an annual total discharge of $36 \cdot 10^6$ m^3 (Arctic station administration, 2014). Red River drains an area of 66 km^2 and 21 % of the drainage area is covered by glaciers (Hasholt, 1996). The main glacier contributing to the runoff is Chamberlain Glacier. Red River is primarily a braided river but the last 3 kilometers of the river are straight. Braided rivers often transport large amounts of sediment and are very characteristic in glacial areas (Humlum, 2006). The large sediment transport is caused by the relatively low water depth compared with other types of rivers with the same discharge levels. As a result, a large part of the water is in contact with the bottom, which creates a very turbulent flow (Humlum, 2006).

The glacial runoff contains suspended sediment which is a source of iron that originates from the surrounding basaltic rocks and gives the water its red color. The river enters Disko Bay and a plume spreads out into the bay.

The discharge measurements and water sampling carried out for this study took place around 700 meters from the river mouth of Red River. At this location the width of the river was 18 meters. At the deepest part of the river the depth was varying between 0.7 and 0.8 meter during the study period.

2.2 Disko Fjord

Disko Fjord (Kangerdluk) is located in the southwestern part of Disko Island (figure 1). Disko Fjord has a drainage area of 531 km^2 with 68 % of the area covered in ice (Møller et al., 2001). The maximum depth in inner Disko Fjord is 120 meters (Gilbert, 1997). This study focus on the inner part of Disko Fjord, the northeastern arm called Kuannersuit Sulluat. A braided river, Kuannersuit Kuussuat, drains the Kuannersuit Glacier that is an outlet glacier of the largest ice cap on Disko Island (Knudsen et al., 2007). The river enters the fjord in an extensive delta creating a freshwater plume. The water from the river transports sediment from the glacier and the surrounding areas (Møller et al., 2001). Because of suspended sediment from the ferrous basaltic rocks dominating the area, the water has a characteristic red color and is creating a plume in the fjord. The salinity in the top layer of the fjord is around 1 ‰. In the bottom water of the fjord the salinity is around 30 ‰.

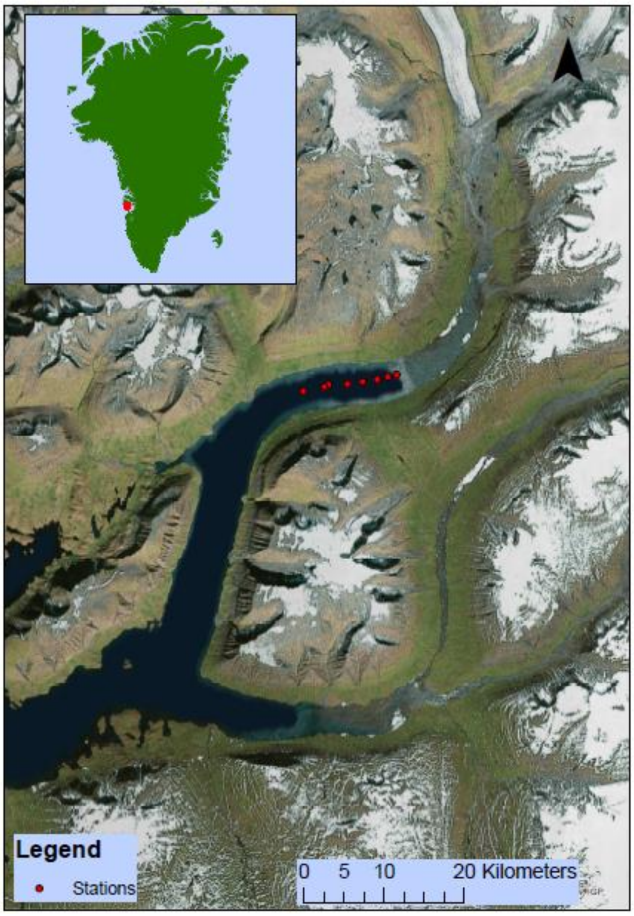

Figure 1: The Disko Fjord area, and the stations used for measurements in this study. Station 1 is the most eastern located station, and station 8 is the most western located station.

Disko Fjord is microtidal with a semi-diurnal range of 1.4 meters. The river supplies the fjord with $325 \cdot 10^6$ m^3 of water on average per year (Gilbert, 1997).

Measurements for this project were carried out in the inner part of Disko Fjord, Kuannersuit Sulluat. Red dots in figure 1 mark the location of station 1 through 8 where measurements for transects were carried out. Station 1 is closest to the river outlet and station 8 is the station furthest away from the outlet. For some transects measurements were conducted in additional stations between the eight stations. The added station between station 2 and 3 is named 2.5. The additional stations are 2.5, 3.5, 4.5, 5.5 and 6.5. All stationary measurements were conducted in station 1. The transects are measured over a distance of 12 kilometers away from the river outlet. The water depth at station 1 is 31 meter and at station 8 the depth is 110 meter.

3. Methods

3.1 Measurements from the boat

A partcam was used together with a YSI 6600-V2 CTD and a YSI Castaway CTD to get measurements of the general water column properties and the flocculation processes. These instruments were used for both stationary measurements and transects. Furthermore a Ruttner watersampler with a capacity of 2 liters was used to take water-samples during some of the profile-measurements.

The CTDs measure Conductivity, Temperature, Pressure, Salinity, Sound Speed, Density, Depth, Specific conductivity and more (YSI, 2010). The Castaway CTD was only used for the boat measurements because the pressure censor in the YSI 6600-V2 CTD was out of order, and so the depth was calibrated between the two instruments.

The partcam is developed in MARUM at the Bremen University in Germany. It uses a polyoxymethylene waterproof housing that makes the camera submersible. The camera model is a Digital SLR Canon EOS 50D together with a Canon EF-S 60mm lens. The camera and lens properties give the device a lower particle size limit of 20 µm and an upper particle size limit of more than 2 mm (Winter et al., 2012).

The particles are made visible by a 80 mW laser with a wavelength of 532nm (Green), which is collimated by a planoconvex lens reducing distortion effects (Winter et al., 2012).

Furthermore an Aanderaa RCM-9 was used to measure current during some of the stationary profiles.

A Sea-Bird 19plus v2 CTD was used together with a LISST-100C to obtain measurements at depths deeper than 50 meters, but was also used in higher parts of the water column. The LISST emits a laser beam and measures the scattering on the beam from particles in the water column. This is done in 32 different angles, and is hereafter converted to a particle size distribution. The matrix used for converting to the particle size distribution is assuming that the particles have different surface shapes, which has shown to give the most precise results (Andrews et al., 2010). In course of the matrix assuming random particle shapes, the lower particle size limit is 2 µm and the upper particle size limit is 400 µm.

3.2 Measurements on land

A hike up through the braided river system towards the glacier was conducted, and measurements were taken on the way. The Castaway CTD was used to obtain values for salinity and temperature throughout the river system, and water samples were taken in 1 liter bottles in order to calculate the SPMC of the river. Furthermore two Eijkelkamp Divers with a range of 5 meters was placed in the river in order to record the tidal range.

3.3 Measurements in the Red River

A Valeport model 801 current meter was used in the Red River to measure the discharge through the river system. The flat type sensor was used, which makes the measurements more sensitive to turbulence, and an averaging period of 30 seconds with a fixed average was applied. By applying the relative large averaging period, the effect of turbulence on the flat sensor was minimized (Valeport limited, 1999).

Furthermore 1 liter water samples were taken on different days, and the SPMC was calculated. Data extracted from a YSI 6600-V2 CTD placed in the river was used to calibrated the SPMC calculations, and to obtain knowledge about the general river properties.

3.4 Data management

A MATLAB script is used to differentiate the particles detected by the partcamera. The different images are converted to a binary format based on brightness intensity, and the different particles are detected through the intensity image. However particles with a maximum intensity lower than half of the overall maximum intensity are neglected because these particles are not in focus.

Through lab-work, the primary particle size is found for each of the water samples. 0.2 M ammoniumoxalat/oxalacid is added to each sample, and the samples are shaken for 4 hours in a Gerhardt Laboshaker. Hereafter the samples are filtered again, the dissolved sediments are added to a MALVERN 2000, and the primary particle size is found for each sample.

4. Results

4.1 Red River

The annual discharge in Red River has been estimated to be $36 * 10^6$ m^3, and the summer run off values generally lie between 3 and 5 m^3/sec (Arctic station administration, 2014). Nevertheless measurements conducted through this study show larger discharge values (table 1).

Date	Discharge [m3/sec]
10-aug	5.21
11-aug	8.0
12-aug	7.04
15-aug	7.0

Table 1: Discharge measurements from Red River for the 10th, 11th, 12th and 15th of August.

Bhatia et al. (2011) measured discharge values at a small outlet glacier from the Greenlandic Ice Sheet and showed results from July ranging between 1 and 2 m^3/sec. However Knudsen et al. (2007) investigated the sediment load and general discharge after a glacier surge in the Kuannersuit Glacier, and found that the mean discharge for late July was 68 m^3/sec. The glacier surge in the Kuannersuit Glacier had a large impact on the discharge, and it is well understood that measurements of run off and discharge from glaciers vary much between different glaciers.

Since Red River only partly drains glacier water, the measured values between 5 and 8 m^3/sec seems quite high; this can be because of the large rainfall during the observation period.

The measured sediment concentrations vary between 134 mg/L and 11037 mg/L for the period 26th of July until 13th of August. The reason for the huge variance in the concentrations is the cloudburst that occurred on the 9th of August. In this way, the measurements from that day show concentrations ranging between 4053 mg/L and 11037 mg/L, whereas the values range between 134 mg/L and 655 mg/L for the period before and after the cloudburst. This means that the rainfall has a huge impact on the measured concentrations even though the system partly drains from the Chamberlain Glacier.

The Red River system and the glacial river system in the Disko Fjord lies approximately 40 kilometers apart, and is hereby affected by more or less the same climate. It is therefore argued that the response to the climate in the two different catchments is comparable too. This does not mean that the response to climate is exactly the same in both catchments, but a measured increase in SPMC in the Red River system will presumably correspond to an increase in SPMC of approximately the same order of magnitude in the Disko Fjord system. However, the river system in the Disko Fjord is almost only draining a glacier whilst the Red River only partly drains a glacier. This difference between the two systems could have an influence on the effect of a cloudburst, and further investigation should be put into this.

4.2 Disko Fjord

The water samples taken in 1 meter depth generally show the highest SPMC values; between 303 mg/l and 1755 mg/l for station 1. The 20 meter samples show remarkably lower SPMC values; between 10.89 mg/l and 187 mg/l for station 1. The tendency is the same throughout the system and the concentrations decrease the further from the outlet the measurements are taken. In the actual river, the measurements of SPMC are quite high; between 1228 mg/l and 1879 mg/l. However, no trend in change throughout the river is detected, and this indicates that the river does not receive any significant amount of sediment from other sources than the glacier.

The stationary measurements conducted during the 4th, 5th and 7th of August over the night in approximately 5 meters depth, just below the plume, show the highest detections of SPMC during slack water (figure 2). During slack water the current velocity is at a low, and hereby the settling velocity increases. Especially the measurements during low water slack show large SPMC values; respectively 210 mg/L

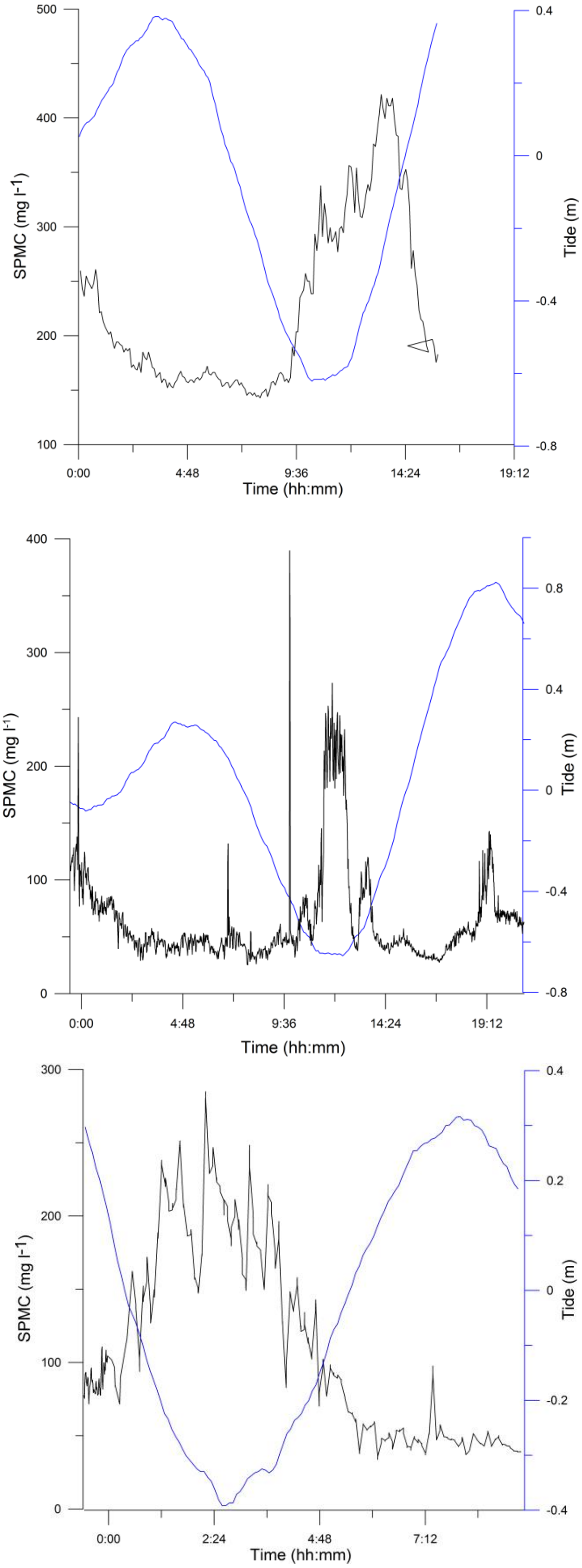

Figure 2: The top graph shows data from the 4th, the middle graph from the 5th and the bottom graph is from the 7th of August. SPMC values measured in 5 meters depth during nighttime on these dates at station 1 are shown. The measurements on the 4th and 5th of August were conducted during low water slack, and the measurements on the 7th were conducted during high water slack.

and 200mg/L larger than just before slack for the 4th and the 5th of August. The reason for the larger values during low water slack are probably due to the large amount of sediment coming from the glacial river system during ebb. In comparison the increase during high water slack is only around 50 mg/L.

Figure 2 shows that the effect of slack water on the SPMC below the plume is quite short, but it surely gives an indication that current velocity is an important factor for the settling of particles. However it cannot be seen directly from the graphs that low velocity corresponds to settling.

An increase in salinity with depth is detected, during the stationary profiling conducted on the 4th and 5th of August, see figure 3 and appendix 1. The temperature declines with depth, with the exception of the top most layers where the water is quite cold. The reason for this is probably the cold freshwater coming into the fjord from the river system. In general the temperature and salinity does not change much during the stationary profiling. A clear tendency between SPMC and mean diameter is however seen in figure 3. Mean diameter rises with a rise in SPMC. The correspondence of these two variables indicate an aggregation of the particles and hereby flocculation. The larger mean diameter size could also be due to large sand particles settling from the river, but the MALVERN 2000 results indicate a mean primary grain size of 35 µm, meaning silt, in 20 meters depth (table 2) thus the increase in mean diameter with depth at station 1 is probably caused by flocculation processes.

	1 m	20 m
Mean primary particle size (µm)	86.83	34.72
Minimum (µm)	16.53	2.81
Maximum (µm)	230.52	85.74

Table 2: Mean primary particle sizes in 1 and 20 meters depth at station 1 calculated with MALVERN 2000.

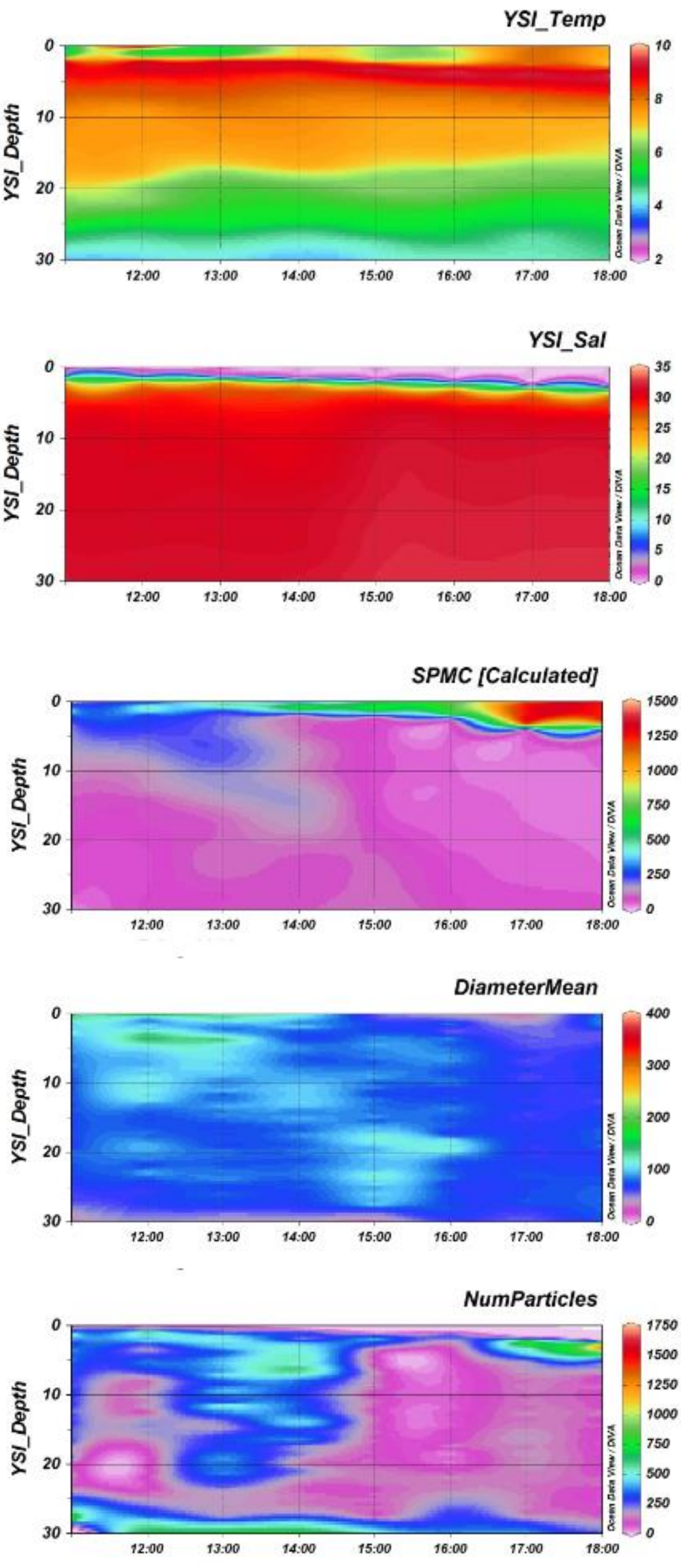

Figure 3: Stationary profiling measurements from the 5th of August, showing temperature, salinity, SPMC, mean diameter and number of particles.

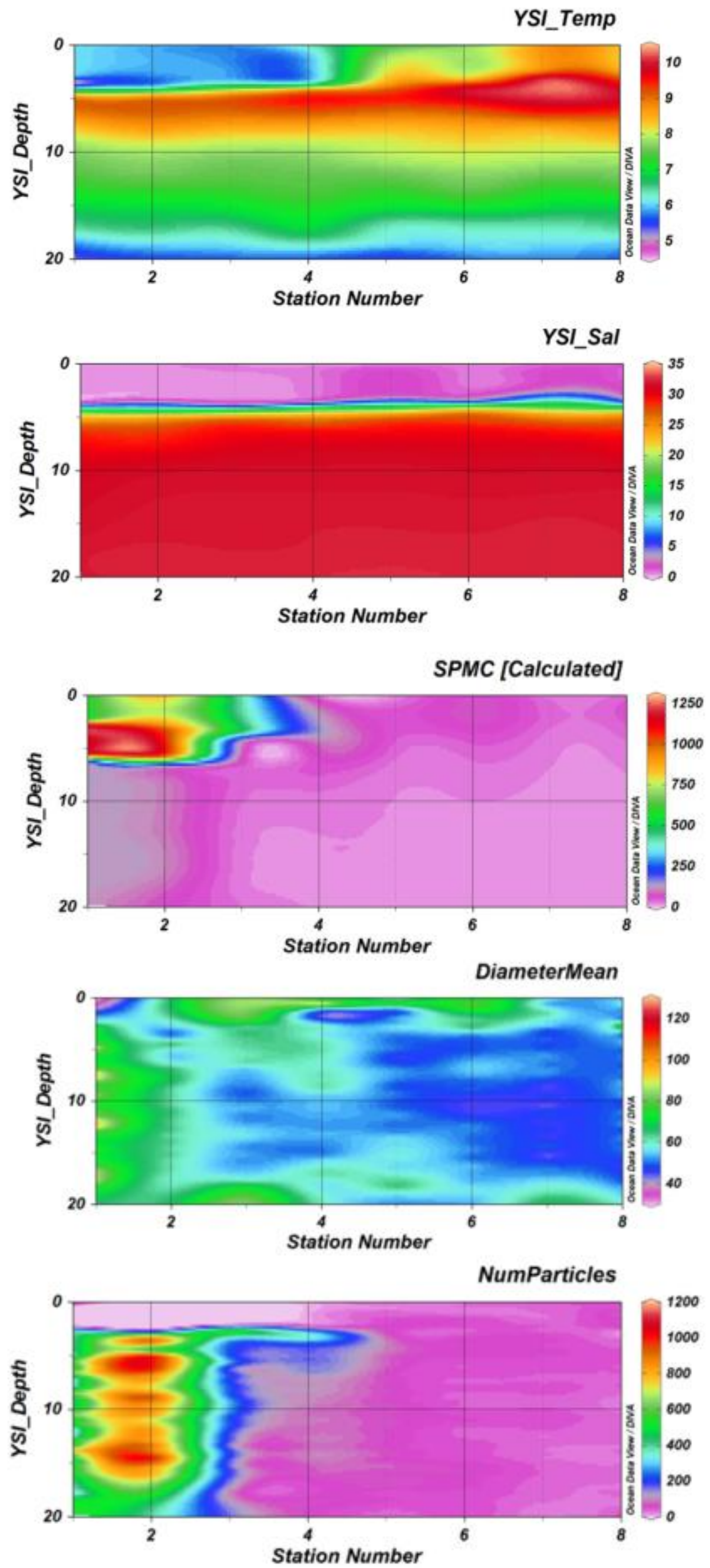

Figure 4: Transect measurements from the 7th of August, showing temperature, salinity, SPMC, mean diameter and number of particles.

On the 5th of August (figure 3), low water slack occurred at approximately 11:30 am, and it is seen from figure 3 that the SPMC starts to rise with depth from this time. Furthermore the number of particles is increasing with depth from this period too. This indicates that the particles are settling, and that the settling is caused by the low velocity at low water slack. In the same period of time, the diameter mean is increasing too, which indicates flocculation.

The results for the stationary profiles hereby indicate that flocculation is occurring, and that the processes are highly dependent on the amount of sediment available for aggregation. However the settling velocity is also increased during slack water. Since the SPMC is highly dependent on the current velocity, the amount of flocculation is also dependent on the velocity. Yet, when the current velocity becomes too high, settling is decreased, and the turbulent shear forces are increased (Pejrup & Mikkelsen, 2010).

The salinity is quite stable throughout the transect measurements, and rises with depth, but the temperature changes a little bit, probably in cause of mixing (figure 4 and appendix 2). In this way, the temperature is decreasing with depth at the part of the plume furthest away from the river outlet.

A clear tendency in SPMC throughout the transect is observed; the concentration is highest closest to the river outlet, and declines further away from the outlet. The decrease in SPMC is probably caused by settling and not because of the plume spreading; this is assumed because the mixing detected is quite little when looking at the general water properties.

As for the stationary measurements, coherence between diameter mean and SPMC can be detected. The mean diameter decreases from the outlet and outwards, indicating that the increased size close to the outlet is caused by the large amount of sediment provided by the river at the same station. Furthermore the number of particles is decreasing away from the outlet too. This does not document that flocculation is happening, but since the mean primary particle size at twenty meters depth is 35 µm at station 1, the results suggest that flocculation is occurring, and that it is happening relatively close to the outlet.

On the 7th of August (figure 4), a quite sudden decrease in concentration in the upper layers of the water column is detected between station 3 and 4. This sudden decrease in SPMC corresponds to a decline in number of particles, indicating settling from the top layers of the water column.

5. Discussion

The general pattern in the measurements between the LISST and the camera are quite equal when looking at the stationary measurements. However, the magnitude of the measurements differs between the two instruments. A general tendency is that the LISST shows mean particle values that are higher than the camera. The reason for this can be that the LISST is not able to detect the different particles if the turbidity is quite high. In this way, small particles can be detected as one bigger particle. Since the LISST only gives the measurements of a particle distribution but not the number of detected particles, this theory is hard to prove. When looking at the lower layers of the water column, the LISST also shows an overestimation of the mean particle size compared to the camera. This indicates that the turbidity is not the only factor with regards to the overestimation.

The overestimation from the LISST compared to the camera is not constant, and in this way, it is hard to correct the data between the two instruments such that they show comparable results.

In the transect measurements, the difference between the LISST and the camera are quite big. The reason for this could be the stratification of the water column, which causes Schlieren when using the LISST.

Agrawal & Pottsmith (2000) showed that when the optical transmission is less than 30%, multiple scattering effects will occur when using the LISST.

The turbidity in the top layers of the water column is really high, and in this way, the scattering effects can have an influence on the results. Since the LISST in this way has shown to be flawed, it can be argued that the camera gives the most sufficient results. In cause of this, the results shown in this study are obtained by the camera, and the LISST measurements have been omitted.

Some of the measurements in figure 3 and 4, and in appendix 1 and 2, show remarkably strange SPMC values in some areas of the top layers of the water column. The reason for these values is probably a very dense concentration that is too dense for the camera to detect correctly. By this if the concentration becomes too high; the camera has problems detecting the different particles from each other. These wrong values disseminate through the other variables, and in this way show results that are flawed by the high SPMC values. However, the results still show reasonable detections compared to the LISST, so the loss of accuracy caused by the high concentration is not as pronounced for the camera as for the LISST.

The issue of condensation when working with lens instruments in water is quite important. In this way condensation was observed for many of the measurements conducted with the camera. When interpreting the data with the MATLAB script, no caution has been brought towards the condensation issue. However, when looking at the images conducted by the camera, the amount of haloes is quite small. Only the brightest particles show sign of being affected by the condensation, so it can be argued that the overall effect of the condensation is neglectable. However since the effect of condensation is only present at the deepest depths, the measurements could be biased towards measuring larger particles at deep depths compared to higher up in the water column. The effect of this bias should be further investigated.

When plotting the results of both the stationary measurements and the transects in Ocean Data View, the DIVA interpolation type which is an advanced weighted average interpolation taking both coastline and bathymetry into account, has been used. The use of interpolation is needed, because none of the measurements are continuous. In this way, interpolation is needed in order to obtain knowledge about what is happening between measurements. The scale-length is different between the variables and measurements, but is set so that the results are coherent. However, some irregularities between the stations and time steps can be detected on some of the measurements. These irregularities caused by the interpolation needs to be taken into account when analyzing the results, but the overall tendencies between the variables are not affected by the interpolation. Therefore it is argued that the interpolated results are fulfilling the purpose of detecting the overall tendencies within the variables.

During the field campaign some sources of error have been detected. When using the winch for some of the instruments while lowering other instruments by hand at the same time, the devices are probably not in the exact same depth of the water column at the same time. However, since the difference between the measuring depths of the instruments is very little and that the data is measured continuously through a profile, the effect of this delay is neglectable.

When doing the stationary measurements, the instruments were lowered to a certain depth and held there for a given period of time. Most days, the sea was calm and therefore the boat did not move a lot with the swirl. However, in the end of the field campaign the wind increased, hence making the boat move more. This movement can be detected in the stationary measurements. The movement caused by waves is, for this campaign, very small and does not have a pronounced effect on the results.

The partcam has a video-function making it possible to film and measure settling velocity in situ. In order to get sufficient results from these measurements, the movement of the boat has to be minimal. During the campaign, a couple of films with varying lengths were conducted, but no other measurements were recorded. The settling velocity is an important parameter, as it can give an indication of how fast the flocculated particles are settling, hence making the analysis of the results more robust. Unfortunately no useful films were shot during the days with calm sea, but for future investigation on the subject, in situ measurements of the settling velocity could be important.

When doing the filtrations, it was in the beginning assumed that the sample bottles contained 1 liter of water, but the bottles held a bit more than 1 liter of water. This means that the measured concentrations for the first 78 samples are slightly off. However when filtrating the rest of the samples, the average water sample size was calculated to be 1.03 liters, which means that the concentrations for the first 78 samples are slightly overestimated. However, this overestimation is so small that it has been neglected through this study.

In general, a coherence between measurements of SPMC and the detection of a rise in mean diameter size is found in both the stationary measurements and the transect measurements. It can be argued that because the number of particles rises where the mean diameter measurements does too, this does not have to indicate flocculation. However the MALVERN results show that the mean primary particle size at the different stations is quite low. With this in mind, the coherence between SPMC, mean diameter size and number of particles suggest that flocculation is happening.

The results indicate that most of the flocculated particles settle within the first stations. Further from the outlet, the SPMC decreases quite rapidly and it is also seen that the number of particles decreases equally rapidly. This gives an indication of SPMC being an important parameter with regards to the flocculation.

The fact that a lot of the particles precipitate close to the outlet can be a problem related to the redistribution of the nutrients. Since iron and other nutrients in the sediment acts as fertilizers for phytoplankton, the quick settling decreases the availability of nutrients, thus minimizing the photosynthesis from the phytoplankton. Further investigation towards the direct effect of the settling on the primary production should be done in order to elaborate on this important issue.

From the results in Red River, it is seen that the cloudburst on the 9th of August had a huge impact on the measured concentrations in the river. Since the Glacial river system in the Disko Fjord and the Red River system are comparable, the impact of a cloudburst would probably be extensive in the Disko Fjord system too. What the exact consequences of a cloudburst would be are hard to estimate, but the SPMC in the glacial river would probably rise. This would have an influence on the plume system in general, and hereby also on the flocculation processes. Further investigation should be done regarding climate changes and the fjord dynamics in arctic fjords in order to obtain knowledge about the consequences of the occurring changes in climate.

6. Conclusions

Through this study, the effect of different variables on the flocculation processes in the Disko Fjord has been investigated. The study shows how camera measurements, supplied with CTD measurements and water samples, can give knowledge about the system and the different interactions between the oceanographic variables. The following 5 conclusions have been conducted upon finishing the study:

1. Cloudbursts have a large short term influence on the SPMC in partly glacial river systems. The effect is possibly also large in glacial river systems.
2. SPMC levels are one of the main controlling factors of the flocculation happening in the fjord. Furthermore the current velocity, and hereby also the shear stress, is an important factor as well.
3. The settling of the flocculated particles is happening primarily during slack water. Especially low water slack shows a large increase in settling.

4. Most of the flocculated particles precipitate close to the outlet, making the redistribution of nutrients sparse with regards to phytoplankton.
5. The LISST has shown to be insufficient when measuring flocculated particles compared to the partcam. Especially in waters with a high turbidity, the LISST has problems with the differentiation of the particles.

Further investigations need to be done in order to obtain knowledge about some of the specific dynamic relations between the variables. Future important studies could be of the settling velocities via in situ measurements with the partcamera, and investigations of the effect of the flocculation happening relative close to the outlet.

7. Acknowledgements

The Center for Permafrost (CENPERM) is thanked for the financially support to the conducted field course in Greenland. PhD student Thor Markussen is thanked for his help throughout the study, both with regards to tuition and for guidance in data management.

8. References

Agrawal, Y.C., Pottsmith, H.C., 2000. *Instruments for particle size and settling velocity observations in sediment transport.* Marine Geology. 168, 89 - 114.

Andrews, S., Nover, D., Schladow, S.G., 2010. *Using laser diffraction data to obtain accurate particle size distributions: the role of particle composition.* Limnol. Oceanogr: Methods. 8, 507-526

Arctic station administration. Faculty of Science, University of Copenhagen, 2014. *The landscape at the Arctic Station.*

http://arktiskstation.ku.dk/english/about/environment/the_nature/the_landscape_at_the_arctic_station/

Last visited: 20th of October 2014

Bhatia, M.P., Das, S.B., Kujawinski, E.B., Henderson, P., Burke, A., Charette, M.A., 2011. *Seasonal evolution of water contributions to discharge from a Greenland outlet glacier: Insight from a new isotope-mixing model.* Journal of Glaciology. 57, 929-941.

Dugdale, R.C., 1967. *Nutrient limitation in the sea: Dynamics, identification, and significance.* Institute of marine science, University of Alaska. 685-695.

Gilbert, R., Nielsen, N., Desloges, J.R., Rasch, M., 1998. *Contrasting glacimarine sedimentary environments of two arctic fiords on Disko, West Greenland.* Marine Geology. 147, 63–83.

Hasholt, B., 1996. *Sediment Transport in Greenland. In Erosion and Sediment Yield: Global and Regional Perspectives*, Walling DE, Webb BW (eds). Publication 236, International Association of Hydrological Sciences: Wallingford; 105–114.

Humlum, O. 2006. *Geografien*. pp 38 in Bruun, L., Kristensen, R.M., Nielsen, N., Pedersen, G.K., Pedersen, P.M. (2006). *Arktisk Station 1906-2006*. University of Copenhagen, Rhodos.

Knudsen, N.T., Yde, J.C., Gasser, G., 2007. *Suspended sediment transport in glacial meltwater during the initial quiescent phase after a major surge event at Kuannersuit Glacier, Greenland.* Danish Journal of Geography. 107, 1 – 7.

Markussen, T.N., Andersen, T.J., 2014. *Flocculation and floc break-up related to tidally induced turbulent shear in a low-turbidity, microtidal estuary.* Journal of Sea Research. 89, 1–11.

Møller, H.S., Christiansen, C., Nielsen, N., Rasch, M., 2001. *Investigation of a modern glacimarine sedimentary environment in the fjord Kuannersuit Sulluat, Disko, West Greenland.* Danish Journal of Geography. 101, 1–10.

Pejrup, M., Mikkelsen, O.A., 2010. *Factors controlling the field settling velocity of cohesive sediment in estuaries*. Estuar. Coast. Shelf Sci. 87, 177–185.

Raiswell, R., 2013. *Rusty Meltwaters*. Nature Geoscience. Vol 6, 251-252, 2013.

Sholkovitz, E.R., 1978. *The flocculation of dissolved Fe, Mn, Al, Cu, Ni, Co and Cd during estuarine mixing.* Earth and Planetary Science Letters, 41, 77-86.

Tranter, M., Brown, G.H., Hodson, A., Gurnell, A.M., Sharp, M.J., 1993. *Variations in the nitrate concentration of glacial runoff in Alpine and sub-Polar environments.* Procedings of Yokohama Symposia J2 and J5, July 1993.

Valeport Limited, 1999. *Model 801, Electromagnetic Flow Meter, Operation Manual.* Valeport Limited, Devon, UK.

Winter, C., Herbst, G., Saworski, B., Schulz, J., Zielinski, O., 2012. *A photogrammetric method for the in-situ particle size distribution of flocculated sediments: Preliminary concept and comparison to laser-diffraction methods.* MARUM, University of Breen, Germany. 1-9.

YSI, 2010. *The CastAway-CTD, with profiling and analysis software.* YSI Incorporated, printed in USA.

9. Appendix

APPENDIX I

04-08-2014

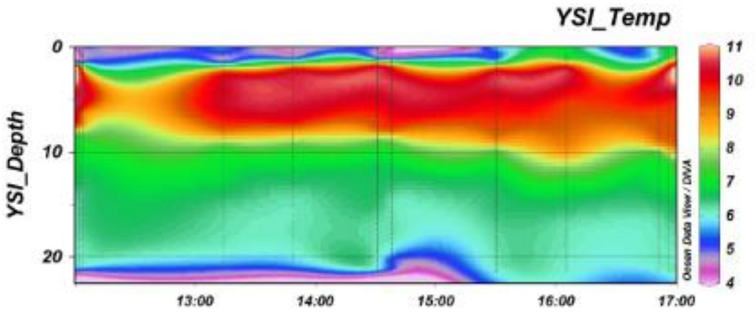

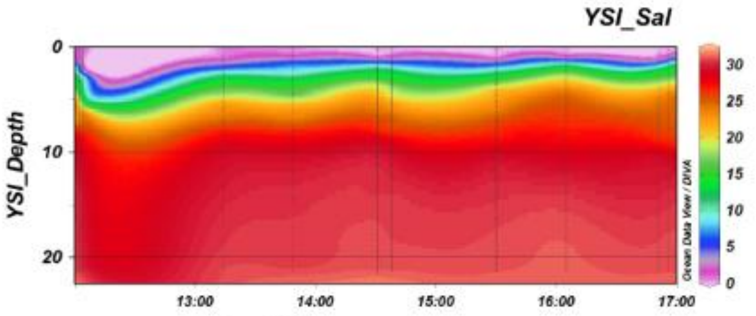

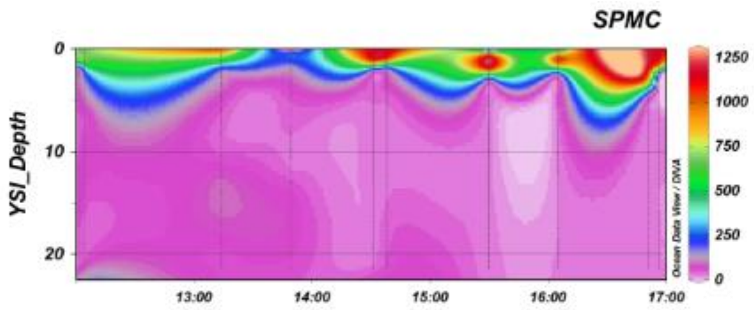

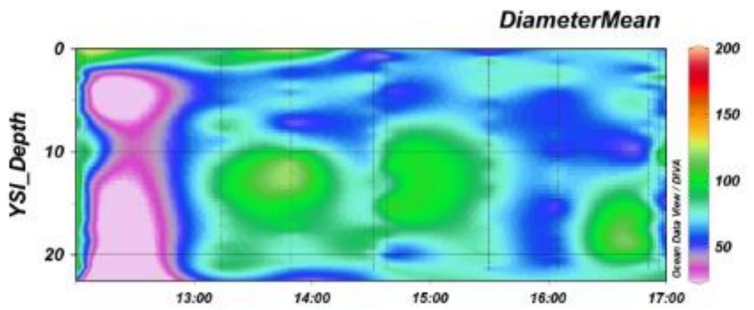

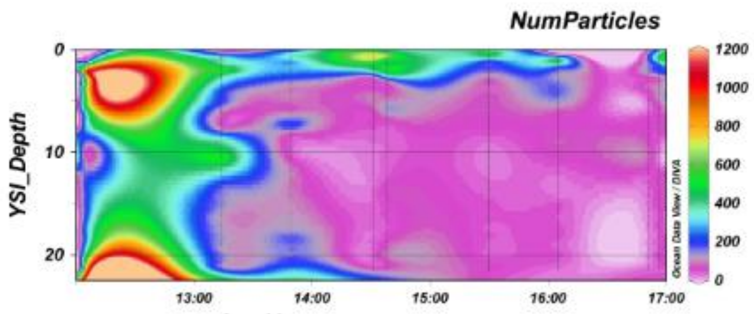

APPENDIX II

05-08-2014

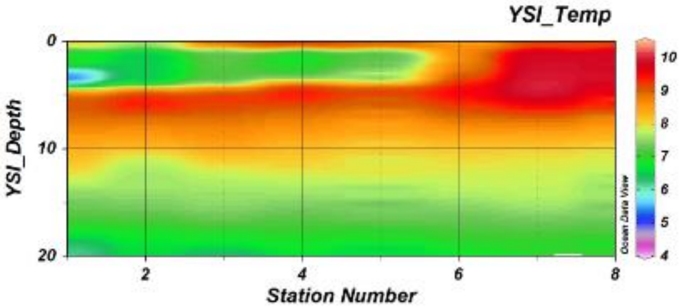

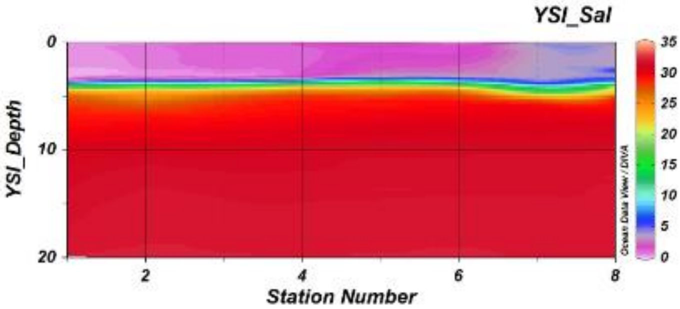

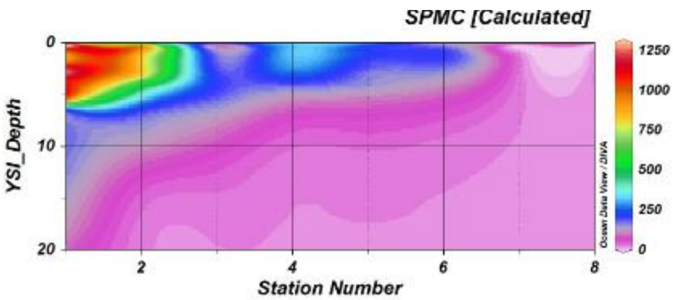

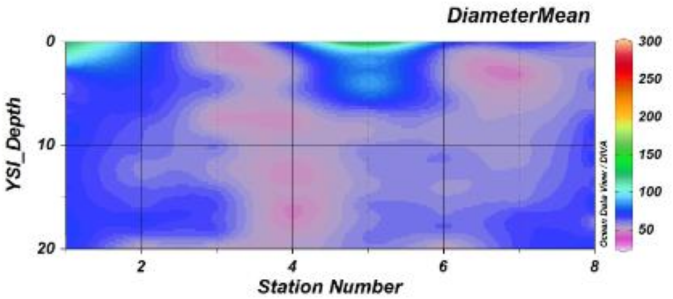

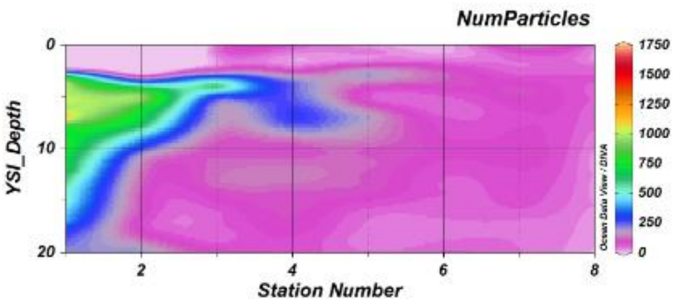

08-08-2014

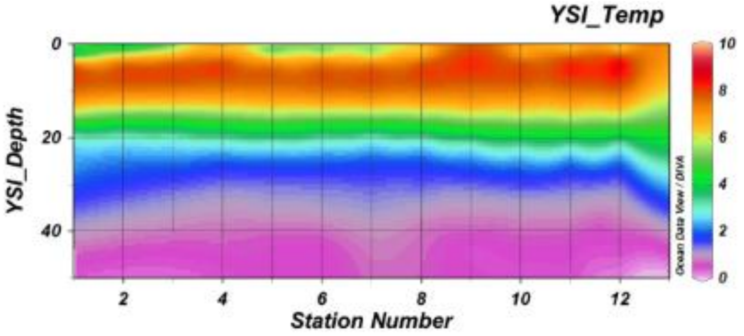
YSI_Temp
YSI_Depth
0
20
40
2
4
6
8
10
12
Station Number
Ocean Data View / DIVA
10
8
6
4
2
0

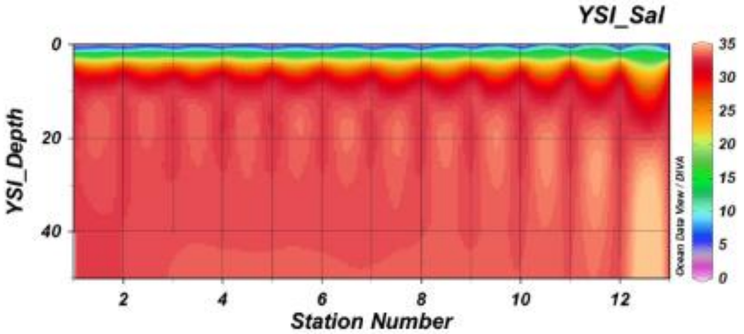
YSI_Sal
YSI_Depth
0
20
40
2
4
6
8
10
12
Station Number
Ocean Data View / DIVA
35
30
25
20
15
10
5
0

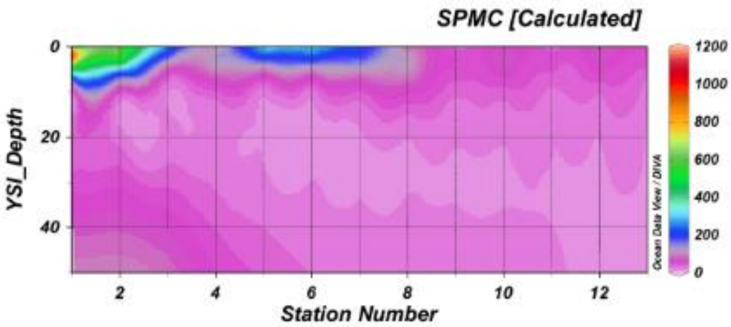
SPMC [Calculated]
YSI_Depth
0
20
40
2
4
6
8
10
12
Station Number
Ocean Data View / DIVA
1200
1000
800
600
400
200
0

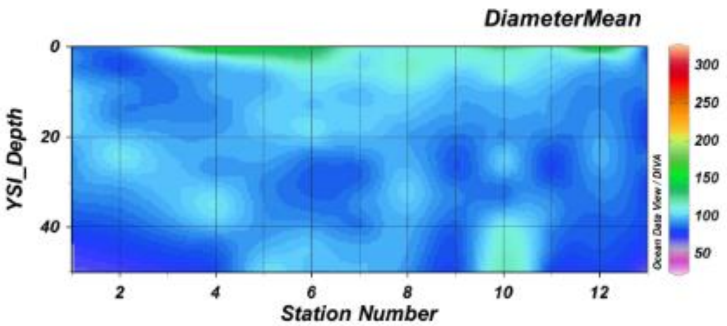
DiameterMean
YSI_Depth
0
20
40
2
4
6
8
10
12
Station Number
Ocean Data View / DIVA
300
250
200
150
100
50

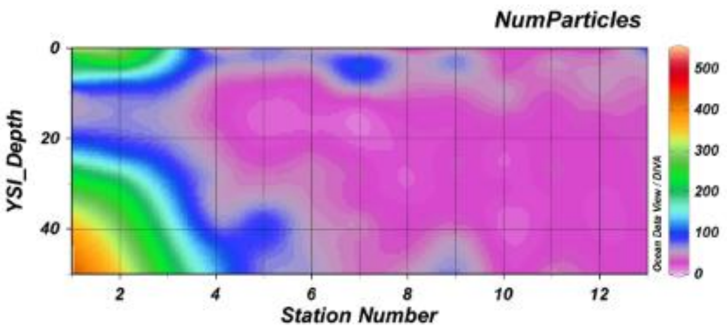
NumParticles
YSI_Depth
0
20
40
2
4
6
8
10
12
Station Number
Ocean Data View / DIVA
500
400
300
200
100
0

Edaphic factor of soils in Blæsedalen, Disko Island

A pedological study of the abiotic factors controlling the edaphic factor

Tue Mariager[1] and Ellen Lindholt Nissen[1]
[1] Cand.Scient Stud, Geography and Geoinformatics, Department of Geosciences and Natural Resource Management, University of Copenhagen

---

Abstract

Edaphic factors have been calculated based on a combination of field measurements, laboratory analysis and theoretical studies of the abiotic factors controlling the edaphic factor. The study has been conducted on 29 sample points from 6 different sites at Blæsedalen, Disko Island using the Stefan solution. Significant negative correlations were found between the water content and the edaphic factors of the soil samples (for both mineral and organic soils). Thus, the edaphic factors have been categorized into three different wetness classes (wet, saturated and moist) based on water content. The associated edaphic factors were determined to 0.029, 0.037 and 0.043 respectively, which will later be used for the active layer modeling of Disko Island.

Key words: *Stefan solution, edaphic factor, thermal conductivity, bulk density, soil moisture, organic matter content.*

Introduction

The aim of this article is to determine an edaphic factor (**E**) for Disko Island. The edaphic factor is being used in the Stefans solution to determine the thawing depth. The Stefan solution is defined as follows by Nelson (1987):

Equation 1.1

$$Z = \mathbf{E}\sqrt{\mathrm{nt} * \mathrm{PRI} * \mathrm{DDT}}$$

An edaphic factor is a term that describes one or more abiotic factors controlling soil properties. It ranges from soil texture, water content, air temperature and solar radiations influence on plant growth and is well known from plant science (Ji, Zhou and New 2009). Edaphic factors are mostly looked at separately, but Nelson (1987) has summed several abiotic factors so it is possible to have an overall soil parameter for the calculation of thawing depth as in (Zhang, Frauenfeld and Serreze, et al. 2005). The sum of abiotic factors, and hereby the edaphic factor is expressed in the following equation:

Equation 1.2

$$\boldsymbol{E} = \sqrt{\frac{2K_t}{P_b wL}}$$

Where E is the edaphic factor, K_t is the thermal conductivity, P_b is the bulk density, w is the water content and L is the latent heat of fusion (Zhang & Barry, 2006). Thermal conductivity, bulk density, soil moisture are incorporated as important parts of the Stefans solution for active layer modeling (Nelson and Outcalt 1987). Edaphic factor can also be calculated using:

Equation 1.3

$$\boldsymbol{E} = \frac{Z}{\sqrt{DDT}}$$

Where E is the edaphic factor, Z is the thawing depth and DDT is the summed degree days. The measured thawing depths and DDT of 1000[1] are used to this equation. Mathematically this gives a

[1] This value has been based on climatic data from Arctic Station.

relation were a higher edaphic factor gives a deeper thawing depth, see Figure 1. This relation does not show which soil properties that determine the edaphic factor. To do this and to achieve a more accurate edaphic factor, the results for each parameter in equation (1.2) will be presented in the following section. Furthermore the edaphic factor based on equation (1.2) will be used to perform an active layer model of Disko Island.

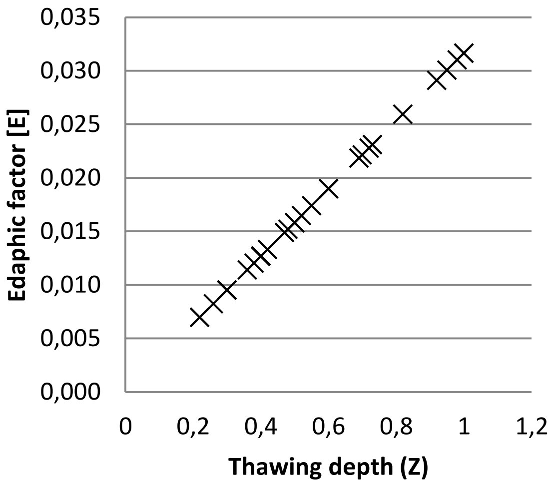

Figure 1 – Graphic illustration of the relationship between edaphic factor and thawing depth.

As mentioned, the edaphic factor is formed by Nelson (1987) and contains four elements which affect the soil; thermal conductivity, bulk density, water content and latent heat of fusion. In the following these parameters will be introduced.

Thermal conductivity is the ability of a material to conduct heat and is defined as:

$$K = -\frac{\vec{Q}}{\vec{\nabla T}}$$

Where, $\vec{Q}$ is the heat flux and T is the absolute temperature (Tritt 2004). The unit of thermal conductivity is $Wm^{-1}K^{-1}$ and a material which has a high thermal conductivity is diamonds which has a thermal conductivity at 1000 $Wm^{-1}K^{-1}$, whereas oxygen has a thermal conductivity at 0.038 $Wm^{-1}K^{-1}$. According to Tritt (2004) soils with organic matter have a thermal conductivity at 0.15-2 $Wm^{-1}K^{-1}$ and saturated soils have a thermal conductivity at 0.6-4 $Wm^{-1}K^{-1}$, at 25C.

Bulk density express how compact a soil is and is calculated by how much weight of dry soil there is per unit volume. The unit is typically g cm^{-3} and compact subsoil often have bulk densities around 2.0 g cm^{-3}, whereas less compact soils have bulk densities around 1.1 g cm^{-3} and organic soil have bulk densities around 0.3 g cm^{-3} (Breuning-Madsen and Krogh 2005). Bulk densities are shown in Table 1, according to U.S texture classes (Campbell, et al. 1994).

The **water content** in the edaphic factor equation is expressed by m^3 m^{-3} (Nelson and Outcalt 1987). The pore volume of a certain soil type determines when a soil is saturated with water. The pore volume for the U.S. texture classes is seen in Table 1. In arctic the water content in soil is highly variable through a year and is mainly controlled by precipitation, see introduction. The soils in arctic regions have limited horizontal drainage because of permafrost which leads the water into depressions and lowland areas. Furthermore, low temperatures in the arctic region results in a low amount of evaporation, also leading to an increased water content of the soils (Hinkel, paetzold, et al. 2001).

Soil type	Bulk Density g cm^{-3}	Porevolumen Θ_s (m^3m^{-3})
Sand	1,79	0,43
Loamy Sand	1,66	0,401
Sandy Loam	1,54	0,412
Silt Loam	1,43	0,486
Silt	1,55	0,46
Loam	1,43	0,434
Sandy Clay Loam	1,4	0,33
Silty Clay Loam	1,27	0,432
Clay Loam	1,31	0,39
Sandy Clay	1,32	0,321
Silty Clay	1,22	0,423
Clay	1,22	0,385
Organic soil	0,3	0,863

Table 1 - US Texture classes.

Latent heat of fusion is the required energy when a material changes phase from solid to liquid without any change in temperature of the specific matter. The unit of latent heat fusion is J kg^{-1} and the required energy to convert one kg of ice from solid to liquid mass is 333660 J kg^{-1} (Nelson, 1987). This constant is necessary in Stefans solution since the equation aims to find where solid and liquid mass interface as mentioned in the introduction chapter, *Stefans solution.*

The reference value EASE

The result of edaphic factor will be compared with edaphic factor values calculated by the National Snow and Ice Data Center (NSIDC). These values are based on remotely sensed data of the land cover types in a grid of 25x25 km (Zhang, McCreight and Barry 2012).

Method

Field work and sampling strategy

The field work for this soil survey took place between the 1st of August and the 15th of August 2014 at different sites in Blæsedalen. In total 9 sampling sites have been investigated, covering a little less than 200 sample points. For most sampling points the active layer depth, soil moisture and soil temperature have been measured, while the thermal conductivity and soil sampling only have taken place at selected sites[2]. The collected data for this soil survey will be divided into two different datasets; (**1**) addressing the soil sampling sites and (**2**) addressing the active layer depth validation. The soil sampling sites covers six different areas in Blæsedalen (see Table 2), which have been selected using a stratified random sampling method (Dinkins & Jones, 2008). Based on either knowledge of the vegetation cover from satellite images (Area 1-4) or from field trips (Cotton Grass site and Horsetail site) locations where chosen for further studies. Table 2 additionally describes the vegetation cover and landscape characterizing the different sites, while Figure 2 shows pictures from four of the sampling sites and Box 1 inform about the different vegetation types at the sites.

Common to the six sites, are as mentioned, measurements of soil moisture, soil temperature, active layer depth and soil sampling, while the thermal conductivity have only been measured for the Cotton Grass- and Horsetail site[3]. Active layer depth have additionally been measured for three other sites (CALM site, CALM site transect and Coast/land transect. The measures from these three sampling sites will be part of the validation of the active layer map in (Modelling Active Layer at Disko Island). For an overview of the spatial distribution of the sampling sites see Figure 4 in the introduction.

Thermal conductivity was measured using a KD-2 pro Thermal Properties Instrument. The instrument sends a current through a heating sensor and the instrument monitors the temperature of the sensor over time. Bias can be related to this instrument since the measured material can change during the monitoring. A really small sensor would minimize changes in the material, but would be too fragile to handle in the field **(Decagon 2014)**[4].

Sample site	Sample numbers	Thermal conductivity	Dominating vegetation	Landscape*
Area 1	1-5	No	Mixed heath vegetation	Hilly terrain
Area 2	6-10	No	Tall willow, horse tail	Steep slope
Area 3	11-15	No	Mixed vegetation	Cryoturbation
Area 4	16-20	No	Willow, mosses, horse tail	Cryoturbation
Cotton grass	21-24	Yes	Cotton Grass	Wetland
Horsetail	25-29	Yes	Horsetail	Wetland

Table 2 - An overview of the six sampling sites
*** Note that all sample sites showed evidence of cryoturbation.**

[2] The soil samples have been taken in a depth of 20-30 cm.

[3] Thermal conductivity measurements were limited due to logistical challenges.

[4] The water content has been measured using a Tetra Probe.

Figure 2 – Pictures from 4 of the sample site (A) Area 1, (B) Area 2, (C) Area 3 and (D) Cotton Grass Site.

Crowberry was very common. It is a plant that grows in heaths and bogs especially in coastal areas. In west Greenland it is seen northwards to 79°N.

Dwarf birch was also very common and is a dominating plant at heaths and fell-field areas. It was 15-20 cm tall and was creeping across the surface.

Salix - Northern willow was also a common vegetation type in Blæsedalen and it grows all over Greenland. The plant was up until one meter tall in Blæsedalen and was hereby the tallest vegetation type in the area

Clubmosses is common at heaths and fell-field sites. It is a perennial plant that is 3-30 cm tall.

Cotton grass was seen on peaty, marchy ground. It is a perennial plant that grows on wet clay or sand all over Greenland**.**

Horsetail was seen in wet areas as well. It is a plant with a very simple plant structure and it grows on moist and clayey ground in all of Greenland.

Box 1 - Main vegetation types of Disko Island (Rune 2011).

Laboratory work and analysis

The total 29 soil samples have been collected with 2 replicates (1 for wet-soil analysis and 1 for dry-soil analysis) using ring samplers. Some of the samples were dried using a microwave own at Arctic Station, while the rest have been freeze dried in the lab at IGN. The dried samples have subsequently been sieved to remove the >2mm fraction. The wet soil samples have been used for the particle size distribution analysis, while the dried samples have been used for, Total Carbon and Calcium carbonate determination.

Particles size distribution

The particle size distribution analysis has been done using a laser diffraction method, resulting in a fractioned distribution of clay, silt and sand for the soil samples. The analysis does not take organic matter into consideration and therefor there are uncertainties related to do the analysis on samples containing large amounts of organic matter[5]. The particle size distribution has been

[5] In this case three samples were excluded from the analysis (Area 1.3, Horsetail 3 and Horsetail 4). Bulk densities for these samples have later been estimated to around 1.50 g/cm^3.

used to classify the soil samples and to determine bulk densities using a bulk density calculator at pedosphere.com, based on U.S. texture triangle (see Figure 3).

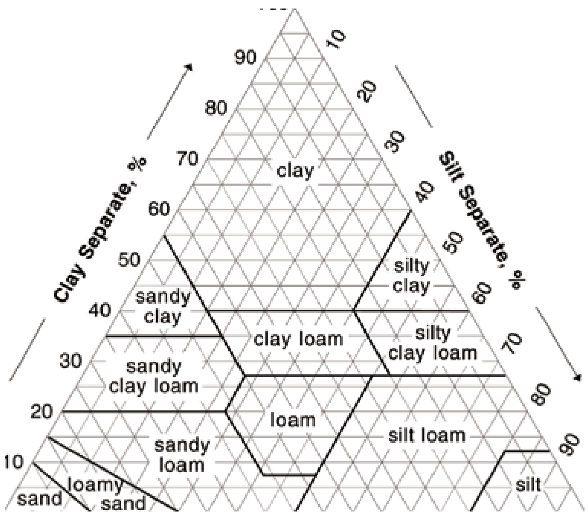

Figure 3 – U.S. texture triangle (Pedosphere.com 2014).

Bulk density and total carbon

Bulk densities have initially been determined based on ring sampling. The ring sample bulk densities have been determined using the weight of the samples and the volume of the ring ($89.3cm^{-3}$). Bulk density have also been calculated based on the distribution between humus, silicates and Calcium carbonate, called the actual bulk densities (Breuning-Madsen & Krogh, 2005). The actual bulk densities can be calculated using the following equation:

$$Actual\ bulk\ density = \frac{(1{,}3 * 2{,}65 * 2{,}8)}{(2{,}65 * 2{,}8 * X) + (1{,}3 * 2{,}8 * Y) + (1{,}3 * 2{,}65 * Z)}$$

Where X is the fraction of humus (%), Y is the fraction of silicates (%) and Z is the fraction of $CaCO_3$ (%) (Breuning-Madsen & Krogh, 2005). To determine the actual bulk density, it is necessary to know the distribution of these three components. Whether the soil samples contain Calcium Carbonate has been examined by adding a small amount of acid (HCl) to a small fraction of the soil samples.

The fraction of humus in the soil samples have been calculated by the amount of total carbon which have been analyzed by dry combustion using an Eltra CS 500 analyzer. The calculation is as follows:

$$OM = A * 1.72$$

Where A is the amount of carbon and 1.72 is the conversion factor between carbon and humus (Breuning-Madsen & Krogh, 2005). The fractions of silicates have subsequent been determined as the residual. The total carbon analysis has further been used to classify organic soil samples (OM content >10%) despite the U.S. triangle classification.

Image 1 – Ring sample.

Results and discussion

The results and discussion section will describe the different inputs to the edaphic factor calculation. Hence the structural composition will be as follows; bulk density, soil classification, thermal conductivity, water content and finally the edaphic factor.

Bulk density

As mentioned in the previous, bulk densities have been determined by three different methods (Ring sampling, actual bulk density and determination by the bulk density calculator at pedosphere.com). As illustrated in Figure 4 the bulk densities vary quite a lot among the different methods. Ring sampling is often difficult to perform due to the porosity of soil and the

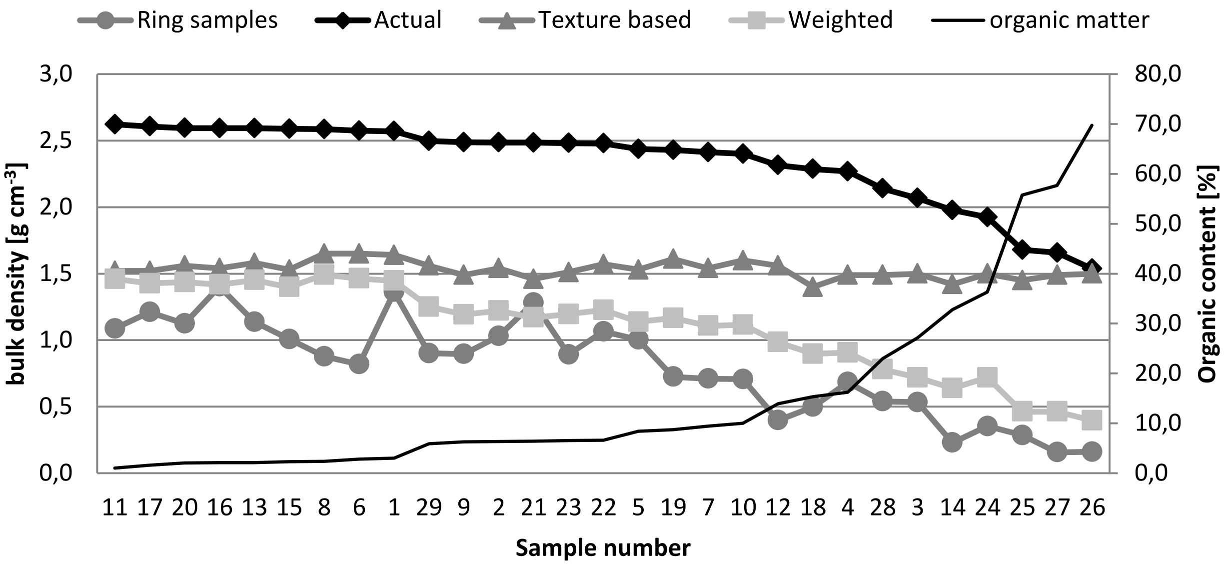

Figure 4 - Bulk density by the three different methods; actual bulk densities, ring samples and texture based + the weighted bulk densities. The samples have been plotted by increasing organic matter content illustrated with the chart of organic matter.

presence of roots and stones (McKenzie, Coughian and Cresswell 2002). The difficulty is to do a ring sample which reflect the exact conditions where nor to less or too much soil is sampled to the ring than the amount there is in the horizon for the volume of the ring, see Image 1. The bulk densities from the ring sampling might therefore be affected by some uncertainties and seems to be underestimated, though they also seem to reflect organic matter content quite well (illustrated in Figure 4), where two clusters can be located; one with high organic matter content and low bulk densities, and one with low organic matter content and higher bulk densities. The actual bulk densities on the other hand, seem to be overestimated. This method is a theoretical pendent to a pygnometer analysis of the soil samples and does not take pore volume properly into consideration (Breuning-Madsen and Krogh 2005). The actual bulk density assumes that the soil is compact, but this is not the case due to cryobatic processes in the area (White 1999). This is reflected in the high values of actual bulk density compared to the other results of bulk density (see Figure 4) As the organic matter content is included in the determination of the actual bulk density the results again reflect the organic matter content quite well.

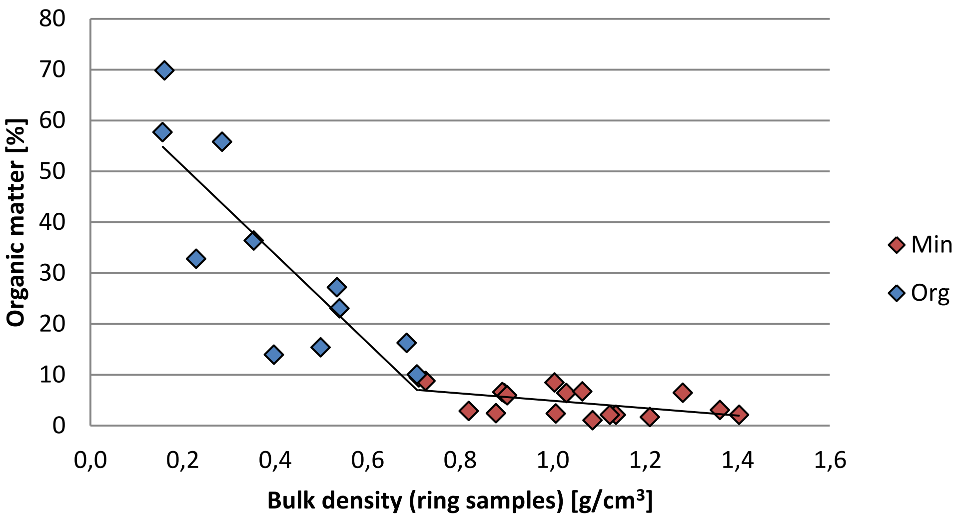

Figure 5 - Correlation between organic matter content and bulk density (ring samples) for the 29 samples, divided into organic and mineral soil samples.

The third method for bulk density determination is based on the particle size analysis. Without exception, this method presents values somewhere between the ring sampling method

and the actual bulk density method, though they seem to be higher than the results presented by (Michaelson and Ping 1996) [6]. This method does not take the organic matter into consideration and therefore the bulk densities seem unsatisfying.
To overcome the disadvantages from the described methods, a weighting of the texture based bulk density results have been performed (See Box 2).

As illustrated in Figure 4, the weighted bulk densities, except for samples 21, are within the boundaries of the ring sample- and texture based bulk density results, and therefore seem to be a nice compromise between the underestimated ring sample bulk densities and the overestimated texture based bulk densities. Instead of ranging from 0.16 - 1.40 g cm^{-3} like the ring samples or between 1.40 and 1.64 g cm^{-3} like the texture based bulk densities, the weighted bulk densities range from 0.46 – 1.49 g cm^{-3}, which correlate with the result found by (Michaelson and Ping 1996), who also argues that a high organic matter content results in a low bulk density, see Figure 5. The results are also corresponding to results found by (Elberling, et al. 2004). The clear distinction between bulk densities for mineral (subsoil) and organic (topsoil) soil samples (as illustrated in Figure 5) could indicate that a two-layer model of the thaw depth advantageously could have been implemented. This however has not been done since the bulk densities that are used for the calculation of edaphic factor have been weighted according to the organic matter. For this reason a one-layer model is evaluated to be representative in the further calculation. The weighted bulk densities are therefore trusted in order to calculate edaphic factor.

Since the classification of the soil into either mineral or organic soil is quite rough, adjustments have been conducted on the bulk densities and thermal conductivities. Based on the amounts of organic matter from the total carbon analysis and the amount of silicate soil, weighted values have been determined using the following equation (Rawls, 1983):

$$Bulk\ density/Thermal\ conductivity = \frac{100}{\left(\frac{OM}{X}\right) + \left(\frac{100 - OM}{Y}\right)}$$

Where OM is the percentile amount of organic matter, X is respectively the bulk density of OM or the associated thermal conductivity for OM with a certain water content and Y is respectively the bulk density for the mineral soil classification and the thermal conductivity for mineral soil with a certain water content. Example of the bulk density and thermal conductivity corrections (Area 1.4):

$$Bulk\ density = \frac{100}{\left(\frac{16.21}{0.30}\right) + \left(\frac{100 - 16.21}{1.49}\right)} = 0.91$$

$$Thermal\ conductivity = \frac{100}{\left(\frac{16.21}{0.26}\right) + \left(\frac{100 - 16.21}{1.39}\right)} = 0.82$$

Sample ID	OM [%]	Bulk density of OM	Bulk density of mineral soil	Weighted bulk density	Thermal conductivity mineral soil	Thermal conductivity organic soil	Weighted Thermal conductivity
A1.4	16.21	0.30	1.49	0.91	1.39	0.26	0.82

Box 2 - Correction of bulk density and thermal conductivity (Rawls, Estimating Soil Bluk Density from ParticleSize Analysis and Organic Matter Content 1983)

[6] Because of high visible organic matter content the particle size analysis have not been conducted on sample 3, 26 and 27. Therefor bulk densities in these cases have been estimated to be around 1.5 g/cm^3.

Soil classification

To determine thermal conductivities a classification of the soil samples have been necessary. The samples have been classified by two different steps; (1) classification according to the U.S. texture triangle and (2) classification according to the organic matter content. The results from the particle size analysis have been plotted in the U.S. texture triangle and thereby three different soil types have been found. Five samples were classified as sandy loam, twenty as silt loam and one as silt[7]. The distribution of the soil samples in the U.S. texture triangle have been illustrated in Figure 6. Secondly the soil samples have been classified as organic soil if the organic matter content exceeds 10%. This is the case for 11 of the 29 samples (An overview of the soil classification can be seen in Table 3).

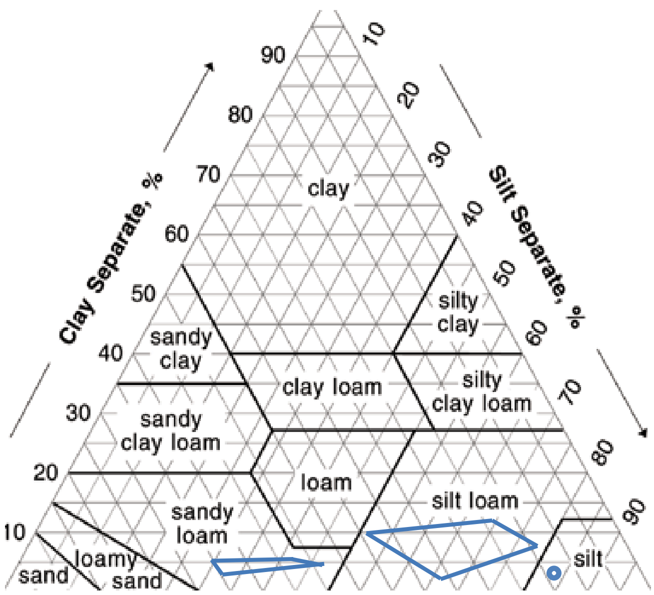

Figure 6 - U.S. texture triangle with the distribution of the bulk density of the soil samples according to pedosphere.com (illustrated with blue markings).

[7] Since the particle size analysis was not conducted on the last 3 samples, these have not been classified directly according to the U.S. texture triangle, but as the classification will later be used for the thermal conductivity, the 3 samples have been classified into silt loam.

	Classification according to U.S. texture triangle	Classification into organic soil
Sandy loam	5	0
Silt loam	20	7
Silt	1	1
no classification	3	3

Table 3 – Classification of soil samples.

Thermal conductivity

The thermal conductivity has only been measured in the field for 9 out of the 29 samples point, and it has therefor been necessary to estimate thermal conductivity values for the rest of the data points. For this purpose, the Campbell thermal conductivity excel sheet have been conducted (Campbell, et al. 1994). Based on the soil classification and the water content of the soil samples thermal conductivities have been determined as illustrated in Figure 7 (Black diamonds). These thermal conductivities clearly do not correspond to the measured thermal conductivities (Orange diamonds). The thermal conductivities for four of the silt loam soils and one of the sandy loam soils have a higher content of water than theoretically possible (Breuning-Madsen and Krogh 2005). This obviously point out that the theoretical thermal conductivities from Campbell are insufficient. This can, as for the soil classification, be explained by the lack of consideration for organic matter content in the mineral soils and the mineral content in the organic soils. To overcome this problem the thermal conductivities have been weighted based on the distribution of organic matter and mineral soil in the soil samples (See Box 2). The weighted thermal conductivity values have been plotted in Figure 7 together with the original sandy loam and organic soil curves, and four different corrections of sandy loam based on different organic matter contents[8].

[8] Note that the dashed lines have been drawn to illustrate the continued progress of the thermal conductivities.

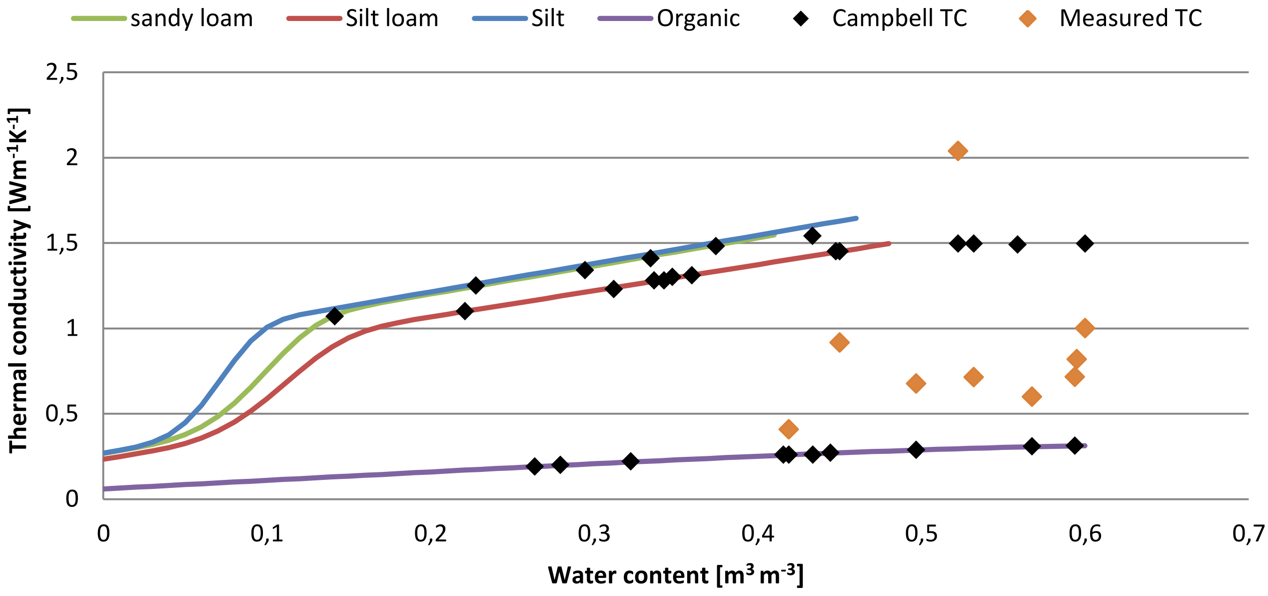

Figure 7 – Measured and estimated thermal conductivity for the soil samples together with soil specific thermal conductivity curves for the 4 classified soil types.

Subsequently to the weighting of the thermal conductivities a distinction between the organic and mineral soils still appears. The organic soils do not exceed 0.9 $Wm^{-1}K^{-1}$, while the mineral soils almost do not undergoes 0.9 $Wm^{-1}K^{-1}$. As for the bulk density determination, this once again indicates a necessity of a two layer model that distinguishes between organic topsoil and mineralogical subsoil, when processing thermal conductivity data.

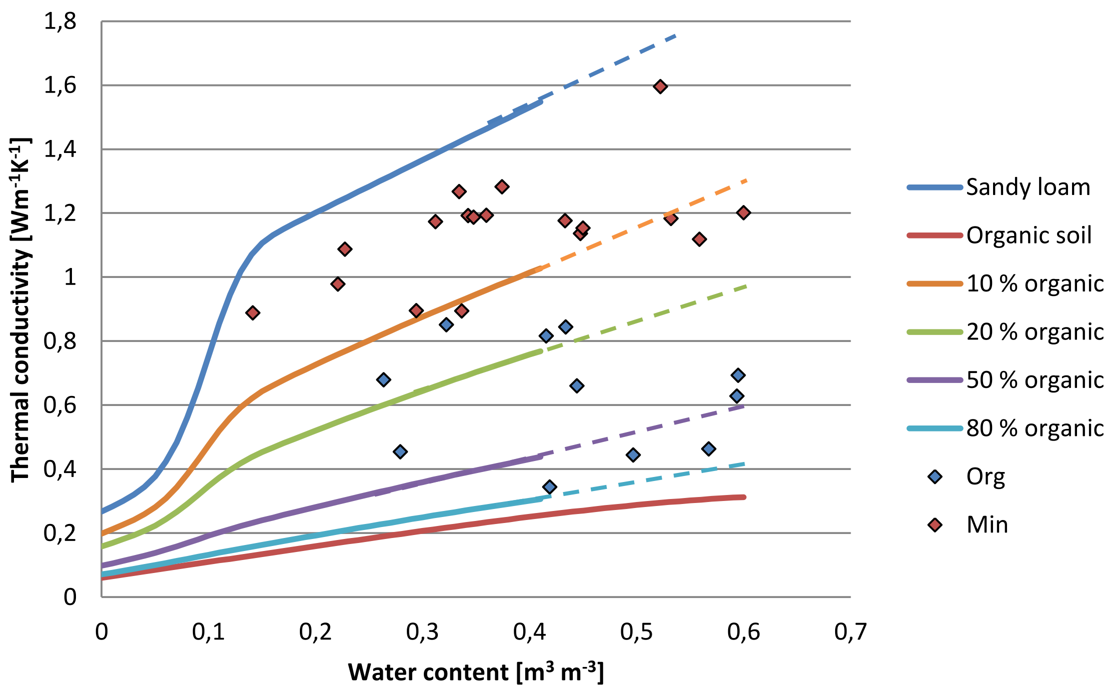

Figure 8 – Weighted thermal conductivities and corrected Sandy loam curves by organic matter content.

In Figure 8 it is shown how the organic material has an influence on the thermal conductivity. The main parts of the mineral plots are placed in between an organic function of 10% and the sandy loam function and they have a higher thermal conductivity than all of the organic samples. It should be noted that the dashed lines illustrate how it would look if thermal conductivity was calculated with a higher pore volume than 0.43 m3 m-3 for sandy loam. However the pore volume is defined to be 0.43 m^3 m^{-3} according to the US texture class, which Campbell (1994) uses to calculate thermal conductivity. As higher water content is not theoretically possible, these lines should be seen as imaginary extensions to the plots to allow the influence of organic matter content to change the water capacity. The obtained thermal conductivity values correlate quite well to the values found by Romanovsky (1997) for arctic regions in Alaska (Romanovsky and Osterkamp 1997).

A comparison of the measured thermal conductivities, the Campbell determined thermal conductivities and the weighted thermal conductivities are shown in Figure 9.

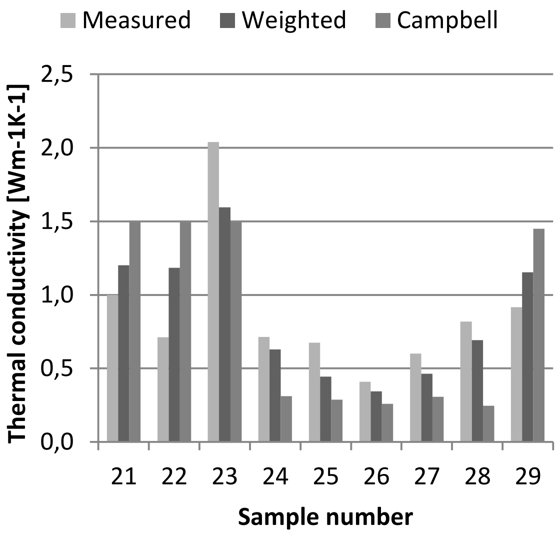

Figure 9 – Comparison between the measured, weighted and Campbell thermal conductivities.

Obviously there is no perfect fit between the measured and Campbell determined thermal conductivities. For six of the samples the measured values are higher than the Campbell values, while the opposite asserts for the three remaining samples. Based on the nine samples no clear patterns can be detected, though the organic soils (sample 24-28) clearly shows lower thermal conductivities (especially for the Campbell values). The weighting of the thermal conductivities for all nine samples seem to minimize the distance between the values and is therefore chosen in order to calculate edaphic factor.

Water content

The results of water content for the samples are shown in Figure 10. The water content ranges from 0.14 m^3 m^{-3} to 0.6 m^3 m^{-3} for the mineral soils and from 0.26 m^3 m^{-3} to 0.59 m^3 m^{-3} for organic soils, which corresponds to values found by (Elberling, et al. 2004). A significant correlation have been found between the soil moisture and OM for the mineral soils (P=0.020), while no significant correlation have been found between the soil moisture and OM for the organic soils (P=0.240). As high, medium and low water contents are found regardless of organic matter content; the water content will later be used to categorize the edaphic factor into three different moisture intervals.

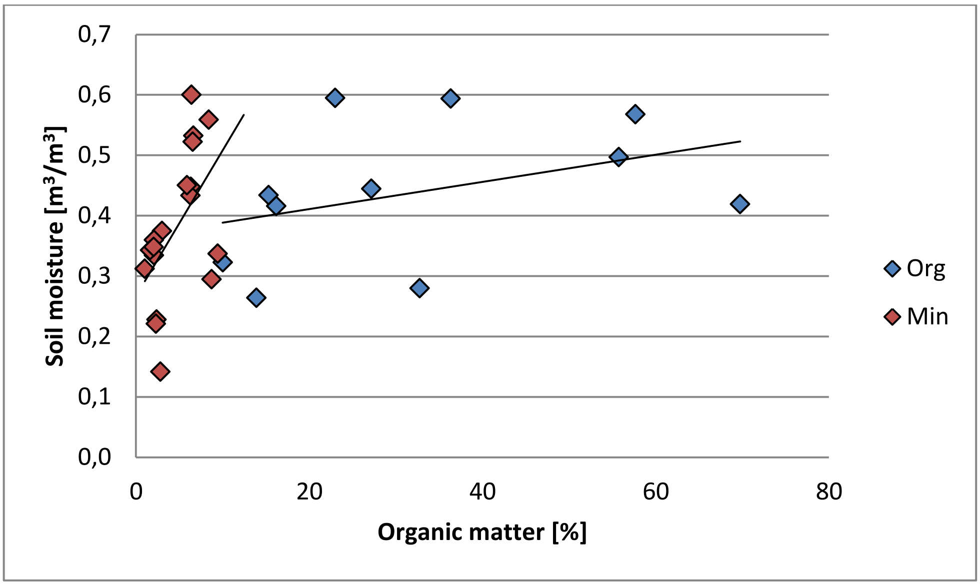

Figure 10 – Correlation between soil moisture and organic matter content for organic and mineral samples.

Edaphic factor

Thermal conductivity, bulk density and the water content have been determined in the above sections by the methods that were evaluated to give the most accurate and precise results. With these results edaphic factor has been calculated for the 29 samples points with the equation:

$$E = \sqrt{\frac{2K_t}{P_b w L}}$$

The results of edaphic factors range from 0.02 to 0.06 in the area. In order to use the edaphic factor in active layer modelling the results have been divided into three wetness classes: wet, saturated and moist. The categories with the respective water content and edaphic factors are shown in Table 4[9].

Wetness	Water content ($m^3 m^{-3}$)	Edaphic factor
Wet	>0,5	0,029
Saturated	0,3-0,5	0,037
Moist	<0,3	0,043

Table 4 – Edaphic factors by soil moisture classification.

These values are within the same range as the edaphic factors found by Zhang et.al in a Russian arctic drainage basin in 2005 (see Table 5) (Zhang, Frauenfeld and Mark, et al. 2005). The edaphic factors from the study of Zhang though seem to indicate an opposite correlation between water content and edaphic factors, than the one found in this study. This discrepancy might be due to the different subdivisions. While this study have categorized the edaphic factors entirely based on the water content, the study by Zhang et.al have categorized their edaphic factors based on landscape characteristics.

Landscape	Edaphic factor
Permanent wetland	0.064
Open and low shrublands	0.05
Barren and sparsely vegetated	0.038
Grassland	0.033

Table 5 – Edaphic factors from Russia by Zhang et al. 2005.

Figure 11 shows the relationship between the calculated edaphic factors and the three main components of Stefan solution. As illustrated in Figure 11A, a pronounced negative correlation is found between the edaphic factors and the soil moisture for both the mineral and organic soil samples. These correlations are supported by regression analysis showing a very significant

[9] The table does not show an edaphic factor for dry areas, since the in situ measurement not focused on dry areas.

correlation for the mineral soil (P>0.001) and a significant correlation for the organic soils (P=0.010). The results of these statistical tests support the conducted categorization based on water content.

For thermal conductivity (Figure 11B) the correlation pattern does not show the same uniformity. For the organic soil samples a positive correlation between the edaphic factors and thermal conductivities are found. This correlation is supported statistically to be very significant (P=0.007). On the other hand the correlation for the mineral soils is negative, indicating an increasing edaphic factor by decreasing thermal conductivity. This does not correspond to the expectation, but are neither supported statistically by the regression analysis (P=0.276).

The relationship between the edaphic factors and bulk densities are shown in Figure 11C. For both the mineral and organic soils there seem to be a positive correlation. This correlation though, is not supported statistically for the organic soils (P=0.240), but are on the other hand very significant for the mineral soils (P>0.001).

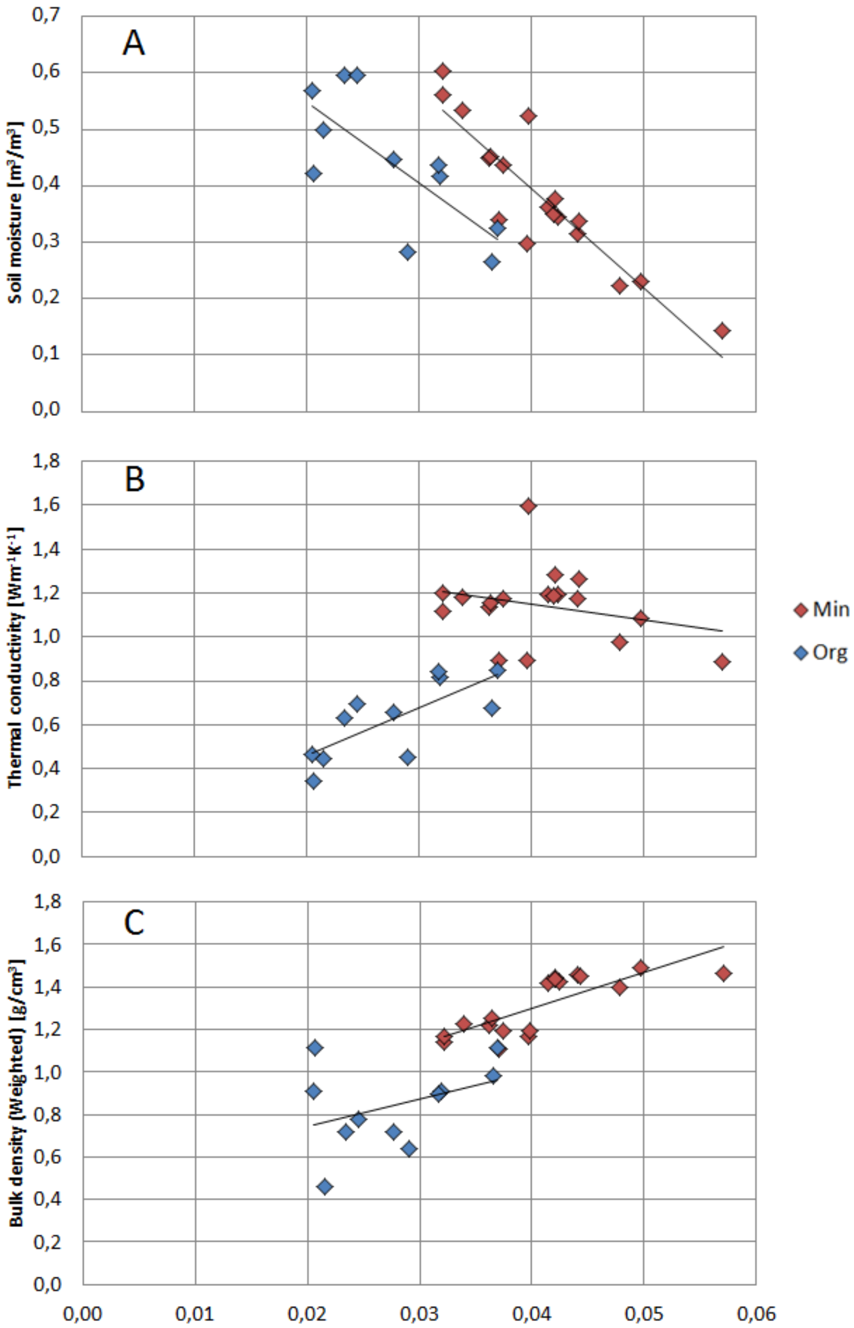

Figure 11 - Correlation between edaphic factors and soil moisture (A), thermal conductivities (B) and bulk densities (C). Black lines illustrate linear regression for the mineral and organic soil samples.

From the entire figure (A, B & C) it can be derived that the edaphic factor in general is lower for the organic soil samples than for the mineral soil samples. This once again indicates that it is necessary to distinguish between topsoil and subsoil and that it therefore could have been advantageously to perform a two layer model of the active layer depth.

As a validation of the calculated edaphic factors, a comparison between these and the EASE edaphic factors of Disko Island have been conducted (See Figure 12). Once again the calculated values seem to be within the same boundaries, though none of the calculated values ± standard deviation overlaps with the EASE edaphic factors. Undoubtedly the rough spatial distribution of the EASE grid (See Figure 13) affects the accuracy and precision of these values. But also the small scale and stratified sampling methods might have affected the calculated values. For example, the fact that the Cotton Grass site and Horsetail site were specifically chosen based on presumed high water content clearly influenced the field measurement towards wetter parts of Blæsedalen. Together with a rather small spatial distribution of the sample sites, this might question the representativeness of the field measurements. If, for example, field measurements had been conducted in dryer areas, edaphic factors closer to the EASE 1 edaphic factor, might have been found. On the other hand the EASE 2 edaphic factor compared to the edaphic factors found in this study seems to be too high. As illustrated in Figure 13, the three EASE 2 values for Disko Island are found at high latitudes in areas clearly affected by snow cover in form of glaciers and since the EASE values are calculated based on land cover data (Zhang, Frauenfeld and Mark, et al. 2005), snow can cause biases to the result. However the remotely sensed data from NSIDC is useful to validate the calculated edaphic factor.

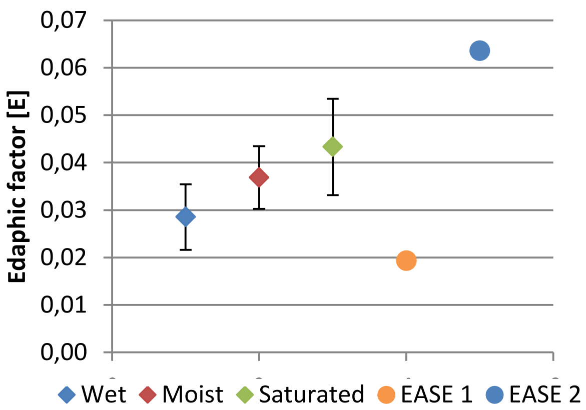

Figure 12 – Comparison between calculated edaphic factors and EASE edaphic factors.

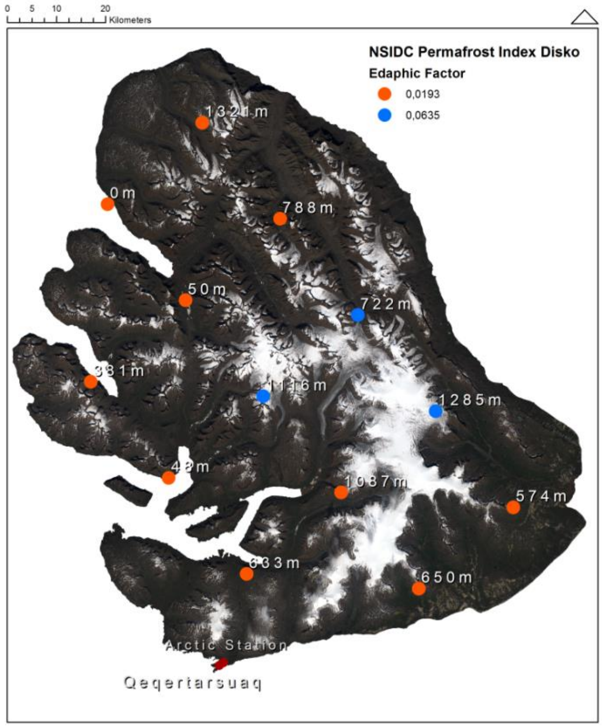

Figure 13 – EASE edaphic factors for Disko Island.

As mentioned in the introduction, the edaphic factor can also be calculated based on measured active layer depth (Z) and DDT[10]. For 27[11] of the sample point, active layer depths have been determined using an active layer probe and the related edaphic factors[12] (2) have been calculated.

These edaphic factors have been plotted against the calculated edaphic factors (1) in Figure 14. From the 1:1 line it can be drawn that the calculated edaphic factors overall are higher than the edaphic factors (2). This discrepancy is expected since the edaphic factors (2) are done during the thawing season and the calculated edaphic factors (1) calculate the maximum thaw depth (which obviously will be at the end of the thawing season). Furthermore there is a risk of hitting stones instead of permafrost during the active layer measurement, in which cases Z will be incorrect and thereby affect the edaphic factors (2) to be higher than they are. It has statistically been tested whether the plotted data correlates significantly.

---

[10] In the following named – edaphic factor (2)

11 An active layer depth has not been determined for sample 12 and 17, as a result of stones in the soil.

[12] In the following named - edaphic factor (1)

This was not the case for the neither the organic soils (P=0.434) or mineral soils, though the edaphic factors for the mineral soils showed a tendency towards a positive correlation (P=0.054). Another reason could be if the collected samples to the study had an extraordinary short depth towards the permafrost, and hereby not represented the total area of Blæsedalen.

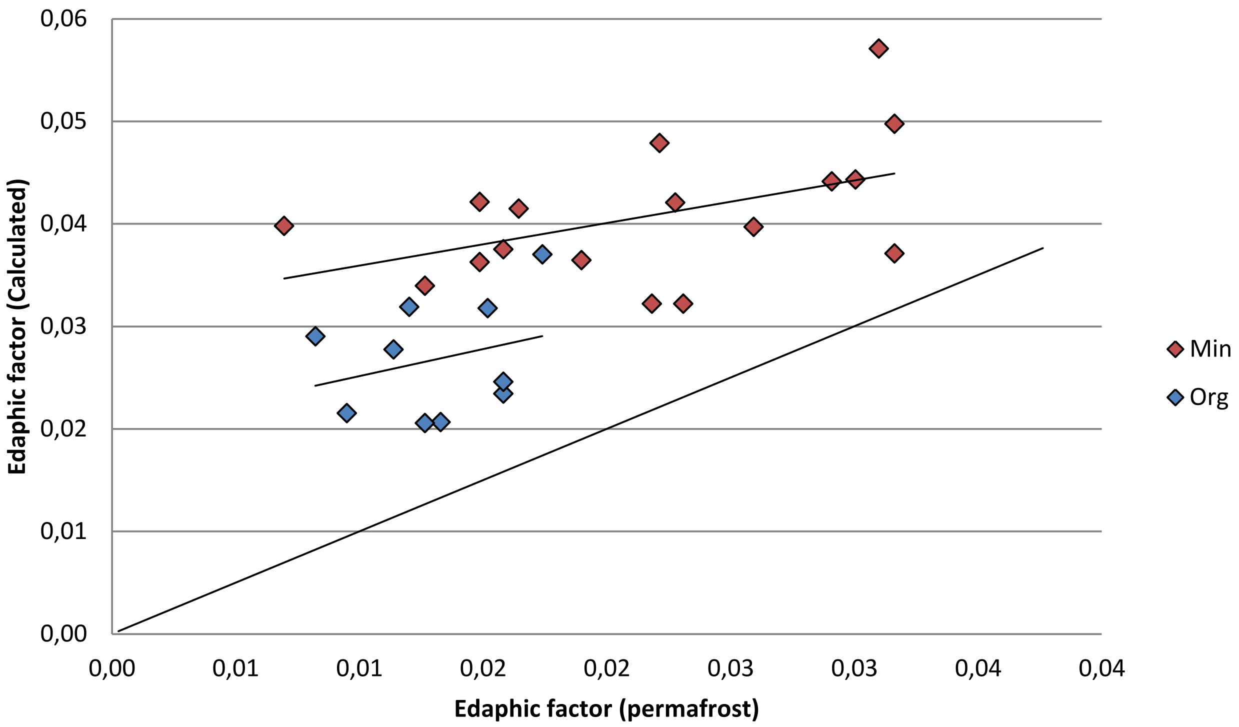

Figure 14 – Correlation between calculated edaphic factors and permafrost edaphic factors + a 1:1 line.

Conclusion

Edaphic factors for three different wetness classes have been determined based on 29 sample point throughout 6 sites at Blæsedalen, Disko Island. For wet soils (w > 0.5 m^3/m^3) the edaphic factor have been calculated to 0.029, for saturated soils (w = 0.3-0.5) the edaphic factor have been calculated to 0.037 and for moist soils (w < 0.3) the edaphic factor have been calculated to 0.043. The edaphic factors have been calculated using the Stefan solution, which summarize abiotic factors such as bulk density, thermal conductivity and soil moisture into a single number. The results of water content and weighted bulk density are accepted to be at a precise and accurate level, whereas the results of thermal conductivity were difficult to measure and validate. However the results of edaphic factor is evaluated to be reliable, compared with (Zhang et al, 2005) and Ease values from NDCSI. Furthermore it can be concluded that organic material has a major impact on the soil properties and that feature studies therefor might have to consider a two layer modeling of the active layer depth. All abiotic factors determined in this study, seemed to differ between the mineral and organic soils, except for the water content.

Bibliography

Nelson, Frederick E, and Samuel I Outcalt. "A Computational Method for Prediction and Regionalization of Permafrost." *Alpine and Arctic Reseach*, 1987: 279-288.

Breuning-Madsen, Henrik, and Lars Krogh. *Kompendium i jordbundsgeografi.* Copenhagen: Geografisk insistitut, Københavns Universitet, 2005.

Campbell, G. S., J. D. Jungbauer, W. R. Bidlake, and R. D. Hugerford. "Predicting the effect of temperature on soil thermal." (Soil science) 1994.

Decagon. *KD2 Thermal Properties Analyzer, operator's manual.* Pullman: Decagon Devices, 2014.

Elberling, Bo, Bjarne H. Jakobsen, Jens Søndergaard, and Charlotte Sigsgaard. "Influence of Vegetation, Temperature, and Water Content on Soil Carbon Distribution and Mineralization in four High Arctic Soils." (Arctic, Anartic and Alpine Research) 36, no. 4 (2004).

engeeringtoolbox. n.d. http://www.engineeringtoolbox.com/thermal-conductivity-d_429.html (accessed 10 29, 2014).

Hinkel, K. M., and F. E. Nelson. "Spatial and temporal patterns of active layer thickness at Circumpolar Active Layer Monitoring (CALM) sites in northern Alaska, 1995–2000." *Journal of Geophysical Research: Atmospheres*, 2003: 9-13.

Hinkel, K. M., F. paetzold, Frederick E. Nelson, and J. G. Bockheim. "Patterns of soil temperature and moisture in the active layer and upper permafrost at Barrow, Alaska: 1993–1999." *Global and Planetary Change*, 2001: 293–309.

Hinzman , L. D., D. L. Kane, R. E. Gieck, and K. R. Everett. "Hydrologic and thermal properties of the active layer in the Alaskan Arctic." (Elsevier Science) 1990.

Hudson, Berman D. "Soil organic matter and water capacity." *Journal of Soil and Water Conservation*, 1994: 189-194.

Ji, Yehe, Guangsheng Zhou, and Thomas New. "Abiotic Factors Influencing the Distribution of Vegetation in Coastal Estuary of the Liaohe Delta, Northeast China." *Estuaries and Coasts*, 2009: 937-942.

McKenzie, Neil, Kep Coughian, and Hamish Cresswell. *Soil physical meassurement and interpretation for land evaluation.* Collingwood: CSIRO, 2002.

Michaelson, G. J., and C. L. Ping. "Carbon Storage and Distributionn Tundra Soils of Arctic Alaska, U.S.A." *Arctic and Alpine Research*, 1996: 414-424.

Nelson, Frederick E., N. I. Shiklomanov, G. R. Mueller, K. M. Hinkel, D. A. Walker, and J. G. Bockheim. *Estimating Active-Layer Thickness over a Large Region: Kuparuk River Basin, Alaska, U.S.A.* Colorado: INSTAAR, University of Colorado, 1997.

Pedosphere.com. *Soil Bulk Density Calculator (U.S. Texture Triangle).* 2014. http://www.pedosphere.com/resources/bulkdensity/triangle_us.cfm (accessed october 24, 2014).

Rawls, Walter J. "Estimating Soil Bluk Density from ParticleSize Analysis and Organic Matter Content." *Soil Science*, 1983: 123-125.

Rawls, Walter J. "ESTIMATING SOIL BULK DENSITY FROM PARTICLE SIZE ANALYSIS AND ORGANIC MATTER CONTENT." *Soil Science*, 1983: 123-125.

Romanovsky, Vladimir E., and T. E. Osterkamp. "Thawing of the Active Layer on the Coastal Plain of the Alaskan Arctic." *Permafrost and Periglacial Processes*, 1997: 1-22.

Rune, Flemming. *Wild flowers of Greenland.* Gyldenlund, 2011.

Sochan, A., A. Bieganowski, M. Ry¿ak, R. Dobrowolski, and P. Bartmiñski. "Comparison of soil texture determined by two dispersion units of Mastersizer 2000." *International agrophysics*, 2011: 99-102.

Tritt, Terry M. *Thermal conductivity Theory, Properties and Applications.* New york: Plenum, 2004.

White, Thomas Leslie . "Soil microstructure and the thermodynamic behaviour of permafrost affected soils." In *Advances in Cold-Region Thermal Engineering and Sciences*, by Kolumban Hutter, Yongqi Wang and Hans Beer, 519-532. Damstadt: Springer, 1999.

Zhang, T., J. McCreight, and R. G. Barry. *Arctic EASE-Grid freeze and thaw depths, 1901 - 2002.* Boulder, Chicago: Natonal Snow and Ice Data Center, 2012.

Zhang, Tingjun, and Richard Armstrong. *NSIDC.* Vers. 2. National Snow and Ice Data Center. 2003. http://nsidc.org/data/ggd641 (accessed 10 23, 2014).

Zhang, Tingjun, et al. "Spatial and temporal variability in active layer thickness over the Russian Arctic drainage basin." *Journal of Geophysical Research: Atmospheres*, 2005: 1-14.

Zhang, Tingjun, et al. "Spatial and temporal variability in active layer thickness over the Russian Arctic drainage basin." (Journal of geophysical Research) 110, no. D16 (2005).

Østerby, Ole. *Analysis of nummerical solution of the stefan problem.* Århus: Institute of mathematics, 1974.

Nt-factor for Disko Island based on NDVI

Andreas Hvam Hoffmann[1], Andreas Elmelund Hass[1]

[1] Cand.Scient Stud, Geography and Geoinformatics, Department of Geosciences and Natural Resource Management, University of Copenhagen

Abstract

Vegetation is an important parameter when determining the thaw depths in the permafrost environments. In relation to the estimations of thaw depth over the area of Disko Island, this study aims to account for the nt- factor based on Normalized Difference Vegetation Index (NDVI) estimations, as well as the relationship between these two parameters and correspondence to the in-situ measurements. NDVI values were calculated from remotely sensed data of Landsat-8 that possesses a spatial resolution of 30x30 and bit depth of 2^{16}*, as well as WorldView scene with a resolution of (2x2m) and resembling bit depth. The estimations have shown that the highest NDVI values were concentrated in low-lying valleys, on south-facing slopes and along the coast, which can be explained by close reliance on the temperatures and solar radiation. Subsequently, nt factor – a ratio of ground surface and air temperatures, was derived from NDVI values through established correlation. It has been found that nt patterns are strongly influenced by surface energy balance. However, when validating the results with in-situ measurements, correspondence was very week, mainly due to the number and location of in-situ observations and continuous temperature gradient established for other geographical location in Greenland.*

Key words: *Stefan solution, nt, NDVI, remote sensing,*

Introduction

In arctic environments vegetation constitute an important variable in determining *thaw depths* (Hollesen 2011). Even though the growing season is short and the biomass is sparse relative to more temperate regions, it still has significant influence on the subsurface. An understanding of arctic vegetation is therefore essential in assessing the depths to which layers of soil is said to be active. Stefan's solution, which is a measure of the thickness of the active layer, is given by:

Equation 1.1

$$Z = E\,x\,\sqrt{\boldsymbol{nt}\,x\,PRI\,x\,DDT}$$

Of these different components, vegetation is included in the *E* and *nt* of the equation. While we will not get into details with the *Edaphic factor* (*E*) for now, we will certainly have a look at *nt*. The edaphic factor only relate to vegetation as a proxy of the degree of wetness of different soils. The other component, *nt,* on the other hand is more directly related to vegetation as it, by detours, can be estimated by utilizing plant interaction with electromagnetic radiation. The theoretical value of *nt* though is known as *n-factor* and it actually covers a dimensionless ratio of ground-surface- and air temperatures (Nelson, et al. 1997):

Equation 1.2

$$nt = \frac{T_s}{T_a}$$

In 2008 Raynolds, et. al found a significant correlation between Summer Warmth Index (SWI) and the Normalized Difference Vegetation Index (NDVI) using satellite imagery for the entire Arctic region (Raynolds, et al. 2008). This eventually formed the basis of comparing the ratio of ground-surface- and air temperatures, the n-factor, with NDVI as done by (Westermann, et al. 2014). Plotting these two variables against each other found the following dependency (Se also Figure 1):

Equation 1.3

$$nt = 2.42\,x\,NDVI^2 - 3.01\,x\,NDVI + 1.54$$

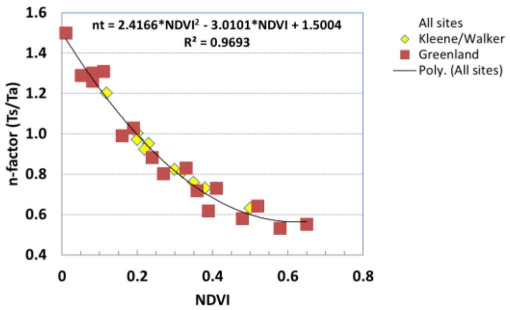

Figure 1 - Correlation between the n-factor and NDVI (Westermann et al., 2014)

The use of indices, such as the mentioned NDVI, has long been applied to remotely sensed data to describe vegetative state. Vegetation indices offer ratio-based (dimensionless), radiometric measures that indicate relative abundance and activity of green vegetation. Most of these indices make use of the inverse relationship between the reflectance in the red (620-750 nm) and near-infrared (750-1400nm) part of the light spectrum and so does NDVI (Jensen 2014)

Data

As we are interested in thaw depths of both the Qeqertarsuaq area and ultimately the whole of Disko Island, remotely sensed data will in this respect be used as a scaling agent that complements the exact but time-consuming ground observations that most often result in a limited areal produce.

Two different satellite sources will be used for the estimation of the n-factor. One will be freely available Landsat-8 images that hold a spatial resolution of 30x30m and a bit depth of 2^{16}. The other, a WorldView scene, has much better spatial resolution (2x2m) and similar bit depth, but covers only a fraction of Disko Island, more precisely the area around Qeqertarsuaq. The coverage of the images is illustrated in Figure 2.

Common for these satellite products, is a band designation, which covers similar wavelengths including visible, near- and mid-infrared. This ensures that an n-factor based on NDVI can be estimated for both images.

World View 2 - RGB Scene 2x2 meters resolution

Landsat 8 - RGB Scene 30x30 meters resolution

Figure 2 - Coverage of Landsat and WorldView scene

Theory & Methods

Normalized Difference Vegetation Index

One of the most widely used vegetative indices is the previously mentioned Normalized Difference Vegetation Index (NDVI). By ratioing the difference of the red and infrared reflectance over their sum it is possible to adjust for multiplicative noise such as sun illumination differences, cloud shadows etc.; this is known as the normalized difference.

In practice the purpose of NDVI (and most other indices) is simply to analyze whether a pixel contains healthy green vegetation or not (relative biomass). For this, the inverse relationship between the red and near-infrared reflectance is used. In a healthy plant, chlorophyll-a strongly absorbs solar energy in red wavelengths, while the near-infrared will be strongly reflected (mainly due to heat compensating in photosynthesizing structures). But a plant is not a being of equilibrium, meaning that their life cycle changes with season, weather, and access to nutrients. During periods of stress (senescence for example) the chlorophyll production decreases and the properties of this absorbance/reflectance ratio will be altered. This divergence is used in the following expression to determine the NDVI (Jensen 2014):

Equation 1.4

$$NDVI = \frac{(NIR-RED)}{(NIR+RED)}$$

NDVI has a range limited to a value from -1 to 1. Vegetated areas will always yield positive NDVI values due to higher near-infrared reflectance than the lower red reflectance. Similarly as the amount of green vegetation increases in a pixel, the NDVI value can increase up to nearly 1. In contrast, bare soils and rocks generally show quite similar reflective patterns in the red and near-infrared, generating positive but often much lower NDVI values closer to 0. Pixels dominated by the presence of water, this could be in the form of lakes, clouds and snow often have higher reflectance in the red than the near-infrared causing the NDVI values to be negative (Smith 2000). According to Raynolds et al. (2008), average NDVI values in the Arctic lie within a range of 0.32, far less than the upper boundary of the index. This is due to a relatively sparse plant cover and patchy distribution. The main force of the NDVI ratioing is that it reduces multiplicative noise, but the index is actually quite sensitive to canopy background, especially in areas with sparse vegetation (Jensen 2014). Here, it could be an idea to look at similar indices that adjust for soil interference (see Box 1), but for now we will not investigate this further as the n-factor dependency has been found to relate to NDVI.

As mentioned, NDVI is sensitive to internal noise, which relate foremost to the visibility of canopy background. By including a soil adjustment factor the influence of these falsely biased pixels can be minimized. The Soil Adjusted Vegetation Index (SAVI) is such a product:

$$SAVI = \frac{(1+L)(NIR - RED)}{(NIR + RED + L)}$$

As seen, the expression covers the same bands used for the NDVI, but included is also a soil adjustment factor, known as *L*. This factor should according to Huete (1988) account for the differential red and near-infrared scatter and extinction through the canopy. This factor is often regarded as a constant of 0.5 but could just as well be continuous according to locality etc. The value of 0.5 has though been found to generally minimizing soil brightness variations best (Jensen, 2013).

Box 1 - Soil Adjusted Vegetation Index (SAVI) (Huete 1988)

As estimation of NDVI have shown to be a quite robust indicator of vegetation health – or a relative measure of primary production - it can safely be scaled over vast geographies with the use of satellite imagery. The NDVI of Disko Island based on Landsat is shown below with a draped hillshade (See Figure 3). It is clear how greenness is affected by terrain as the highest NDVI values are concentrated in low-lying valleys, on south-facing slopes and along the coast. This is an artifact of the main climatic constraints to net primary production in the Arctic; temperature and radiation (Bonan 2009). As seen in Figure 3, incident radiation is dominant at south-facing slopes, but temperature gradients inland as well as with height plays just as significant role for the distribution of relative greenness.

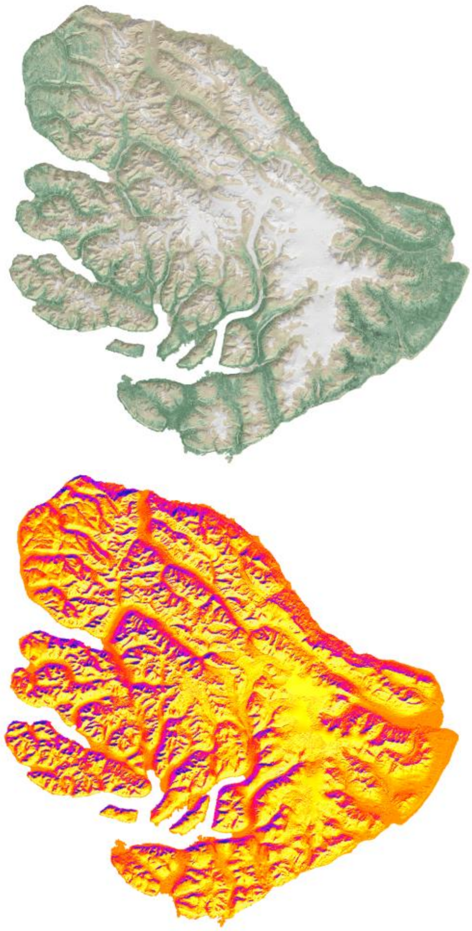

Figure 3 - NDVI of Disko Island with a draped hillshade. On the right is a Potential Radiation Index (PRI) and temperature gradients in height, Tz, and in land, Tc.

Where Raynolds et al. (2008) found average NDVI values of 0.32 in the Arctic the average for Disko Island is only 0.13 (even with negative values ignored). A dominance of rocky surfaces must contribute to a significant lowering of averaged NDVI. According to USGS (U.S. Geological Survey), sparse vegetation such as Arctic shrubs most often result in moderate NDVI values, approx. 0.2 to_0.5 (Brown 2011) In-situ measurements of NDVI (using handheld SKYE NDVI sensor) in the valley of "*Blæsedalen"* near the Qeqertarsuaq settlement in general showed a tendency towards higher values (0.4 in average) - and thereby greening. This corresponds well to above mentioned climatic constraints to primary production. Consequently, in-situ measures will mostly represent places of similar topography, biome and aspect.

Figure 4 – Ground observations of NDVI at Blæsedalen.

Illustrated in Figure 4 is the GPS located ground observations (red dots) of NDVI and other variables related to the soil/surface interface. Underneath these is a NDVI cover based on Landsat and WorldView imagery respectively - with an extent approximating the field study area.

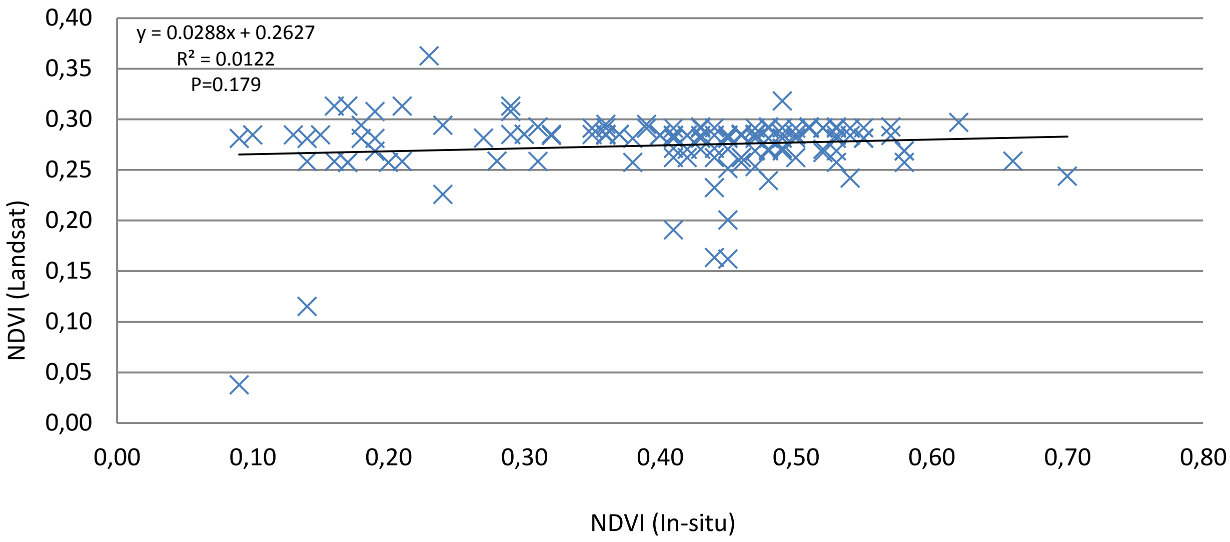

Figure 5 – Landsat derived NDVI plotted against in-situ measurements of NDVI. Note the poor correlation given by high p-value.

We will not linger too much on these measures; only note that within this extent especially Landsat derived NDVI deviates from in-situ measurements – look at the poor correlation of Figure 5. As the homogeneity/heterogeneity of pixel values are mainly controlled by spatial resolution, smaller pixel units will undoubtedly lead to more accurate estimations especially in relation to in-situ measurements. Conversely, less spatial resolute images will be more generalized as every pixel potentially includes several biomes. In the further study, this will be a key issue as our used data material will be of varying spatial quality. It will therefore require some kind of balancing between resolution, accuracy and geographic cover for optimal use. In general it seems that Landsat underestimates and WorldView slightly overestimates relative to ground observations.

The n-factor

According to Riseborough (2003) ground surface- and air temperatures is a key parameter in the thermal regime of both active layer and permafrost (Riseborough 2003). While ground surface temperatures can be measured from space in vast geographies, the other variable of the original *nt* equation (1.2), air temperatures, is a bit more tricky to estimate to a similar extent. Air temperatures above ground surface (2m) are usually measured by climatological stations, which are most often spatially sparse, and therefore provide just as sparse spatial information on these temperatures. While there are several climatological stations on Disko, these would still not be sufficient to estimate a proper temperature range of the whole island; they are mostly located in the south, too clustered and further, simple interpolation methods would not take account for the topography. Ways to circumvent the need for air temperatures would therefore improve the extent to which analysis can be performed without losing too much reliability.

Analysis

With our knowledge on the n-factor and its relation to NDVI we can calculate one of the missing variables in estimating thaw depths on a pixel-by-pixel basis covering the whole of Disko Island. The procedure is quite straight-forward and only requires a simple expression (equation 1.3) in a spatial analyst environment with the only input being the NDVI. Some preprocessing of NDVI is though needed. As thermal regimes are a predominantly land measurable entity, the range of negative values is not of interest as these mainly cover surfaces of either liquid or frozen water. Therefore, these values have been excluded in the further processing, which result in the following *nt* of Disko Island (see Figure 6). Glaciers, rivers and other waterbodies appear without data – additionally a valuable mask for further analysis of thaw depths.

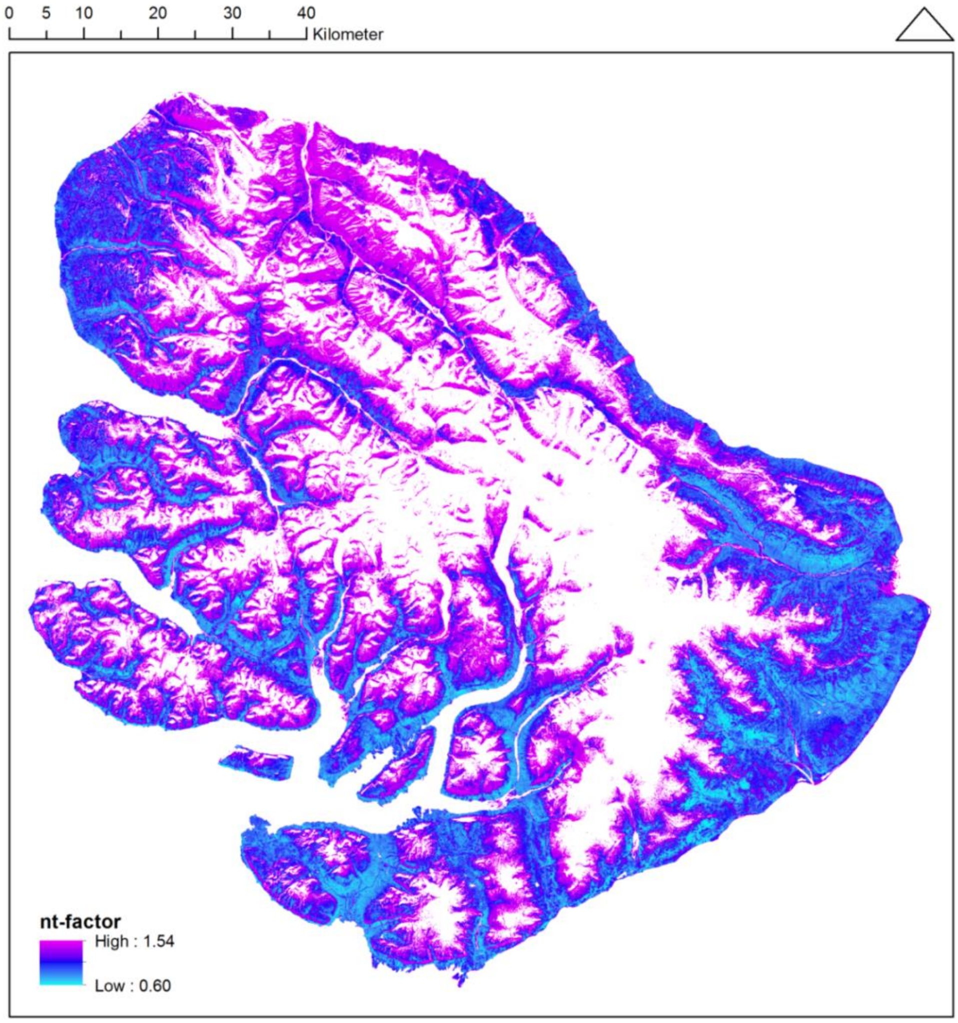

Figure 6 – Landsat derived nt-factor of Disko Island.

Results

According to Karunaratne and Burn (2004) *n*-factors for surfaces have been determined empirically, but the physical contribution of microclimate driving the n-factor relation is not fully understood (Karunaratne and Burn 2004). While an n-factor of 1.0 represents equal surface- and air temperatures (dark blue areas in Figure 6), higher values than one represent relatively warmer surface- than air temperatures (magenta). This gets especially apparent with heights, where surface temperatures often can be considerably warmer due to the atmospherically driven gradients of air temperatures. In our case we have worked with a continuous temperature gradient as proposed by (Fausto 2009)in their Greenland study.

But a single variable cannot explain the *nt* pattern alone as also mentioned by (Karunaratne and Burn 2004). This is partly due to the nature of the surface energy balance. As latent heat, sensible heat and ground heat fluxes - and any combination of these - influences surface temperatures differentially a whole suite of physical attributes are likely to influence the *nt-factor.* Though relatively sparse in nature, canopy cover influences net radiation, while moisture influences both latent- and sensible heat transfer from the surface. Consequently we see low *nt-values* in valleys predominantly occupied by vegetation. These areas are furthermore continuously saturated by topographical catchments; runoff from either rainfall or glacial sources or both. Here, surface temperatures are lowered relatively due to increased energy input for plant growth. Water is absorbed for transpiration with the effect of cooling as water evaporates from stomata by means of radiative heating (Bonan 2009) and (Hendriks 2010). At high altitudes vegetation is generally sparser and therefore more energy is put into heating of the soil. Additionally, slopes are more often drained leaving less to evaporate. Karunaratne and Burn (2004) furthermore mention soil moisture content but also site shading as important variables in controlling *nt*.

In the following we will have a look at a profile of *nt* to see how it relate to other satellite-derived variables (See Figure 7). The profile covers approx. 3 km of relatively distinct topography – to either side a rise in vertical extent, descending to a valley with lower limit in a river bed at about 1.300 m. The most noticeable feature of *nt* is how it fluctuates across the entire profile. As our *nt* is based solely on NDVI, the relation between these variables is quite easily perceived. NDVI and *nt* is almost inversely related. Peaks in NDVI cause depressions in *nt* and vice versa. When assessing our *nt* it should be kept in mind that it originates as a ratio of surface- and air temperatures. To see that this variable relates to both topography and surface temperatures gives the method credibility. As initially argued, higher *nt* values are found with height and only with sudden greening at high slopes, not too steep though, we will see a decline in *nt*, which is a function of either surface- and air temperatures reaching equalization or air temperatures actually raise above surface temperatures due to increased evaporative action. The most noticeable break in *nt* must be the sudden peak 1.350 meters within the profile. A related peak in surface temperature and decrease in NDVI exist within a quite small part of the profile; the river bed. Due to its location within a south-facing valley it generally receives much net radiation. A dominance of rocky surfaces contributes to excessive soil warming but just as much in small NDVI values resulting in the observed peak of *nt*.

As mentioned earlier, our in-situ measurements will mostly represent areas that are similar in topography and biome. As focus during field work were on tedious soil property investigations, ground-to-image (satellite) validation and NDVI, other variables such as air temperatures were not given just as much attention due to the believed significance of the nt/NDVI relation found by Westermann et al. (2014) with the result of minimizing the basis for *nt* validation. In retrospect this unfortunately produce a significant drawback in the future use of *nt*.

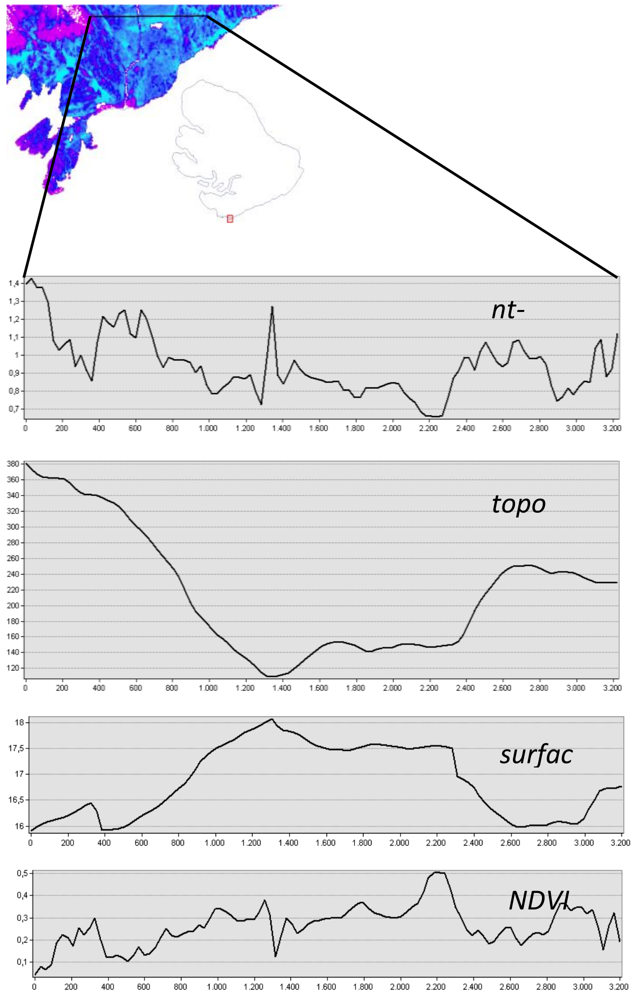

Figure 7 – Profile of satellite derived variables crossing both the Red River and Petturson's Moraine.

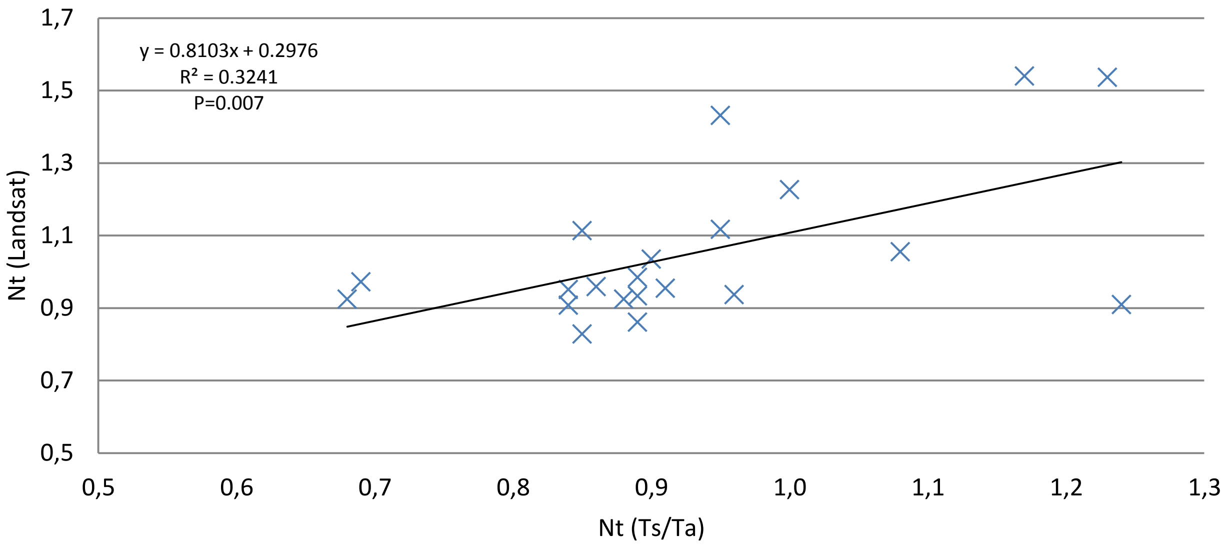

Figure 8 - Landsat derived nt plotted against original nt equation (Ts/Ta) using in-situ measurements of surface- and air temperatures.

The relation above (Figure 8) is based on Landsat derived *nt* and on in-situ measurements relative to the original ratio of surface- over air temperatures. As seen, the degree of determination (R^2) is relatively small and therefore does not account for much variation, but this is likely to be influenced by the number of observations. Furthermore Westermann et al., (2014) used averaged daily Ta values and not just a single observation per in-situ location. Then again a quite small p-value of 0.007 tells us that the pattern is not necessarily due to random chance. Had we had more air temperatures measured at the same locations a more robust relationship could maybe have been found. On the other hand, the following relation of *nt* (Figure 9) based entirely on NDVI (equation 1.3) does not prove any more noteworthy even though it is validated using more comprehensive in-situ measurements.

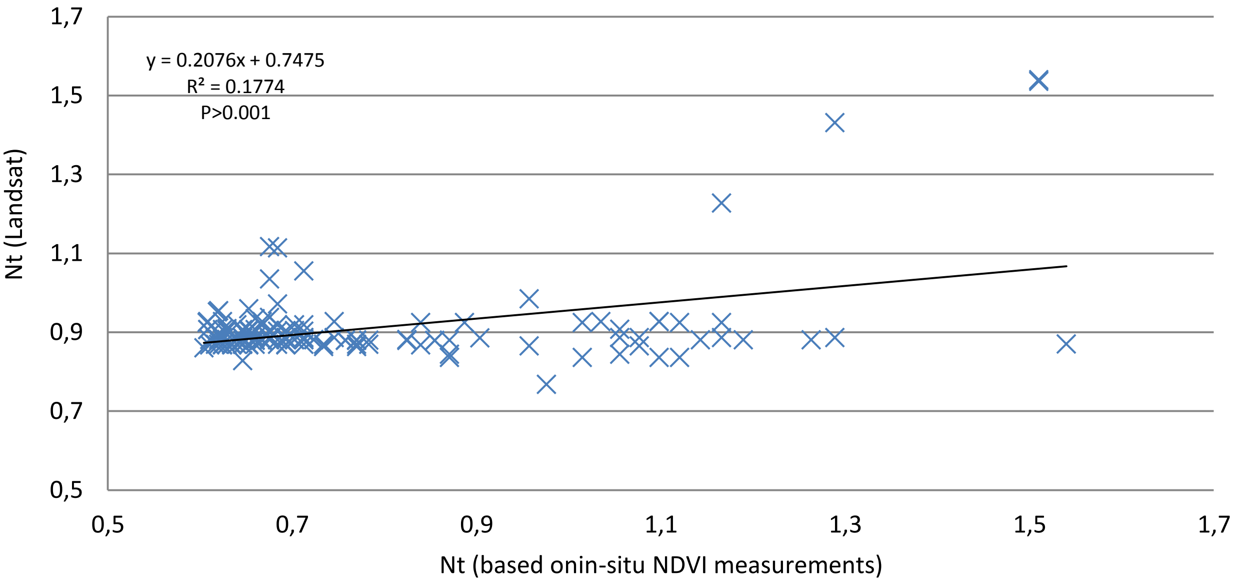

Figure 9 - Landsat derived nt plotted against nt based on in-situ measurements of NDVI

While the pattern is not due to random chance (small p-values), the small degree of determination also associated with our data could be caused by sampling method. As mentioned earlier a key issue in this study is the varying spatial quality of different variables. While Landsat have a spatial resolution of 30x30m we could regard every single in-situ measurement of having a spatial resolution of approx. 1 meter (NDVI measurements were averaged within a square measuring 1x1m). It is obvious that within this span a single in-situ measurement is likely not to represent an area of 30x30m adequately. Measurements should in retrospect have been distributed more evenly in areas that correspond to Landsat pixels. This would have helped in creating more averaged values better suited for comparison. In this respect the high resolution WorldView scene (2x2m) could provide the needed intermediate spatial resolution for compatible scaling between in-situ measurements and the full coverage of the Landsat scene.

A similar plot between *nt* based on WorldView and in-situ measurements can be assessed below (Figure 10). But no better coherences actually exist. One major concern is the time difference involved. For one, the weather often limits the usabilty of satellite products. Clouds can in periods cover most of Disko Island and this can require certain backtracking (even monthly to yearly) to find suitable cloud-free images. As Landsat only recur every 16 days, chances for cloudy conditions is actually quite high, especially in the Arctic. This is unfortunately a necessary trade-off when we want image quality of certain resolution (e.g. spatial). The time difference between in-situ measurements and satellite image weaken the basis for comparison as Arctic vegetation according to Bonan (2013) is both highly seasonal and mainly controlled by temperature and radiation. Difference in general greening, for instance exemplified as NDVI, may vary considerably between years/months due to these climatological constraints.

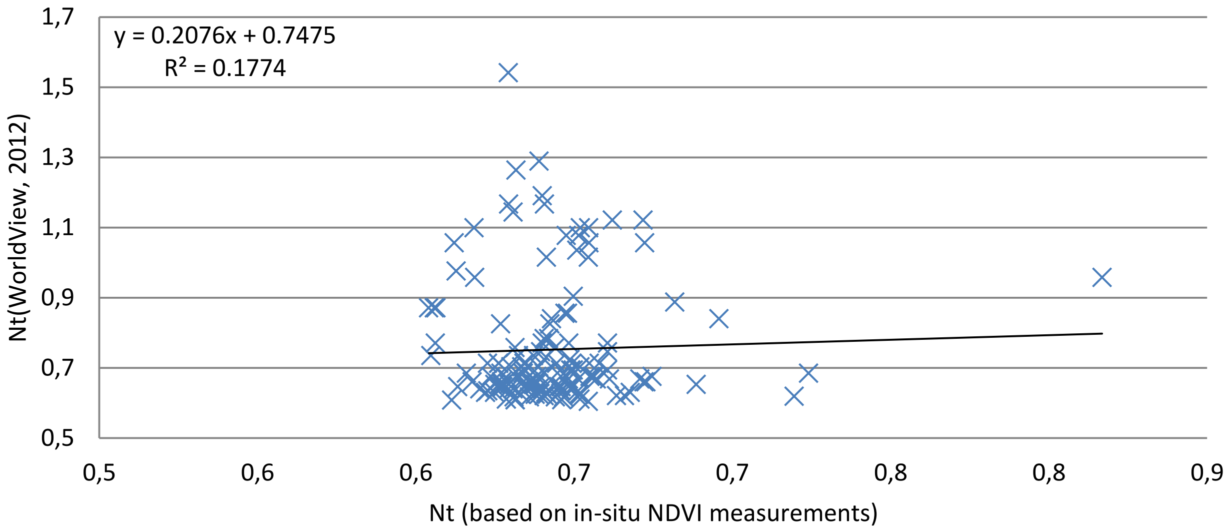

Figure 10 - WorldView derived nt plotted against nt based on in-situ measurements of NDVI

As a last effort, an image recorded in the same period as the in-situ acquisitions will be used with the one purpose of validating our *nt*. Even though most of the scene is dominated by clouds the southern tip of Disko is actually cloud-free. Hopefully, this can serve as an agent of determination that could back up the use of the nt/NDVI relation found by Westermann et al. (2014) even in previous years.

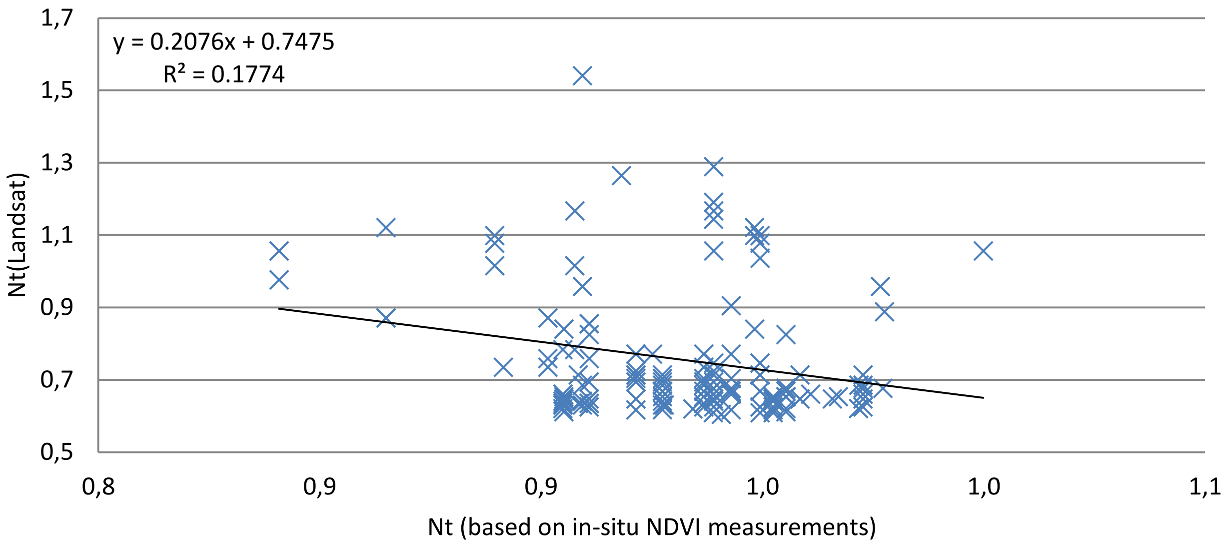

Figure 11 - Landsat derived nt from the same period as in-situ acquistions plotted against nt based on in-situ measurements of NDVI

As we see of Figure 11, even a more contemporary image does not hold any more promise in validating *nt*. We therefore have to rely on NDVI as a scientifically acknowledged means of expressing relative greeness and further, that it is applicable in the expression of calculating *nt* as a product of NDVI.

Conclusion & Perspective

While having derived at a nt-factor covering the whole of Disko, it is important to keep in mind that the procedure involved is theoretical and not necessarily applicable across geographies, meaning that the dominating physical variables controlling this relation may vary relative to a certain region's microclimate, vegetation density and soil properties. The large coefficient of determination (R^2) seen in the relation of NDVI and *nt* (figure 1) may not be as pronounced at Disko Island. Extrapolation of *nt* based on NDVI is in our case done with significant uncertainties. But the fact that air temperatures potentially can be excluded in estimation of *nt* could prove valuable in mapping efforts of thaw depths in Arctic milieus. While we will not go into further details of validating *nt* for now, the later process of estimating thaw depths and validating it relative to in-situ measurements of active layer thickness will additionally conclude on the potential of air temperatures being replaced by vegetation response to electromagnetic radiation in the form of NDVI. In this perspective the potential of mapping vast extents outweighs method weaknesses. As a by-product, theoretical air temperatures (in the growing season) for the whole of Disko Island may be derived from the orginal *nt* equation (equation 1.2), as both surface temperatures and now *nt* is known variables for the island. This can be used in estimating another important variable of the Stefan Solution; Degree Days of Thaw (DDT).

Bibliography

Bonan, Gordon. *Ecological climatology concepts and applications.* Cambridge: Cambridge university Press, 2009.

Brown, Jesslyn F. *USGS.gov.* 01 06, 2011. http://phenology.cr.usgs.gov/ndvi_foundation.php (accessed 10 20, 2014).

Fausto, Robert S. "A new present-day temperature parameterization for Greenland." *Journal of Glaciology*, 2009: 95-105.

Hendriks, Martin R. *Introduction to Physical Hydrology.* Oxford: Oxford University Press, 2010.

Hollesen, et. al. "Future active layer dynamics and carbon dioxide production from thawing permafrost layers in Northeast Greenland." *Global Change Biology*, 2011: 911–926.

Huete, A. R. "A soil-adjusted vegetation index (SAVI)." *Remote Sensing of Environment*, 1988: 295–309.

Jensen, John R. *Pearson New International Edition -Remote Sensing of the Environment An Earth Ressource Perspective.* Essex: Pearson, 2014.

Karunaratne, K. C., and C. R. Burn. "Relations between air and surface temperature in discontinuous permafrost terrain near Mayo, Yukon Territory." *Canadian Journal of Earth Sciences*, 2004: 1437-1451.

Nelson, Frederick E., N. I. Shiklomanov, G. R. Mueller, K. M. Hinkel, D. A. Walker, and J. G. Bockheim. *Estimating Active-Layer Thickness over a Large Region: Kuparuk River Basin, Alaska, U.S.A.* Colorado: INSTAAR, University of Colorado, 1997.

Raynolds, Martha K., Josefino C. Comiso, Donald A. Walker, and David Verbyla. "Relationship between satellite-derived land surface temperatures, arctic vegetation types, and NDVI." *Remote Sensing of Environment*, 2008: 1884–1894.

Riseborough, D. W. "Thawing and freezing indices in the active layer." *Geological survey of Canada*, 2003: 953-958.

Smith, Elizabeth. *Serc catalog.* 06 01, 2000. http://www.ccpo.odu.edu/~lizsmith/SEES/veget/vg_data.htm (accessed 10 29, 2014).

Westermann, S., Bo Elberling, S. Højlund Pedersen, M Stendel, Birger Ulf Hansen, and G. E. Liston. *Future permafrost conditions along environmental gradients in Zackenberg, Greenland.* Discussion paper, Copenhagen: The Cryosphere Discuss, 2014.

Estimating Degree Days of Thaw for Disko Island using Satellite Imagery

Andreas Hvam Hoffmann[1], Andreas Elmelund Hass[1]

[1] Cand.Scient Stud, Geography and Geoinformatics, Department of Geosciences and Natural Resource Management, University of Copenhagen

Abstract

Vegetation is an important parameter when determining the thaw depths in the permafrost environments. In relation to the estimations of thaw depth over the area of Disko Island, this study aims to account for the nt- factor based on Normalized Difference Vegetation Index (NDVI) estimations, as well as the relationship between these two parameters and correspondence to the in-situ measurements. NDVI values were calculated from remotely sensed data of Landsat-8 that possesses a spatial resolution of 30x30 and bit depth of 2^{16}*, as well as WorldView scene with a resolution of (2x2m) and resembling bit depth. The estimations have shown that the highest NDVI values were concentrated in low-lying valleys, on south-facing slopes and along the coast, which can be explained by close reliance on the temperatures and solar radiation. Subsequently, nt factor – a ratio of ground surface and air temperatures, was derived from NDVI values through established correlation. It has been found that nt patterns are strongly influenced by surface energy balance. However, when validating the results with in-situ measurements, correspondence was very week, mainly due to the number and location of in-situ observations and continuous temperature gradient established for other geographical location in Greenland.*

Key words: *Stefan solution, DDT,*

Introduction

During a yearly cycle the period of frost-free days form, in general, the best conditions for vegetation growth. This is also the reason why it is sometimes referred to as the growing season. In arctic environments air temperatures above zero constitute an important variable to permafrost thaw (Jorgenson, et al. 2001).Cumulative temperatures during the growing season are expressed in the notion of Degree Days of Thaw (DDT). The importance of this component to thaw depths can be seen by the Stefan's solution, which is a measure of the thickness of the active layer:

Equation 1.1

$$Z = E\ x \sqrt{nt\ x\ PRI\ x\ \boldsymbol{DDT}}$$

The downside of this cumulative measure is the dependence on air temperatures. As climatological stations are spatially sparse in inaccessible and vast environments, such as the Arctic, measurements will most often be just as equally sparse. By means of spatial interpolation a range of temperatures across geography could be derived. Disko Island, our study area, is a large island with only few stations, which even more are located in relatively near proximity. This would not suffice for interpolation purposes as insecure extrapolation also would be needed. Ways to theoretically derive air temperatures for the whole of Disko Island would prove valuable in generating an energy input expressed by the cumulative temperatures in the growing season, also known as DDT, for estimating thaw depths.

We have previously investigated the *nt-factor* of the Stefan's Solution. Here, a correlation between *nt* and NDVI could potentially substitute the need for air temperatures in the following equation:

Equation 1.2

$$nt = \frac{T_s}{T_a}$$

By isolating T_a in the equation we get:

Equation 1.3

$$T_a = \frac{T_s}{nt}$$

Riseborough (2003) mentions ground surface- and air temperatures as key parameters in the thermal regime of both active layer and permafrost (Riseborough 2003). The only temperature range that can be directly detected from space in vast geographies is surface temperatures. This is due to the nature of electromagnetic radiation reflecting primarily off solid or liquid surfaces and not gaseous constituents just above ground. But as we already have T_s, and additionally have estimated an nt, we can theoretically try to derive above zero air temperatures, T_a, in the growing season in the geographic extent of the satellite image (see equation 1.3).

Data

Moderate Resolution Imaging Spectroradiometer (MODIS) will be used for acquiring surface temperatures. Though, having less spatial resolution than for example Landsat products the level 1 images have been initially processed and corrected for multiplicative noise by service provider, and further contain quality assessments codes for additional control of unreliable pixels. The unreliability of pixels has been considered using the following QC scheme:

MODIS Land Surface Temperature - Quality Control
MOD11A2 LST QC

Evaluation Scheme

Bit position	7	6	5	4	3	2	1	0	Notes
Integer	128	64	32	16	8	4	2	1	
0	0	0	0	0	0	0	0	0	Good Quality, average LST <=1k
1	0	0	0	0	0	0	0	1	LST produced, other quality, recommend examination of more detailed QA
2	0	0	0	0	0	0	1	0	Not Produced, due to cloud effects
3	0	0	0	0	0	0	1	1	Not Produced, primarily due to reasons other than cloud
5	0	0	0	0	0	1	0	1	LST produced, other quality, recommend examination of more detailed QA
17	0	0	0	1	0	0	0	1	LST produced, other quality, Average emissivity error <= 0.02
21	0	0	0	1	0	1	0	1	LST produced, other quality, Average emissivity error <= 0.02
64	0	1	0	0	0	0	0	0	Good Quality, average LST <=2k
65	0	1	0	0	0	0	0	1	LST produced, other quality, Average emissivity error <= 0.01, Average LST error <= 2K
69	0	1	0	0	0	1	0	1	LST produced, other quality, Average emissivity error <= 0.01, Average LST error <= 2K
81	0	1	0	1	0	0	0	1	LST produced, other quality, Average emissivity error <= 0.02, Average LST error <= 2K
85	0	1	0	1	0	1	0	1	LST produced, other quality, Average emissivity error <= 0.02, Average LST error <= 2K
129	1	0	0	0	0	0	0	1	LST produced, other quality, Average emissivity error <= 0.01, Average LST error <= 3K
133	1	0	0	0	0	1	0	1	LST produced, other quality, Average emissivity error <= 0.01, Average LST error <= 3K
145	1	0	0	1	0	0	0	1	LST produced, other quality, Average emissivity error <= 0.02, Average LST error <= 3K
149	1	0	0	1	0	1	0	1	LST produced, other quality, Average emissivity error <= 0.02, Average LST error <= 3K

The color indications are recommendations for the QC pixel values (red: LST pixel to be rejected; orange: LST pixel probably acceptable; green: LST pixel ok). The decision to accept or reject orange indicated values depends on you.

Table 1 – Quality Control Scheme

Consequently, pixels considered unreliable have been excluded in the further analysis. Clouds and probably persistent fog along coasts will produce unreliable temperature measurements. Unreliability then becomes an issue of atmospheric altitude, meaning that bias almost only exist at subzero temperatures (<-30°C). For ease of interpretation, land surface temperatures measured in Kelvin will be converted to Celsius degrees. In a spatial analyst environment this is simply executed by multiplying each digital number (degree in Kelvin) with 0.02 and subtracting by - 273.15°C (absolute zero).

In a former paper we have previously presented *nt* as a product of Landsat imagery (the Red and Near-Infrared bands) and hence this variable hold a much finer resolution than that of MODIS land surface temperatures. Varying spatial resolution will be a key issue when relating products from different sensors. In the case of MODIS thermal images, even adjacent pixels can show quite high variability in temperature range. This is primarily due to the scale of the pixels (1000x1000m). As it is a quite coarse estimate temperatures may actually vary considerably within these specific areas – especially when one pixel e.g. covers both slope and valley. Compared to Landsat derived *nt*, land surface temperatures, T_s - our other variable - seems more rigid as it has coarser spatial resolution and is dominated by sharp data boundaries. This rigidness, if not adjusted for, will manifest itself in the further analysis as pronounced borders between adjacent pixels – ensuring a relatively unlikely and also unrealistic spatial pattern. As land surface temperatures are a product of thermal infrared reflectance, shifting altitudes of surfaces will strongly influence the final detected surface temperature. As minor, but potentially quite influencing, variations in topography are neglected when working with these coarse resolutions and the fact that we work with a one-dimensional raster product; we will look into methods that incorporate more spatially heterogeneous elevation models and thereby hopefully smoother temperature transitions.

Although differences in spatial resolution can prove to weaken overall reliability as variability plays less significance at larger scales, one of the great advantages of using MODIS is the rate of recurrence. Due to requirements of frequent overpasses (high temporal resolution) of these images, satellite orbit is held high in the atmosphere. In this way, in a single scene, larger parts of earth are covered more frequently but with the downside being at a poorer spatial resolution (USGS 2014). The coverage of MODIS land surface temperatures can be seen in Figure 1. Two adjacent scenes are needed as they split exactly at Disko.

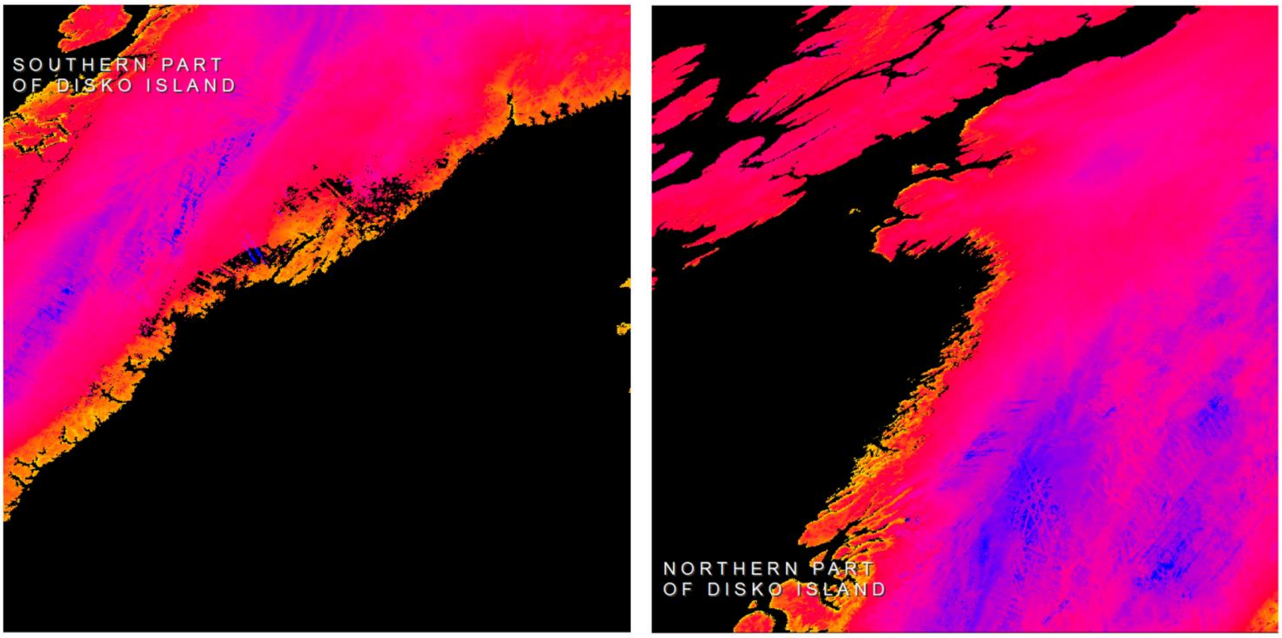

Figure 1 – MODIS LST scenes needed to cover the whole of Disko Island

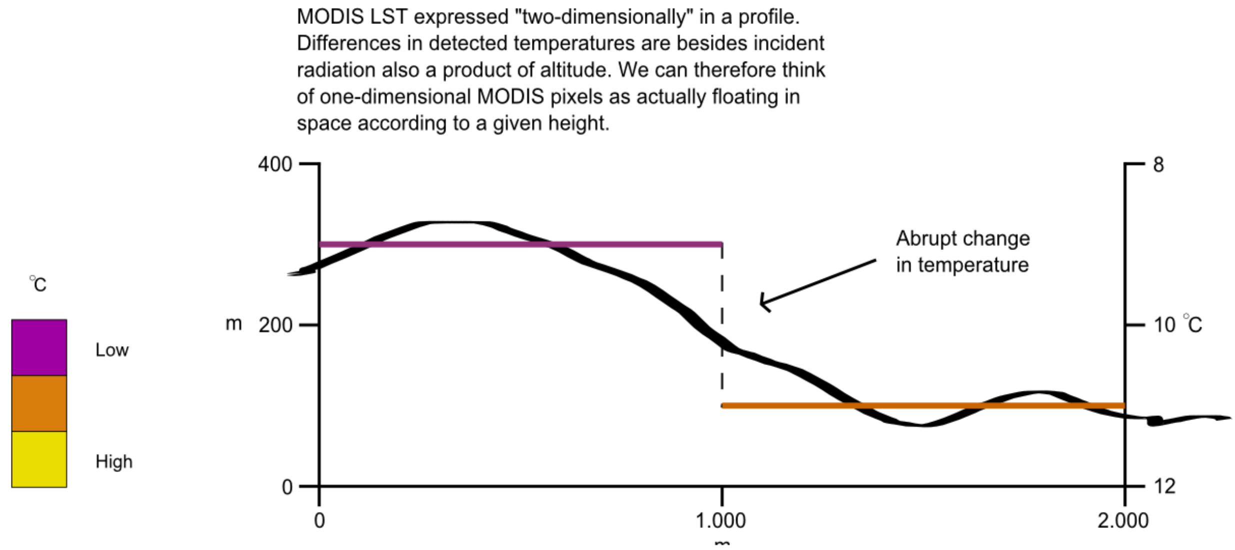

Figure 2 - MODIS LST compared to GIMP DEM. Transitions will be less pronounced if GIMP DEM is used to control MODIS LST relative to an expression of a given continuous temperature gradient.

The topography used is a Digital Elevation Model (DEM) produced during the Greenland Mapping Project (GIMP). Multiple data sources were used in minimizing the root-mean-square error of the DEM. While the GIMP DEM offers some of the best available elevation information for Greenland, the data has a nominal date of 2007 and therefore is of limited use in areas of frequent change (e.g. glacial boundaries). As we mainly study ice-free areas change is expected to be much more moderate. The GIMP DEM has a spatial resolution of 30x30m in ice-free margins (Howat, Negrete and Smith 2014). As more detailed elevation models are not acquirable for the Arctic region, we must accept that quite large deviations may exist in the data, especially at high relief.

Methods

As a preliminary effort we have prepared the images so they only extend to the boundaries of Disko Island and resampled them to a spatial resolution equal to other used image materials. This procedure does not alter data though.

Temperature adjustment

One of the great deficiencies in working with MODIS products is as mentioned its relatively coarse spatial resolution. If we take a look at the illustration below (figure 2), an entirely constructed example, we can imagine how every single pixel in the MODIS image must be located relatively in space according to the surface. A detailed elevation model will in the same profile reveal topographic variations such as slopes, depressions and peaks. Land surface temperatures are thus detected as an average within this topography. To a certain point this is a valid temperature measure, but transitions can be quite abrupt as also illustrated. As we know that temperatures decrease with height even slight altitudinal variations can lead to alterations in surface temperature. Other variables such as slope, shading and aspect certainly also play a major role on surface temperatures (due to its effect on and amount of received incident radiation), but we will not consider this further as a Potential Radiation Index (PRI) will be used as a correcting factor (Nelson, et al. 1997) for the influence of these in the Stefan Solution later on. Instead we will mainly try to control the rigidness of MODIS land surface temperatures using detailed topography (GIMP DEM) together with knowledge on temperature gradients. In this case we will use a continuous temperature gradient as also proposed by (Fausto 2009) in their studies of lapse rates in Greenland (see table 2 below). Hopefully, this can reduce some of the rigidness the coarse images hold and produce smoother transitions that represent reality better.

Table 2 - Mean monthly slope lapse rates and their standard deviation (Fausto et al., 2009

Month	Mean monthly slope lapse rate (std dev.) °C km^{-1}
Jan	−7.9 (±4.6)
Feb	−8.9 (±3.5)
Mar	−7.9 (±2.8)
Apr	−7.3 (±2.3)
May	−5.9 (±2.7)
Jun	−4.7 (±0.6)
Jul	−4.6 (±0.6)
Aug	−5.7 (±0.8)
Sep	−6.9 (±2.2)
Oct	−7.3 (±3.1)
Nov	−6.5 (±3.5)
Dec	−7.6 (±3.7)
Mean	−6.8 (±2.5)

As we are interested in the cumulative temperatures during the growing season we will need to take account for not only continuous changes in lapse rates (temperature gradients) during a year but also for night and day temperatures as subzero degrees at a given time of day can be devastating to vegetation health. Luckily, MODIS provides both night- and daytime coverage of surface temperatures.

Without having adjusted the land surface temperatures yet, we see a beginning of the growing season at approx. the 145th day, late May till the 249th day, in early September (see figure 3). 14 MODIS LST 8-daily images is needed to cover this period. A growing season of approx. 112 days correlates well with other studies of growing season in the Arctic (Tolvanen, et al. 2008). A theoretical temperature gradient, Tz, for the entire Disko Island can be assessed below. Based on heights derived from GIMP DEM (30x30m) and the assumption of temperatures decreasing by an average of -0.68°C/100m (Fausto et al., 2009) it illustrates how any temperatures, be it air- or ground surface, should be adjusted relative to specific altitudes. More technically the temperature gradient is produced by multiplying the topography with the specified temperature gradient and divide it by 100 (m).

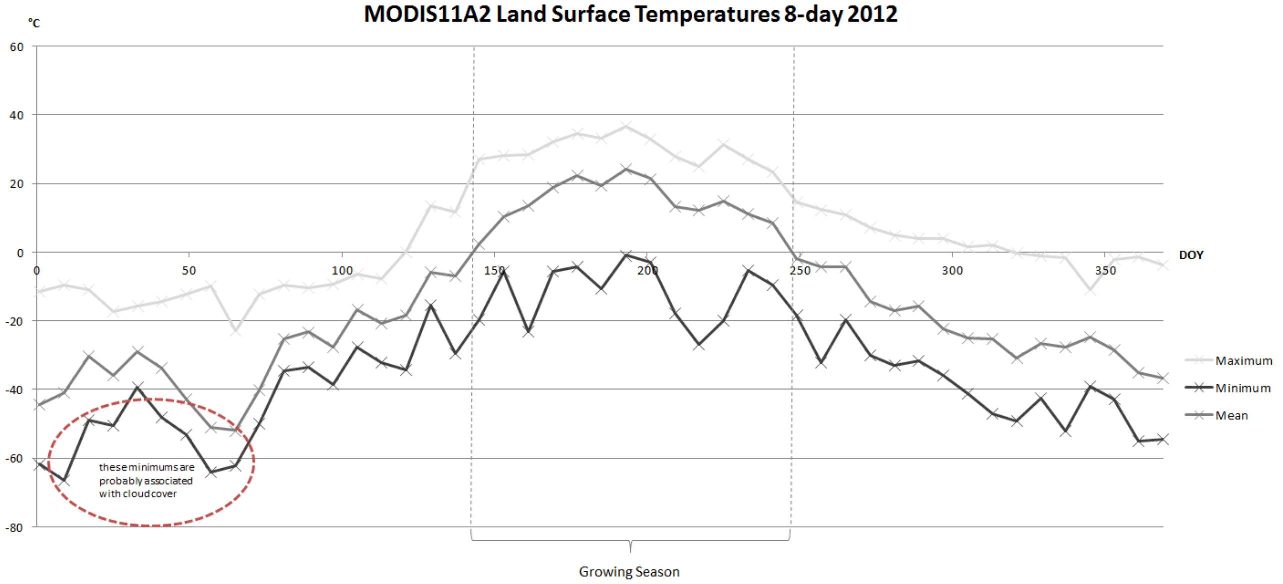

Figure 3 – MODIS Land Surface Temperatures during 2012. Dashed grey lines evaluate on the beginning and end of the growing season using mean land surface temperatures. Dashed red circle on the other hand represent outliers that are probably caused by cloud cover.

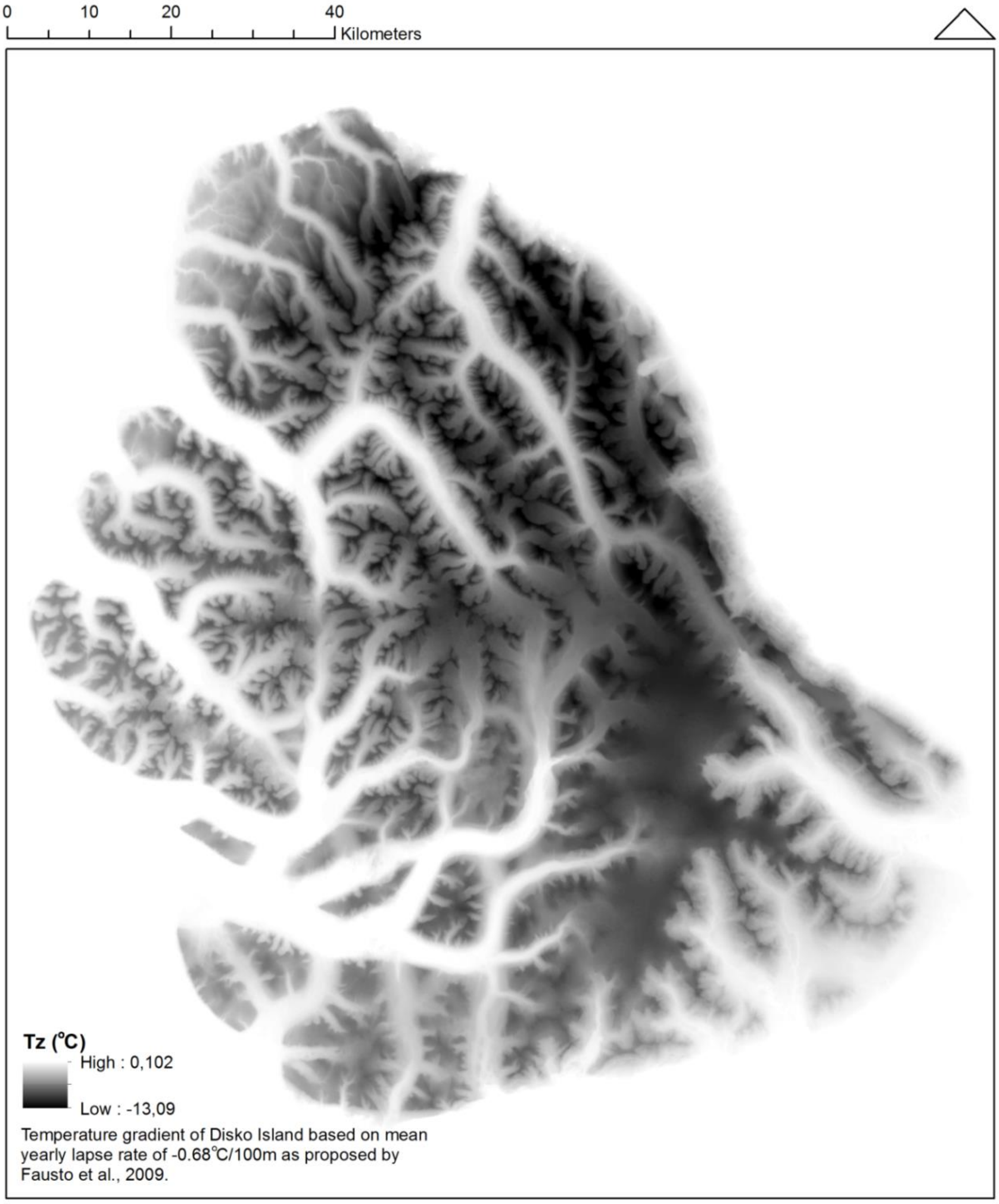

Figure 4 – Example of how temperatures should be adjusted with height. In this case with a mean yearly lapse rate of -0.68°C/100m as proposed by Fausto et al., 2009.

Though this will bring essential insights to how temperatures spatially depend and vary it will not serve as sufficient means to adjust coarse MODIS LST estimates. This is tried illustrated below (figure 5). As mentioned one of the main disadvantages of MODIS products are its coarse spatial resolution that often result in sharp data value boundaries, or said differently, abrupt changes between adjacent data in question. If we regard every MODIS pixel as having a relative location in space (z) and not just being a one-dimensional part of a raster image, as illustrated in the latter (figure 2) and following figures, we should be able to see where it will go wrong. By subtracting Tz from detected MODIS LSTs we only get a general lowering of temperatures and the abrupt changes between adjacent pixels would even more persist.

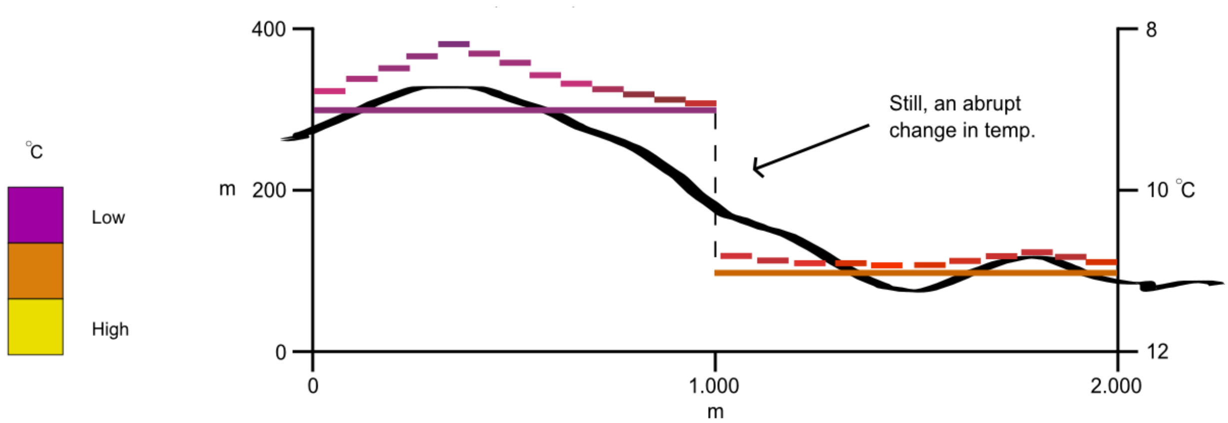

Figure 5 – Adjusting MODIS LST simply using a specified temperature gradient.

While a more smooth transition within every MODIS pixel can be achieved due to the finer spatial resolution of Tz (30x30m), this does not change the fact that the abrupt change we also set out to minimize just will be displaced and continued on in further analyses. While we have considered relative locations of raster-based temperatures, estimates of actual z-placement (location in space) could help decide if temperatures should be lowered or potentially even raised. Consider the following. If every MODIS LST has an associated (actual) location in space, every time the detailed topography (GIMP DEM) is either higher or lower than this, the temperatures should be adjusted accordingly (see figure 6 below).

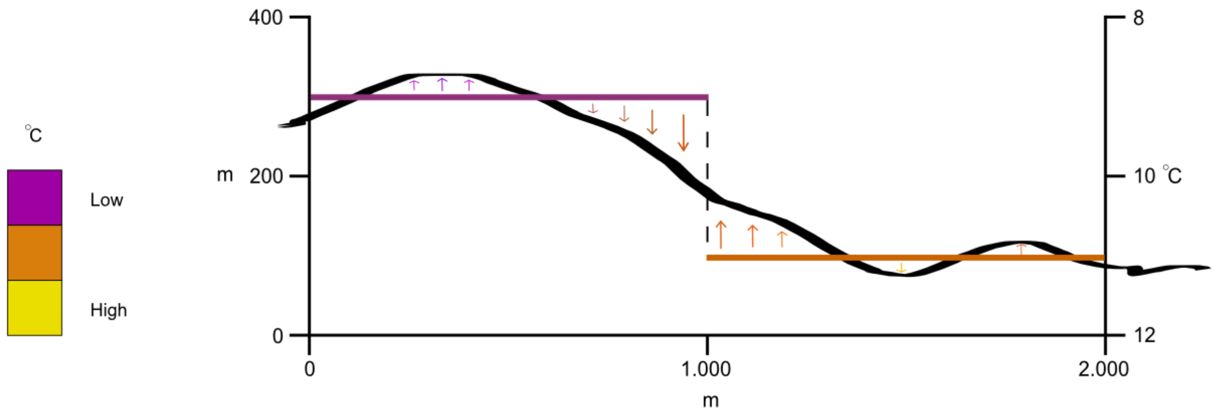

Figure 6 - Adjusting MODIS LST using the difference in height as an estimate for needed temperature correction.

As MODIS products do not hold any usable information on pixel altitude, we will use the GIMP DEM as a surrogate for MODIS LST altitude. Specifically, elevations will be averaged to the extent of every MODIS LST pixel (see figure 7 below).

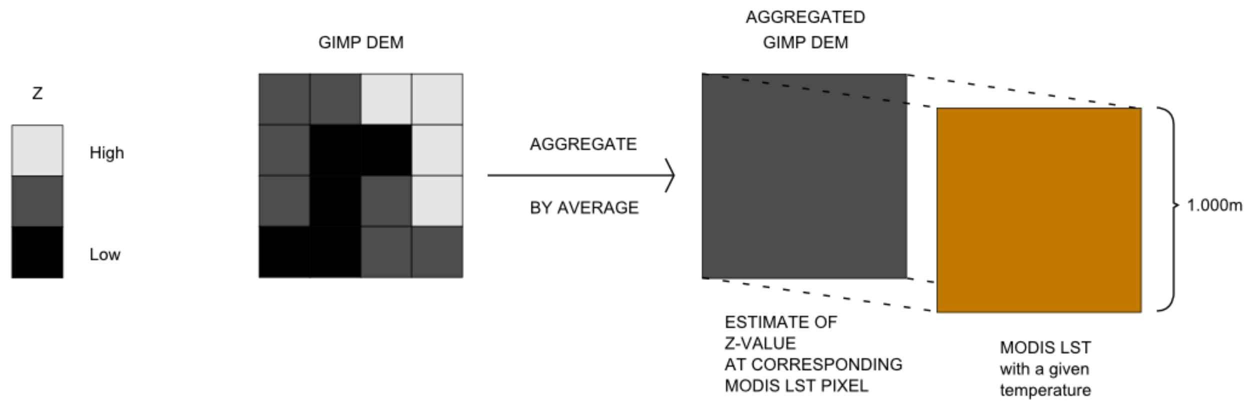

Figure 7 – Example of how a detailed DEM is used as a surrogate of MODIS LST altitude.

The differences in heights between GIMP DEM and the relative (in this case actual) spatial location of MODIS pixels will be the decider of whether a temperature gradient should be added or subtracted from the detected land surface temperature. Again, this will depend on size of difference and the assumption of temperatures decreasing/increasing by a continuous temperature gradient. In the following figure 8 we see an example of how this adjustment can be used to hopefully smooth temperatures more realistically according to the topography.

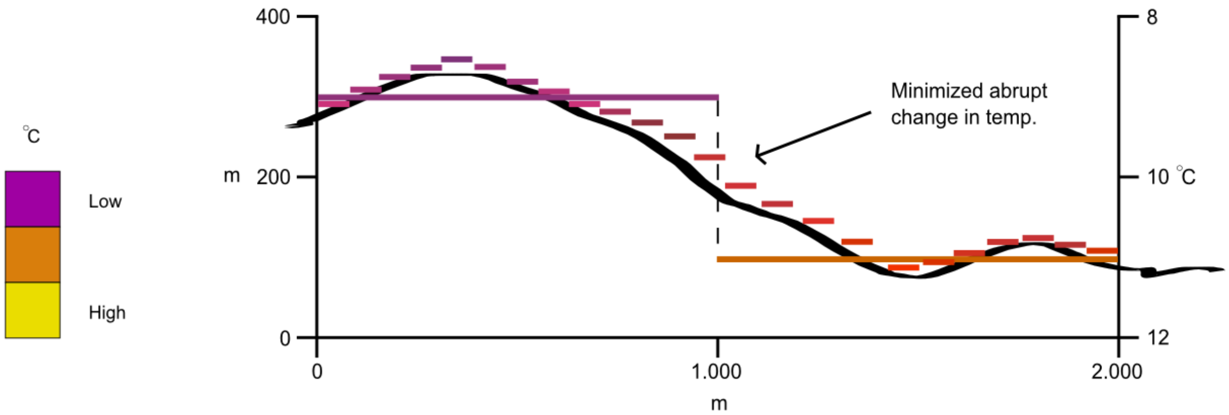

Figure 8 – Adjusted MODIS LST using the difference in height as an estimate for needed temperature correction. Note a slightly smoother transition between adjacent pixels.

As we are mainly interested in the growing season we will primarily look into the period that based in averaged land surface temperatures is defined by above 0°C only. This is a valid approach for two reasons. For one, as we want to derive air temperatures from the relation between surface temperatures and *nt,* which in our case is based on vegetation response to electromagnetic radiation (NDVI), only snow-free days are of interest. Secondly, air temperatures generally tend to be lower than surface temperatures and the growing season would probably only be shortened rather than prolonged. We will therefore apply temperature gradients for 5 months (May – September) similar to those proposed by (Fausto 2009). The Table 3 below shows how every MODIS Land Surface Temperature (night and day) recorded during the growing season should be adjusted.

DOY of MODIS LST recording	Month	Temp. gradient / 100m
145	May	-0,59 °C
153	Jun	-0,47 °C
161	Jun	-0,47 °C
169	Jun	-0,47 °C
177	Jun	-0,47 °C
185	Jul	-0,46 °C
193	Jul	-0,46 °C
201	Jul	-0,46 °C
209	Jul	-0,46 °C
217	Aug	-0,57 °C
225	Aug	-0,57 °C
233	Aug	-0,57 °C
241	Aug	-0,57 °C
249	Sep	-0,69 °C

Table 3 – Continuous temperature gradient needed for adjusting MODIS LST during the growing season. The average lapse rate during the growing season is -0.556°C.

The adjusted night and day surface temperatures are then averaged so we get a single 8-daily temperature estimate. While much consideration have been put in adjusting MODIS LST estimates relative to topography the act of retrieving air temperatures is actually quite straight-forward as it only requires simple division (equation 1.3). Then, to go from 8-daily to cumulative air temperatures through a growing season, we need to assume that every temperature in every image (14 in total) is an average of 8 consecutive days. We therefore need to multiply every temperature estimate with 8 to get the cumulative temperature for that 8-day period (see also Table 4 below for how DDT is calculated):

Analysis & results

While the procedure of retrieving air temperatures was quite straigth-forward the outcome of this is subjected to much uncertainty. The resulting temperatures should be regarded as an ideal (potential maximum) that is not likely to occur in-situ at any given time. As (Karunaratne and Burn 2004) argues the physical contribution of microclimate driving the n-factor relation is not fully understood. Air temperatures are influenced both by heat fluxes from the surface, evaporative action from vegetation and by continuously shifting air masses etc. - physical contributions that probably should be adjusted for, but as we derive our air temperatures from equation 1.3 and we already know surface temperatures and *nt* we are actually limited in our possibility of adjusting these as they according to equation 1.2 should give an *nt*-factor that we already know. A theoretical average of air temperatures during the growing season at a given year (2012/2013) can be assessed below (figure 9):

Table 4 – Calculation of DDT. Note the importance of multiplying every image with 8 (days) to achieve cumulative temperatures, DDT. If not, the growing season will only extent to 14 days instead of 112.

	1	1	1	1	1	1	1	1	1	1	1	1	1	1	14 days	DDT	Avg.
Cum. air temp. (°C)	5	9	12	15	17	18	19	20	20	18	15	12	9	5	SUM	135°C	9.642857
Theoretical air temp. (°C)	5	9	12	15	17	18	19	20	20	18	15	12	9	5			9.642857
Cum. air temp. (°C)	40	72	96	120	136	144	152	160	160	144	120	96	72	40	SUM	**1080°C**	9.642857
	8	8	8	8	8	8	8	8	8	8	8	8	8	8	**112 days**	DDT	Avg.

length of growing season

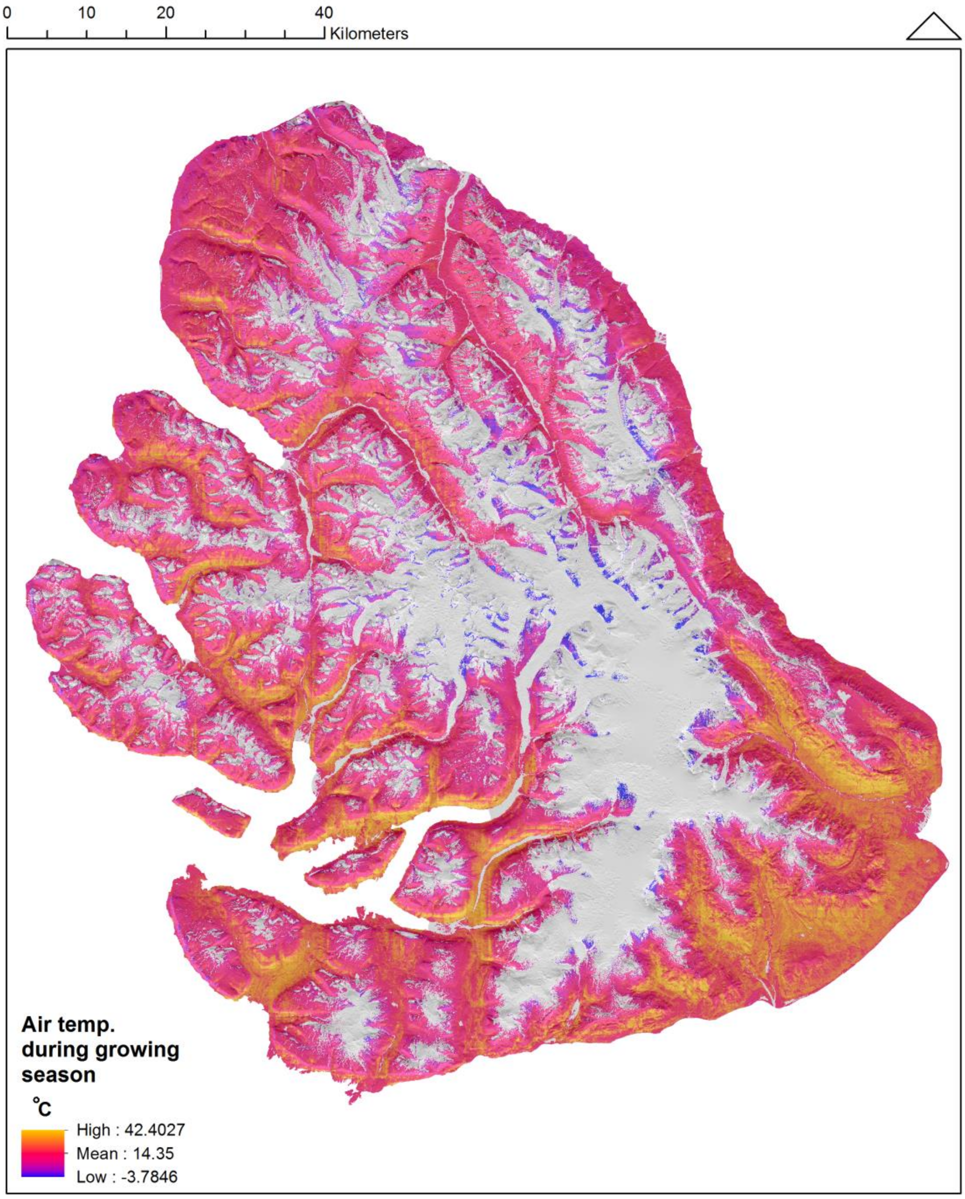

Figure 9 – Average air temperatures during growing season. Draped with hillshade.

In general we have quite high average temperatures, with highly unusual maximum temperatures. This is a product of the relation between surface temperatures and *nt*. Low *nt-values* are found in valleys predominantly occupied by vegetation. When continuously saturated by topographical catchments, surface temperatures are lowered relatively due to increased energy input for plant growth. Water is absorbed for transpiration with the effect of cooling as water evaporates from stomata by means of radiative heating (Bonan 2009) and (Hendriks 2010). This means, that when surface temperatures are quite high e.g. 25°C and we have an associated low *nt* e.g. 0.6 we get, relative to equation 1.3, an air temperature of approx. 41.6°C; which is quite unusual. The used method additionally raises an important issue; the uselessness of the *nt* variable in the Stefan Solution (equation 1.1). Consider the following: as we are only interested in the cumulative temperatures during the growing season, DDT, a given energy input (if we use the same example as before, this could potentially be 4.160°C) would be leveled out when multiplied by *nt* (in this case 0.6) and return to the original value (a surface temperature of 25°C or expressed in DDT as 2.500°C). Furthermore, we saw average *nt* values for the entire Disko Island of about 1.23; a value expressing relatively warmer surface- than air temperatures (figure 9) meaning that the island's land surface in general consists of either barren land, rocks or sparse vegetation (with visible canopy background). This coincides well with quite low NDVI estimates for the island (also figure 10). The nt variable would in this respect only increase the average energy input to further use in the Stefan's Solution but obviously also lower the energy input in areas of low nt input (valleys, depressions etc.). It could be argued that nt may be omitted from the Stefan's Solution as it already is used to theoretically derive air temperatures. Also, high nt values associated with non-vegetated areas are likely to increase the energy input (DDT) to these, which is not necessarily meaningful when seen in relation to slope and high altitudes. While this is an important issue in further active layer modeling, this paper is mostly concerned with temperature adjustment to achieve best-fit DDT. In relation to this we have certainly achieved more detailed temperature gradients in our temperature data, especially within pixels. But relatively distinct boundaries still persist in spite of efforts to reduce these. This is an inevitable artifact of the coarse MODIS LST data, in which abrupt change in data can occur even between adjacent pixels. To assess which level of detail we can express temperature gradients in, we will present the difference between the raw MODIS LST estimates and the one based on the differences in height between MODIS LST and GIMP DEM (figure 8), in the following figure:

Figure 10 – Histograms of *nt* and NDVI respectively

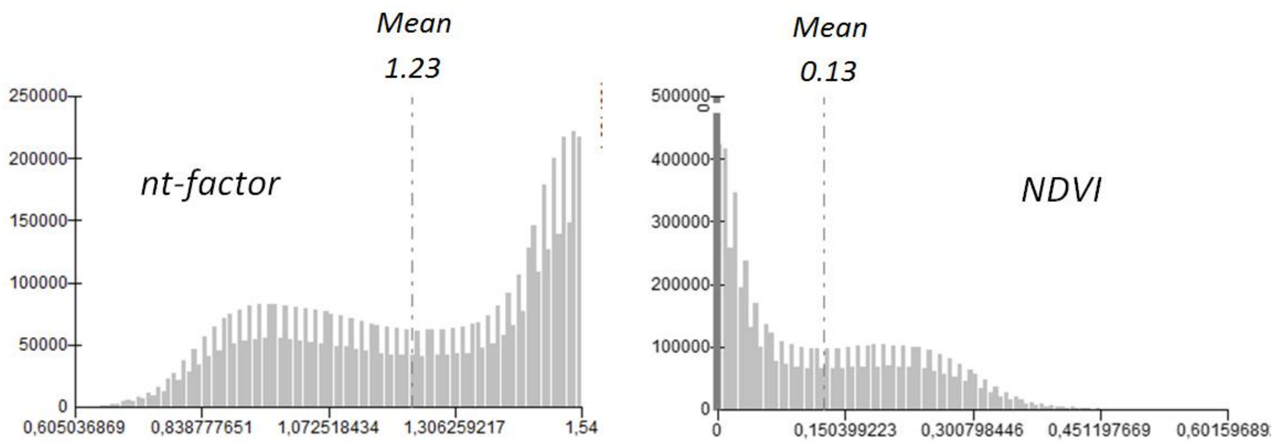

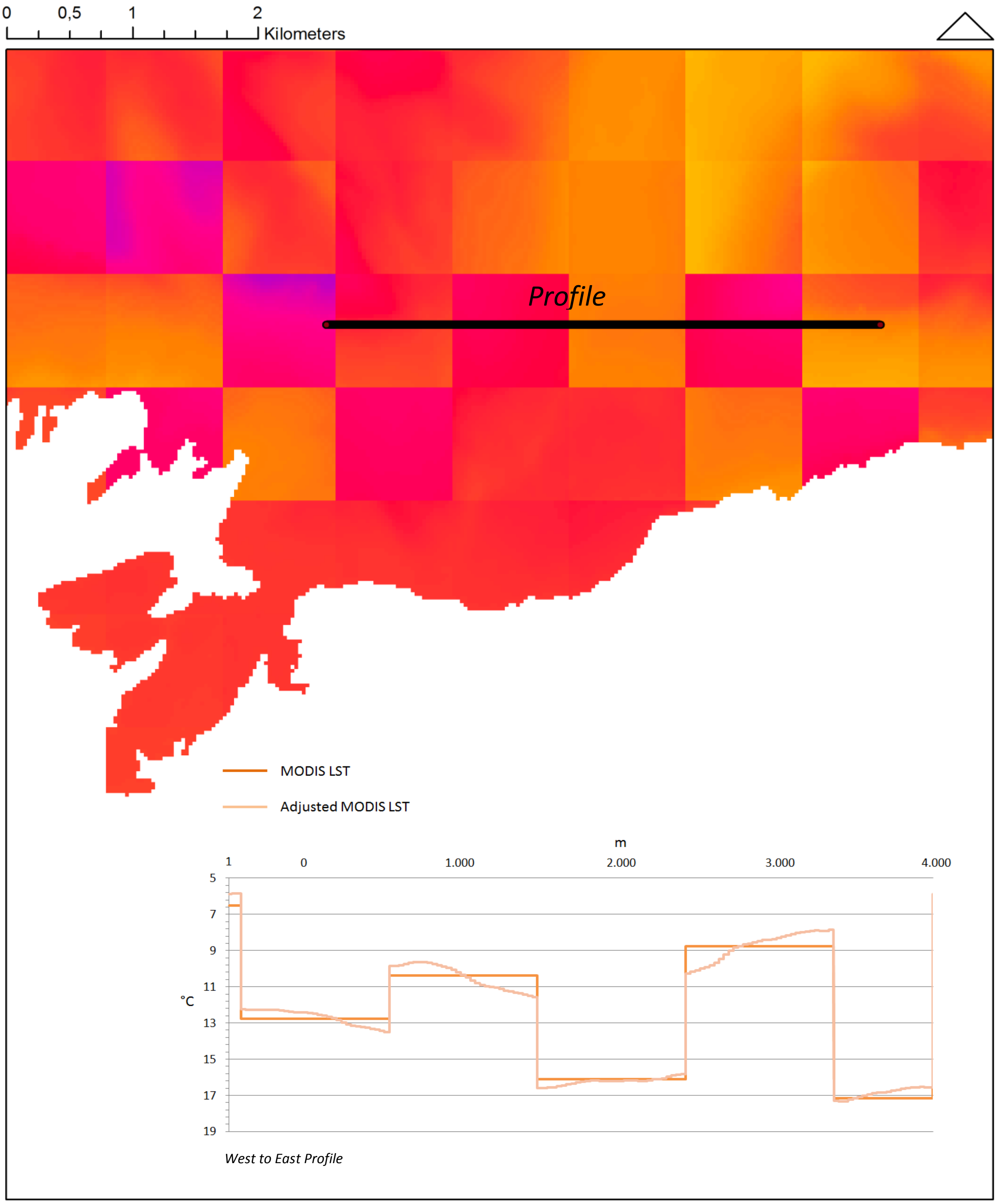

Figure 11- Comparison of raw MODIS LST estimates and adjusted MODIS LST estimates

In general we see a better temperature fit when adjusting temperatures relative to topography; in this case the difference between GIMP DEM and the "relative" MODIS LST location in space. But as mentioned we still see quite abrupt changes between adjacent pixels, and sometimes even more exaggerated. This will unfortunately persist in further analysis of active layer depths. The following figure shows the cumulative temperatures, DDT, during the growing season based on theoretically derived air temperatures:

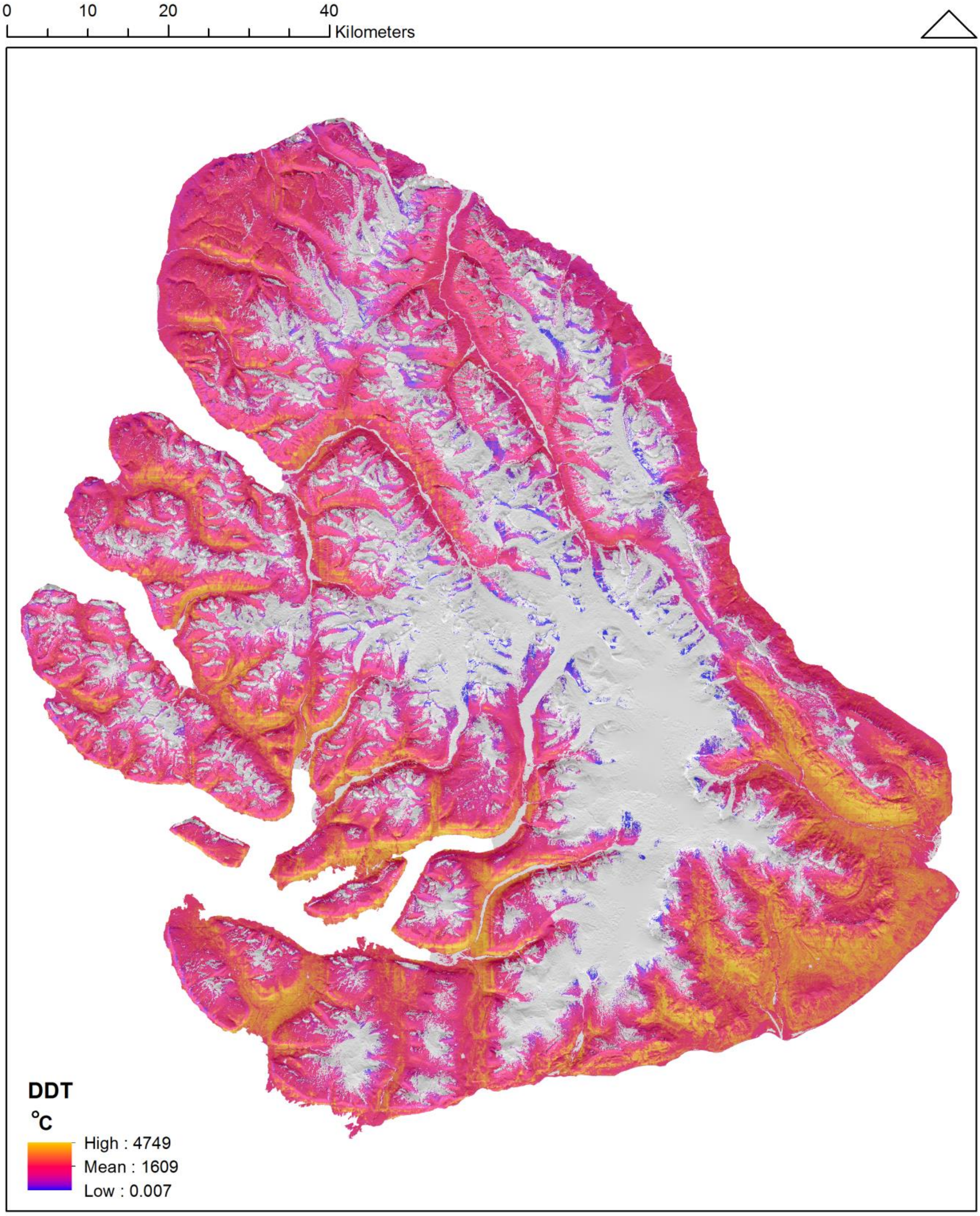

Figure 12 – DDT for Disko Island. Draped with hillshade.

With the distribution of average air temperatures in mind (figure 9), the distribution of DDT (figure 12) is as expected. We see generally higher energy inputs in valleys and at south-facing slopes. Conversely, the energy input gets lower with altitude and latitude (northerly). The main problem with this energy input is that it on average seems to overestimate quite significantly to estimates based on climatic data from Arctic Station (Hansen 2014). Here average DDTs range from 832 in 2012 to 729 in 2014 (figure 13), which is a much lower average than ours (1609). We will therefore try to adjust the DDT to lower the average energy input. As we can tweak and adjust the DDT indefinitely we will only apply a temperature gradient (Tz) that make up for the energy loss that inevitably will happen with increasing altitude. Until now we have only adjusted surface temperatures this way and not air temperatures as they needed to result in a known *nt*. The use of a temperature gradient will when applied on DDT work as a correcting factor that takes altitude into further account. Additionally, when we have a pixel size that now corresponds to, and implements, the detailed topography (GIMP DEM), we do not need to take account for the concerns raised in the methods section. The DDT is corrected by the average lapse rate during the growing season, -0.556°C/100m (see also table 3).). The result (figure 14) has a significant lower average (1379), but still, relative to in-situ data a generally higher energy input.

Figure 13 – Degree Days of Thaw based on historic data and future modeling (Hansen 2014). Red outline indicates approx. years 2000-2020.

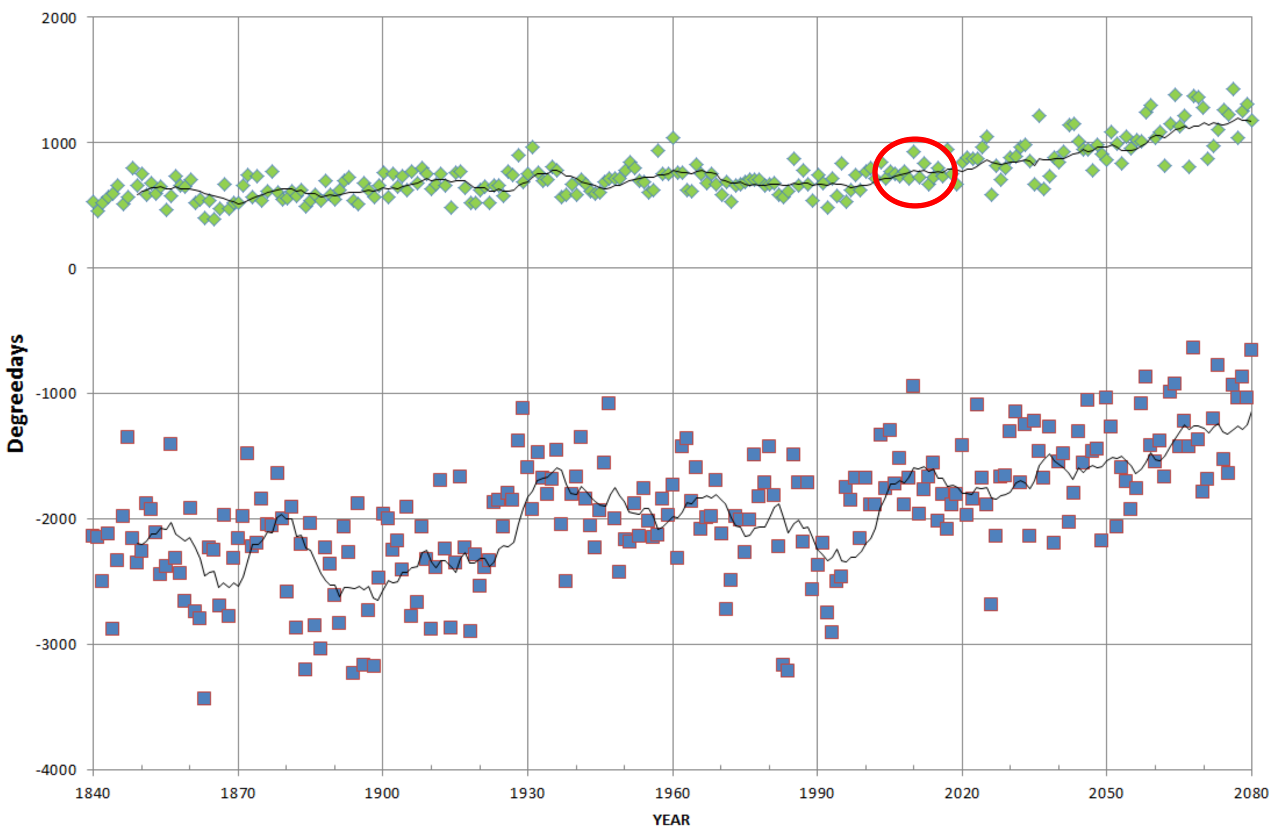

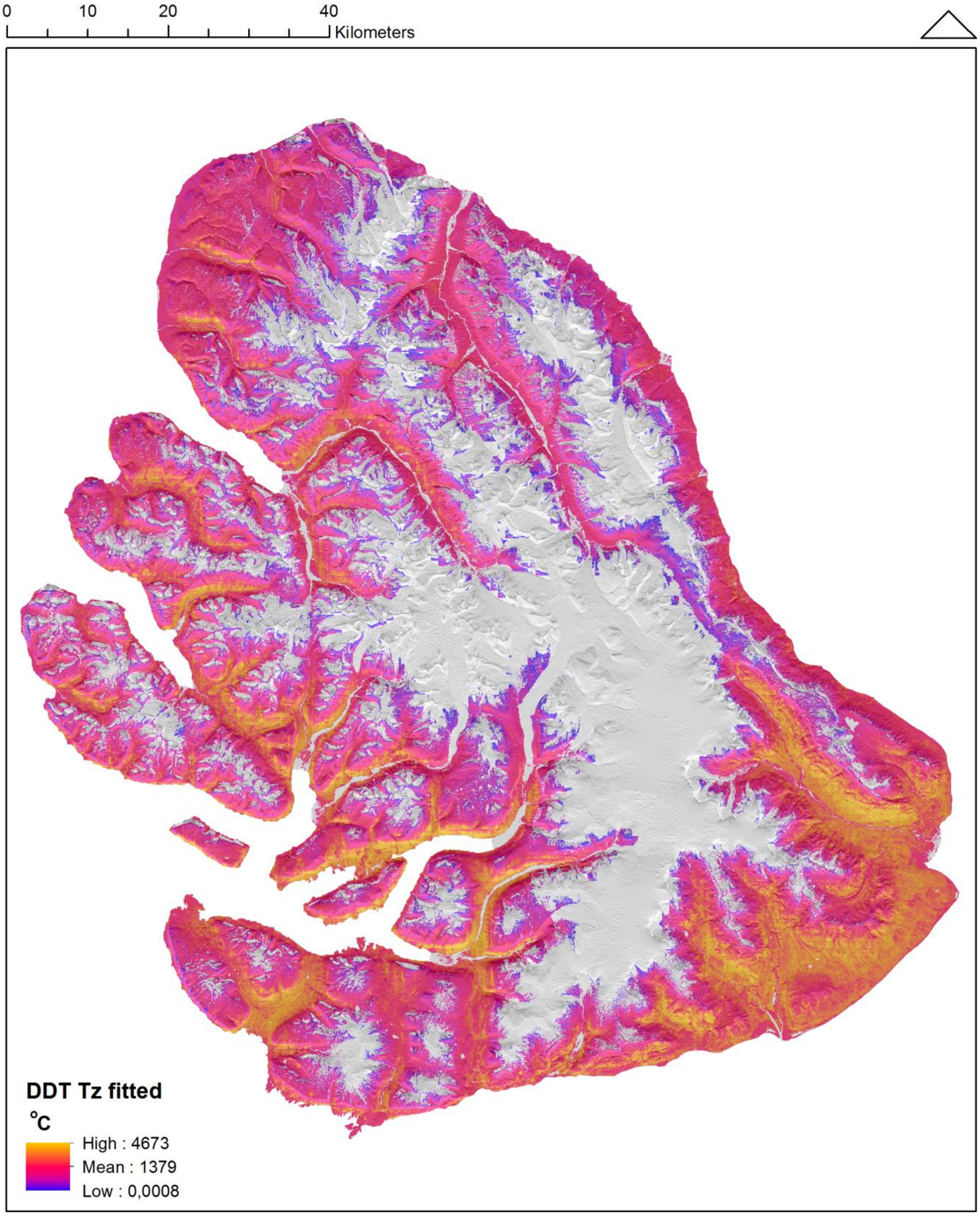

Figure 14 – DDT for Disko Island fitted relative to decreasing temperatures with height (Tz). Draped with hillshade.

Conclusion & perspective

While we are able to theoretically derive air temperatures and following DDT using satellite data alone, temperatures are constantly overestimated relative to in-situ measurements and prognoses. Average DDT values for Disko Island have been estimated to be around 1379, while recent findings show significantly less, approx. 729-832 (Hansen 2014).This is probably a product of the *nt* dependency. Areas of low *nt* input < 0 (valleys, depressions etc.) will be more susceptible to these elevated air temperature estimates as they are already characterized by relatively high surface temperatures. As surface temperatures are remotely sensed, atmospheric influence can be difficult to assess. Moreover, the resolution of MODIS land surface temperatures might be too coarse to give an appropriate temperature range on the scale we work in, which is primarily 30x30m. As a future perspective more detailed thermal images e.g. Landsat could be implemented. As a concluding remark, it could be argued that *nt* may be omitted from the Stefan's Solution as it already is used to theoretically derive air temperatures. Multiplication would only lead to equalization of DDT as this parameter is used in deriving air temperatures. Also, high *nt* values associated with non-vegetated areas are likely to increase the energy input (DDT) to these, which is not necessarily meaningful when seen in relation to slope and high altitudes.

Bibliography

Bonan, Gordon. *Ecological climatology concepts and applications.* Cambridge: Cambridge university Press, 2009.

Brown, Jesslyn F. *USGS.gov.* 01 06, 2011. http://phenology.cr.usgs.gov/ndvi_foundation.php (accessed 10 20, 2014).

Fausto, Robert S. "A new present-day temperature parameterization for Greenland." *Journal of Glaciology*, 2009: 95-105.

Hansen, Birger Ulf. *GodhavnAirTemperatures1840-2080.* Excel data sheet. Copenhagen University. Copenhagen, 2014.

Hendriks, Martin R. *Introduction to Physical Hydrology.* Oxford: Oxford University Press, 2010.

Hollesen, et. al. "Future active layer dynamics and carbon dioxide production from thawing permafrost layers in Northeast Greenland." *Global Change Biology*, 2011: 911–926.

Howat, I. M., A. Negrete, and B. E. Smith. "The Greenland Ice Mapping Project (GIMP) land classification and surface elevation datasets." *The Cryosphere*, 2014: 1509-1518.

Huete, A. R. "A soil-adjusted vegetation index (SAVI)." *Remote Sensing of Environment*, 1988: 295–309.

Jensen, John R. *Pearson New International Edition -Remote Sensing of the Environment An Earth Ressource Perspective.* Essex: Pearson, 2014.

Jorgenson, M. Torre, Charles H. Racine, James C. Walters, and Thomas E. Osterkamp. "Permafrost Degradation and Ecological Changes Associated with a WarmingClimate in Central Alaska." (Climate Change) 48, no. 4 (2001).

Karunaratne, K. C., and C. R. Burn. "Relations between air and surface temperature in discontinuous permafrost terrain near Mayo, Yukon Territory." *Canadian Journal of Earth Sciences*, 2004: 1437-1451.

Nelson, Frederick E., N. I. Shiklomanov, G. R. Mueller, K. M. Hinkel, D. A. Walker, and J. G. Bockheim. *Estimating Active-Layer Thickness over a Large Region: Kuparuk River Basin, Alaska, U.S.A.* Colorado: INSTAAR, University of Colorado, 1997.

Raynolds, Martha K., Josefino C. Comiso, Donald A. Walker, and David Verbyla. "Relationship between satellite-derived land surface temperatures, arctic vegetation types, and NDVI." *Remote Sensing of Environment*, 2008: 1884–1894.

Riseborough, D. W. "Thawing and freezing indices in the active layer." *Geological survey of Canada*, 2003: 953-958.

Smith, Elizabeth. *Serc catalog.* 06 01, 2000. http://www.ccpo.odu.edu/~lizsmith/SEES/veget/vg_data.htm (accessed 10 29, 2014).

Tolvanen, Anne, et al. "MODIS-NDVI-based mapping of the length of the growing season in northern Fennoscandia." (International Journal of Applied Earth Observation and Geoinformation) 10, no. 3 (2008).

USGS. *USGS.gov.* 04 14, 2014. https://lpdaac.usgs.gov/products/modis_products_table/mod11a2 (accessed 10 31, 2014).

Westermann, S., Bo Elberling, S. Højlund Pedersen, M Stendel, Birger Ulf Hansen, and G. E. Liston. *Future permafrost conditions along environmental gradients in Zackenberg, Greenland.* Discussion paper, Copenhagen: The Cryosphere Discuss, 2014.

Potential Radiation Index for Disko Island

Andreas Elmelund Hass[1], Andreas Hvam Hoffmann[1] & Paulina Karkauskaitė[1]
[1] Cand.Scient Stud, Geography and Geoinformatics, Department of Geosciences and Natural Resource Management, University of Copenhagen

This article covers the estimation of a Potential Radiation Index (PRI) for the island of Disko, West Greenland. Various methods for calculating incoming solar radiation, such as extrapolating of local climate station measurements of incoming radiation to larger surface areas have been proposed and investigated throughout previous studies. The Potential Solar Radiation Index derived in this study was designated to be incorporated in a larger model of an Active Layer Thickness spatial presentation covering the whole area of Disko Island. For this reason, the extrapolation method was considered unconfident, due to insufficient amount of climate stations available on Disko Island. Consequently, the most reliable method was identified to be The Area Solar Radiation (ARS) tool in ArcGIS, due to its capabilities to create a complete solar radiation model for a raster surface that contains elevation data. Elevation data was represented through an improved global ASTER digital elevation model established during the Greenland Ice Mapping Project. The results of the derived PRI are discussed, tested and to some extent validated, via in situ measurements of climatic data at Arctic Station. The study has found that applying the ARS tool is a reliable method of estimating the PRI, however it has several discrepancies with regards to transmissivity input, cloud model and in-situ measurements that hindered the obtainment of truthful results of the model.

Keywords: *Potential Radiation Index, PRI, Area Solar Radiation tool, ARS, Aster DEM, GIS, Stefan Solution, Energy input.*

Introduction

When computing an energy input for Disko, the incoming solar radiation and the temperature throughout the growing season, is the main driver[1] (Bonan, 2008).

Insolation is the primary energy source that drives many of the natural processes on Disko, both the physical and the biological. It is therefore vital to know the correct energy input in for example the Stefan solution, since the vegetation conditions and thaw depth, is coupled to this. It has proven to be a challenge in obtaining valid measures, since remotely derived data is calculated, given the name, from a distance, and will at different stages during its way from the measured object of interest to the sensor, experience obstacles that distort the data quality. We have tried to circumvent these obstacles by different manners, which are explained in the following sections, firstly discussing the theory behind PRI, next validating the results and in the end displaying the PRI product.

Other researchers have tried and to some extent successfully managed to obtain and calculate the insolation over large areas like (Gastli & Charabi, 2010), (Allen, Trezza, & Tasumi, 2006) and (Rich & Dubayah, 1995)

The aim of the following article is therefore to test and explore the potentials the Area Solar Radiation tool might provide for active layer modelling. Through a theoretical review of the algorithm we will explore the mechanics of the tool, and thereafter try and test it against ground measurements.

[1] Before dwelling deeper into this article note that the PRI is a theoretical measurement based on the ASTER Digital Elevation Model of DISKO and DDT is a physical measurement of remotely sensed land surface temperature data (LST MODIS11A2 product) from the year 2012.

Area Solar Radiation

At a large global scale the amount of insolation transmitted to a surface, is a function given by the geometry of the Earth. It determines the amount of solar radiation the atmosphere transits, and the relative location of the Sun. When zooming in to a local and smaller scale, the incoming radiation is influenced by the aspect, elevation and surface slope (Allen, Trezza, & Tasumi, 2006).

Different receipts of solar energy on slopes, varying orientation and gradient can lead to substantial, systematic differences when calculating thaw depth of permafrost (Nelson, Shiklomanov, Mueller, Hinkel, Walker, & Bockheim, 1997). In order to account for the mentioned topoclimatic effects, it is necessary to calculate Potential Radiation Index (PRI), which impart the ratio of extraterrestrial irradiation on a horizontal surface to a potential global radiation incident on a sloping surface.(Nelson et. al, 1997) Potential Radiation Index is expressed through the following equation:

$$PRI = \frac{SlopeGlobal_{tot}}{PlaneGlobal_{tot}}$$

The calculation of the Potential Radiation Index was done through a toolset in ArcGIS (ESRI, 2014). The *Area Solar Radiation* (ARS) tool was applied in order to calculate incoming solar radiation for a raster surface of Disko. In order to do so, the equation provided by the tool was modified into the following:

$$Global_{tot} = Dir_{tot} + Dif_{tot}$$

Where total (global) radiation (*$Global_{tot}$*)is the sum of direct (*Dir_{tot}*) and diffuse radiation (*Dif_{tot}*), as illustrated in Figure 1. Note that reflected radiation is not included in the equation, since it only constitutes a small proportion of the *$Global_{tot}$* in the areas surrounded by low reflectance surfaces (ESRI, 2014).

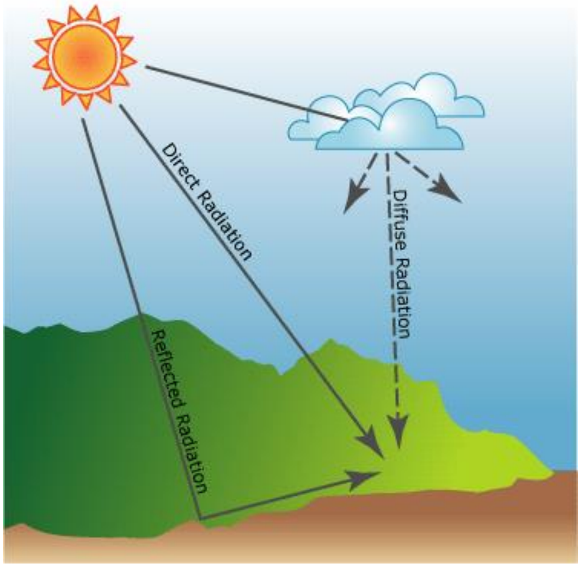

Figure 1 - Model for potential incoming radiation

Although the central parts of Disko Island are covered by ice sheets that exhibit high reflectance of solar radiation, ARS equation could still be applied due to high elevation of the ice sheets. The ice sheets are situated on the top of the mountains and thereby do not have a significant influence on the surfaces of surrounding areas. Subsequently, it was decided to exclude the ice sheets from the estimations, since it also holds negative temperatures that conflicted with the active layer modelling later on.

Direct solar radiation

Calculating the direct radiation is completed by calculating the sum of the insolation for each pixel. The insolation is given by

$$Dir_{tot} = \sum Dir_{\theta,\alpha}$$

The insolation for each pixel ($Dir_{\theta,\alpha)}$) is measured via a *sun map sector*[2] calculation, which determines the amount of radiation at particular intervals during the day. On top of this, a viewshed is being laid, to include obstacles that might hinder the flow of radiation towards the pixel. This is calculated via slope extracted from the ASTER DEM. The expanded equation for each sector where (θ)is the zenith angle and (α)is the azimuth angle, is shown below:

[2] Sun map and sky map is illustrated and explained in the next section.

$$Dir_{\theta,\alpha} = S_{const} * \beta^{m(\theta)} * SunDur_{\theta,\alpha} * SunGap_{\theta,\alpha} * \cos(AngIn_{\theta,\alpha})$$

The solar constant S_{const} is per default 1367 W/m^2 and is a basic constant adopted from the World Radiation Center (Iqbal, 1983). It is obtained by calculating the mean distance between the sun and earth and then estimating the amount of radiation from the sun that travels to the earth's atmosphere. β indicates the transmissivity of the atmosphere, which in our case was set to 70%. This percentage was preferred because normally Disko and coastal Arctic regions experiences clear weather from midday during the growing season, but often there is a heavy fog in the morning and in the afternoon coming from the sea. The angle of the sun (θ) during the day is also low in the northerly Arctic regions, influencing how much radiation is transmitted through the atmosphere, meaning that the Sun's energy has to travel longer through the atmosphere before colliding with the Earth's surface. Note that this variable is an average of the transmissivity of all wavelengths.

Optical path length shown as $m(\theta)$, is the length of the path the radiation follows from the sun to the pixel, and could also be explained as a proportion relative to the zenith path length. The parameters for determining $m(\theta)$ are the solar zenith angle (θ) and the value for the pixel's elevation above sea level (*Elev)*. The elevation is measured from the ASTER Global DEM in a resolution of 30x30 meters.

$$m(\theta) = EXP(-0{,}000118 * Elev - 1{,}638 * 10 - 9 * Elev^2)/cos(\theta)$$

When $m(\theta)$ is calculated, $SunDur_{\theta,\alpha}$ is then measured, representing the time dimension. This variable is equal to the day interval for our determined growing season in 2012 and multiplied by 24, since we want the incoming radiation to be calculated every hour during the season. The Sun's presence, or the amount of time that a pixel receives radiation, is closely related to the aspect of the pixel which is displayed in Figure 2. The color ramp is a bit generalized, but it gives an idea of the input in the equation.

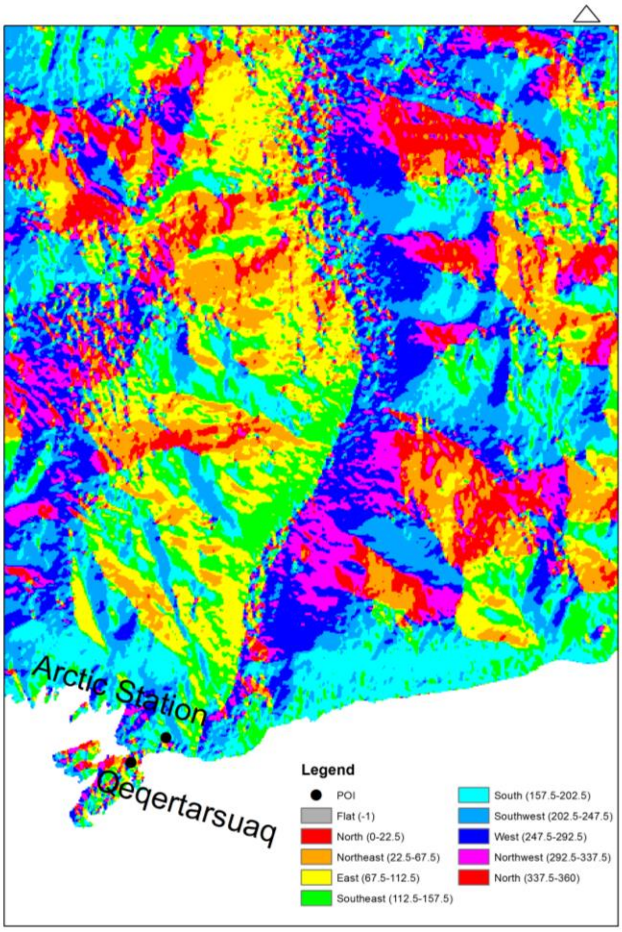

Figure 2 - Aspect of the pixels in the ASTER

$SunGap_{\theta,\alpha}$ is the amount of radiation that travels to a pixel unhindered. For example, if a pixel is placed on a south faced upward going slope, the radiation might be obscured by the above terrain making a gap of incoming radiation in the Sun's map. If more detailed data was available as LIDAR, the obstacles could eventually be trees, man-made structures or even smaller features like shrubs or rocks. The last part of the equation takes in the angle between the incidence of the radiation from the centroid of the sky map and to the axis of the surface. $AngIn_{\theta,\alpha}$is calculate by

$$AngIn_{\theta,\alpha} = \text{acos}(Cos(\theta) * Cos(G_z) + Sin(\theta) * Sin(G_Z) * Cos(\alpha - G_a))$$

$(G_z)$is the surface zenith angle and (G_a) is the surface azimuth angle.

Diffuse radiation calculation

The construction of a sky map is a way of including the diffuse solar radiation, which is the reflected and scattered parts of the Sun's energy, mainly coming from elements and particles in the atmosphere such as clouds and haze. The diffuse radiation is calculated in different sectors above a pixel placed on a surface, as it was done with the direct incoming radiation. When summed with the direct radiation this again provides the total global radiation (*Global_{tot}*).

$$Dif_{tot} = \sum Dif_{\theta,\alpha}$$

$$Dif_{\theta,\alpha} = R_{glb} * P_{dif} * Dur * SkyGap_{\theta,\alpha} * Weight_{\theta,\alpha} * \cos(AngIn_{\theta,\alpha})$$

This equation predicts the diffused radiation ($Dif_{\theta,\alpha}$) in the centroid of the sky sector, integrates it with the time of our growing season and corrects it again, as with the calculation of $Dir_{\theta,\alpha}$, by including the gap fraction and angle of incidence. In this equation, R_{glb} is the global normal radiation measured for each sector in a pixel via measuring the insolation without any obstructions and without the correction for solar incidence angle.

$$R_{glb} = (S_{Const} \sum(\beta^{m(\theta)}))/(1 - P_{dif})$$

The solar constant S_{const} is, as previously, set to 1367 W/m^2, β equals the transmissivity, $m(\theta)$ is the optical path length, while $(1 - P_{dif})$ is the proportion of diffuse radiation. P_{dif} is calculated by determining the sky conditions. Values ranges from 0 to 1 and if it is very clear sky then a value of 0,2 is to be applied and a value of 0,7 if it is very cloudy. A value of 0,3 was applied in our case making the diffuse part of the $Global_{tot}$ quite small. 0.3 makes out for generally clear sky conditions. Dur is the time interval for the analysis. $SkyGap_{\theta,\alpha}$,, as explained in the previous equation, represents the proportion of clear sky, taking into account the obstacles that might influence the incoming radiation. Before calculating the solar incidence angle, a weight is put on the sky map, to ascertain what kind of radiation model is used. In the ArcGIS software you can either chose a uniform sky model or a standard overcast sky model. For the uniform sky model the weight is calculated as

$$Weight_{\theta,\alpha} = (cos\theta_2 - cos\theta_1)/Div_{ati}$$

$\theta_1$and θ_2- Is each of the bounding zenith angles in sky map. Div_{ati} is the number of azimuthal divisions.

We used the uniform sky model because it presumes that the incoming diffuse radiation is the same from all sky directions and because we do not have the needed information to create a standard overcast model. At last, the angle of incidence between the centroid of the sky sector and the intercepting surface is included.

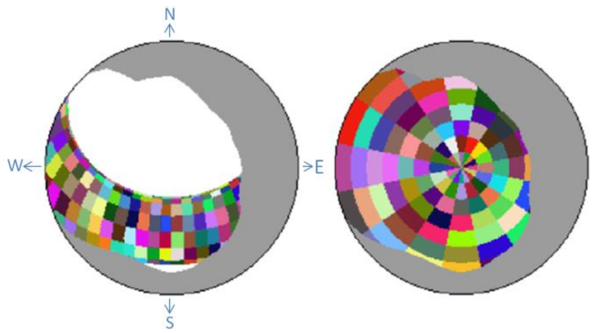

Figure 3 - Left: Viewshed of a sun map. Right: Viewshed of a skymap.

Theoretically, Figure 3 illustrates a pixel's viewshed with resulting sectors of incoming solar radiation. The grey color illustrates the percentage of blocked insolation, due to obstacles in the environment and the topographic shading. The viewshed should be interpreted as a 360° degrees view of the sky from a given pixel on a surface. The multicolored rectangles are visualizing independent sectors where the insolation ($Dir_{\theta,\alpha}$ & $Dif_{\theta,\alpha}$) is calculated and then summarized. As this is done for each pixel it only emphasizes the very time consuming process if creation of PRI are on a larger local scale. What we want to see from the resulting PRI map is low values of radiation on downward north facing slopes and ideally values that correspond with our climate station's values located at Artic Station in Godhavn. In addition, we would like to see a changing PRI on a modelled plane surface, resembling the location of Disko. Since the latitude is shifting from 69,2°N to 70,3°N, throughout 110 km length distance from south to north of Disko Island, PRI should decreasingly become smaller when getting closer to the northern part of Disko. This should inevitably be clear when PRI on a plane surface is calculated.

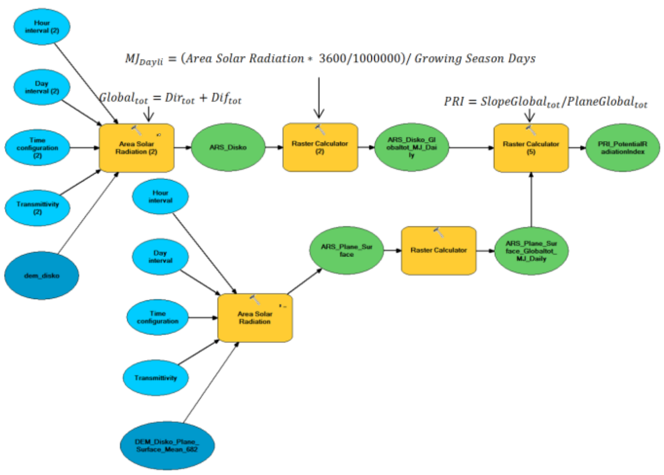

Figure 5 - Workflow in Arcgis 10.2.2

The workflow conducted in ArcGIS is displayed in Figure 5, and illustrates a stepwise approach to the calculation of PRI. This model can be copied and applied to regional places in most parts of the world, because the ASTER elevation model is a global product which is the only actual data input for creating the ARS in ArcGIS.

Potential Radiation Index

A similar procedure was undertaken for the calculation of insolation on plane surfaces. A method developed by (Nelson & Spies, 1991) shows how to address the topoclimatic effects on insolation. The method suggests dividing the above created PRI with a surface containing zero data for slope and aspect, but maintaining the independent elevation, thereby creating the ratio. The plane surface needs to have a height relation, in order to provide a value for the calculation of, for example, optical path length. It could be reasoned that a constant elevation of 0 meters above sea level (MASL), might give a reasonable and neutral PRI, but this would not justify that the average elevation of the island is 682 MASL, as it is in the ASTER digital elevation model (DEM). In a perfect setup we want to have the ARS tool to include the individual elevation for each pixel, but instead of including the slope and aspect for the pixel, we would rather have these two parameters set to zero. This is in fact possible during the setup of the ARS model, by stating that the topographic parameters should only include elevation. By doing this we keep the individual elevation assigned to each pixel. According to (Nelson & Spies, 1991), this should eventually eliminate the topographic effects that incoming radiation and topography have on temperature.

For illustration purposes and testing, a permanent profile line in Blaesedalen was chosen to display the different inputs and products that often are not visual on a 2D map. Therefore, whenever a graph for a profile line is displayed throughout the rest of this section on PRI, it will be placed precisely at the same place. This site in Blaesedalen was preferred since we have a very high resolution World View 2 image covering the area. This can be used together with the ASTER DEM creating a 3D view in ArcScene used to assess the actual shadowing and obstruction in the landscape, making the PRI values a lot easier to interpret. This is illustrated Figure 4.

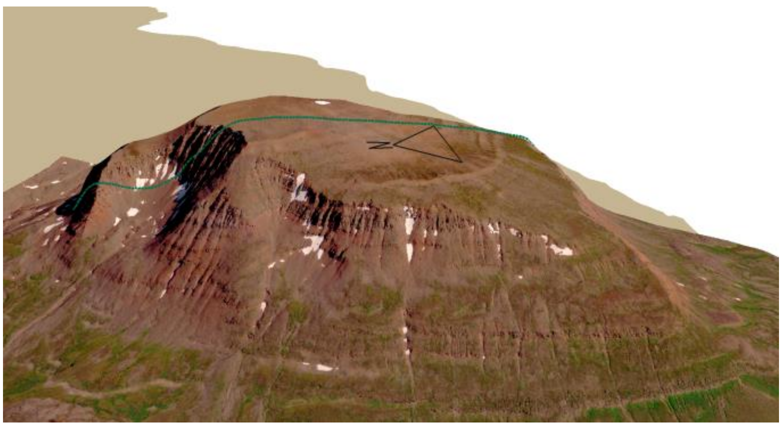

Figure 4 - Profile line over Skarvefjeld, Blaesedalen.

In Figure 6 the final product is presented. The top two maps are illustrating the two inputs in the PRI equation. The graphs below, plots the same profile in Blaesedalen, but with the two different versions of the ARS as inputs. In the left profile it is seen how changes in aspect and slope alters the insolation, and how these changes have no affect on the values displayed in the profile in the second graph. When entering these results in the equation for PRI, the result is produced in the lower left figure. The frequency distribution of PRI values gives out a mean of 0,93. The minimum value of 0,02 is calculated in a pixel that receives very little radiation, which could be because of obstacles from the surrounding terrain, providing a large fraction gap. A high radiation index value (1,25) is seen on southward slopes with a long duration of incoming sun, $SunDur_{\theta,\alpha}$.

This is not uncommon since *"…, South-facing slopes (SFS) may receive six times higher solar radiation than north-facing slopes (NFS). Thus, the SFS has a more xeric environment, that is, warmer, drier and a more variable microclimate, than the mesic NSF. Although located only a few hundred meters apart and sharing the same macroclimatic zone, the microclimatic conditions on the slopes vary dramatically." (Auslander, Nevo, & Inbar, 2002)*. Having said this, one should bear in mind that these significant local variations in slope and aspect, may require a finer resolution in ASTER data to comprehend. At first sight this PRI product in Figure 6 looks good and solid, however further tests had been performed and are presented in the next section. The mean values can be discussed since it is clear that PRI values close to 1 reveals that aspect and slope have not influenced the incoming radiation to a significant degree, over a large part of the data. Therefore it can be argued that there must be large areas with plane or flat surfaces, where slope and aspect have not resulted in differences in ARS.

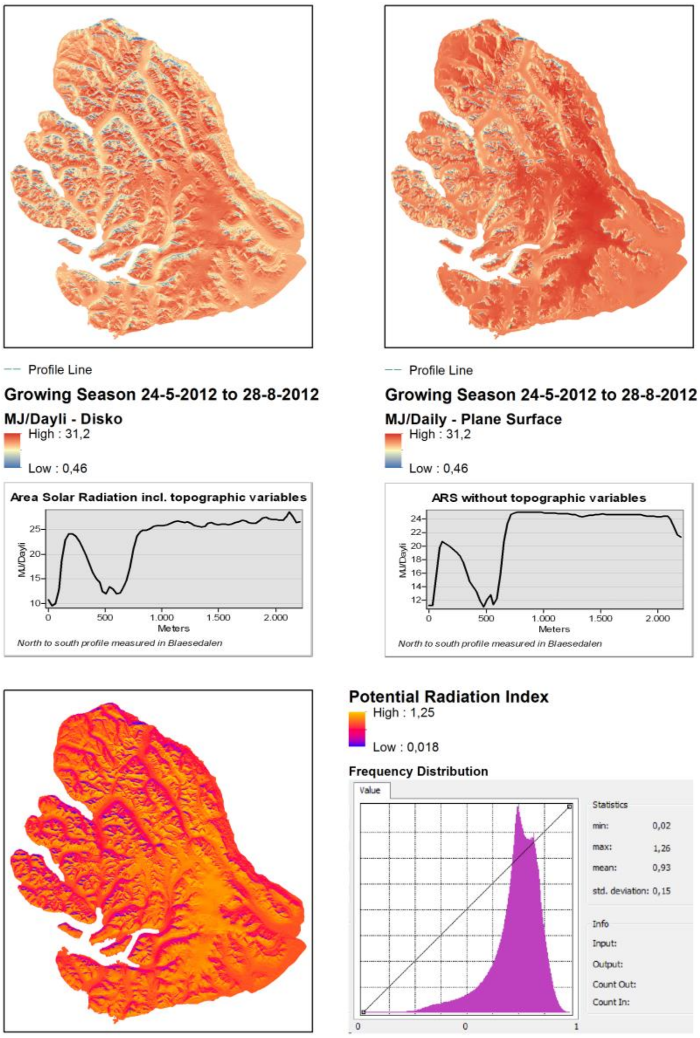

Figure 6 - Process of PRI Creation. UL: Area Solar Radiation with measured slope and aspect. UR: ARS without measured slope and aspect. LL: PRI for Disko during the growing season 2012.

Testing of PRI

In the above sections, the theory and PRI product was presented. This section will cover the testing and validation of the results of the PRI and testing of the algorithm that functions behind the tool. The testing performed in this phase will be according to the *in-situ* measurements derived from our local climate station at Arctic Station. These values have been measured in the same growing season and should likely resemble one another. By applying the second test we want to make sure that the physics of the model is reliable and follows the above reviewed theory. It has been done through testing and examining the PRI on different scales. These values have been tested by using similar equations made for point based theoretical calculation by (Nelson, Shiklomanov, Mueller, Hinkel, Walker, & Bockheim, 1997).

In-Situ testing

During the same growing season a total of 1.140.364 w/m^2 hours were measured at the scientific leaders house at Arctic Station. The ARS tool calculated 717.368 in the same positioned pixel, giving an underestimation of 422.996 w/m^2 hours. The station only measures the shortwave radiation opposite to the ARS tool which calculates the whole spectrum. The difference between in-situ measurements at Arctic station and ARS tool based estimations of insolation might be the reason for the substantial underestimation. A determining input during the setup of the ARS tool was the value for transmissivity, which might have been set to too high, letting only a small fraction of the actual radiation reach the surface. Another source of error could be the choice of cloud model which should be tested against an actual model to create a more realistic setup.

Theoretical testing

Based on a previous mentioned positional importance of latitude (the Sun's position and time duration seen from a pixels view on Disko), we have concluded that the shifting from north to south does not influence the amount of incoming solar radiation when using ARS tool.

The ARS tool calculates an average latitude for the whole of Disko and then uses this value in the equation for the entire set of sky- and Sun maps (ESRI, 2014). In the right row, Table 1 illustrates the extracted PRI values from each side of the island, but with the same slope and aspect values. It can be seen that this is completely the same, which goes for other tested PRI values. This is compared with values calculated via a method for calculating PRI from (Nelson, Shiklomanov, Mueller, Hinkel, Walker, & Bockheim, 1997) and (Iqbal, 1983) . According to their equations, southern latitudes have a higher PRI than the northern latitude, and should likewise have been realized when the ARS tool was launched. Since the actual size of the difference extents to an insignificant amount of 0.00022, we can also conclude that the ARS model is still applicable when area sizes reaches 100km in length. However, it should be possible to account for the pixel's own latitude, through algorithm updates of the ARS tool.

PRI on different latitudes	PRI (growing season) (Iqbal, 1983)	PRI (growing season) (ESRI, 2014)
Latitude: 70.3°N Slope: 10° Aspect: 180°	1.10089	1.08
Latitude: 69.2°N Slope: 10° Aspect: 180°	1.10111	1.08

Table 1 - Comparison of two different calculations of PRI with two different latitudes

Another important factor to check is the optical path length shown before as $m(\theta)$. It is the length of the path the radiation follows from the sun to the pixel, which is applied as a weight to the solar constant. To check if a smaller path length also equals a larger energy input, it has been necessary to find pixels in the dataset that has the same slope and aspect, but a variance in elevation. When comparing these pixels to each other, it is evident that values vary to a very small degree. It has been difficult to assess and check this variation since we have not been able find other equations that includes optical path length for the solar radiation calculation. Figure 7 provides an overview of values for PRI, slope, elevation and aspect along at the above explained profile line. The raster maps visualize the heterogeneity that the tool is able to produce within a small area of a few kilometers.

It is first of all very obvious that PRI is very influenced by aspect since south facing slopes have a much higher PRI than north facing slopes. This is illustrated via the graphs in Figure 7. The graph showing slope also provides valuable information on the importance of this variable when comparing this graph to the PRI. Even though elevation is dropping at 2000 meter along the profile line, the PRI continues to grow because of the extra steepness of the slope. All in all, one can ascertain that the ARS tool takes relatively big amount of variables into consideration when estimating the insolation,

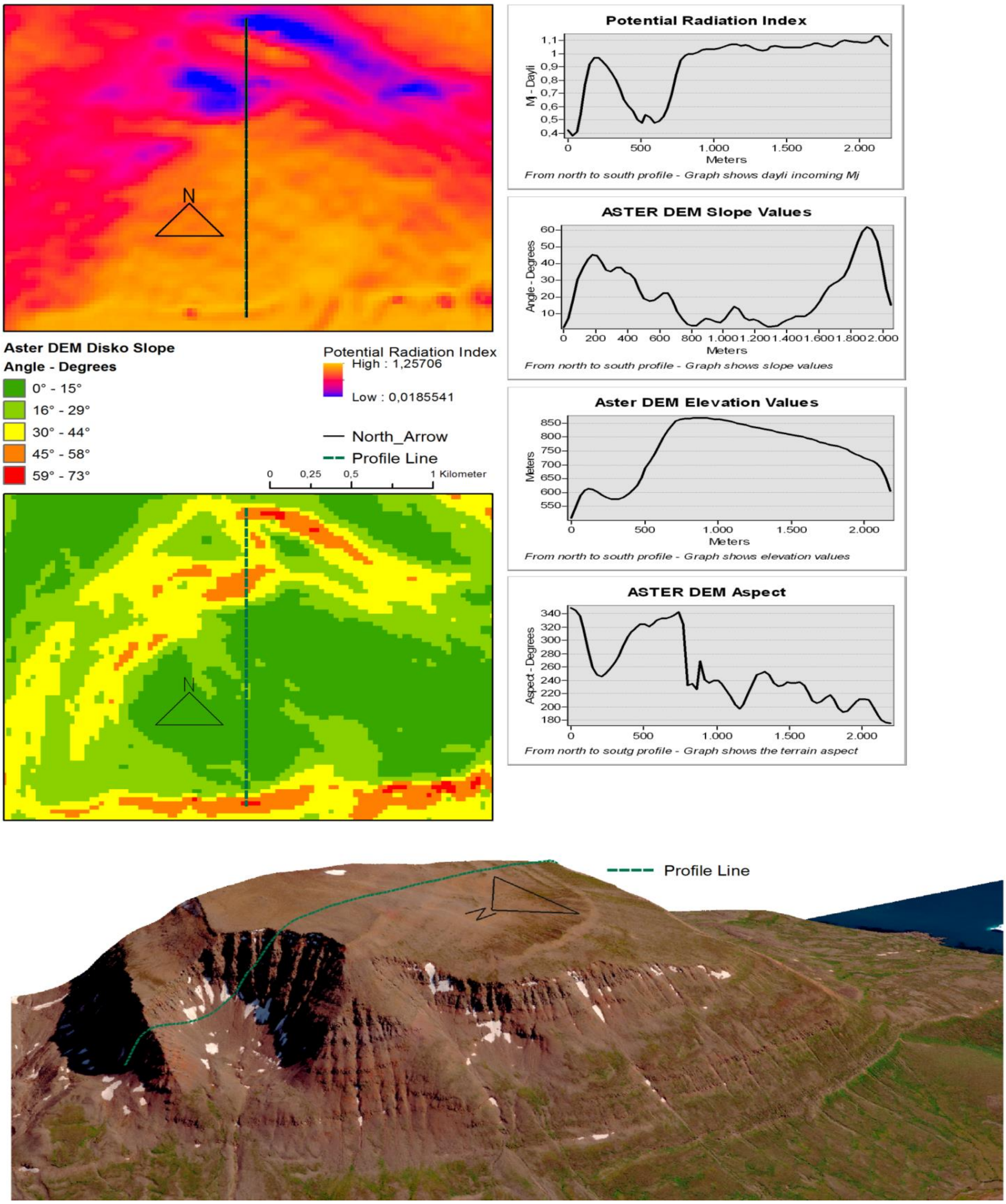

Figure 7 - Profile zoom at Skarvefjeld, Blaesedalen. Graphs show values for the variables along the same profile line from north to south.

however, the question is whether this is valid enough to use for active layer modelling. This will be discussed in the following section.

Conclusion and perspective

The objective of this article was to test and evaluate if the ARS tool is capable of providing adequate and reliable estimates of the incoming solar radiation on Disko Island during the growing season. In order to do so, the process of GIS analysis was undergone and the results were evaluated in accordance to ground truth measurements. It has been found, that the ARS tool provides a relatively useful way of estimating incoming solar radiation. However, it does not entirely correspond to values of ground measurements, due to underestimation of the amount of radiation calculated in the model. The ARS model setup could be fine-tuned to correspond to the higher values measured at Arctic Station, by adjusting the transmissivity and altering cloud model. However, these adjustments are extremely time-consuming and due to limited timeframe of this investigation, the adjustments were not performed, but could be applied for future modelling. In addition to adjustments of transmissivity and cloud model, variety of ground measurements are also important in order to perform a high quality testing. It is recommended to crosscheck the ARS calculation across multiple climate stations that record the same spectrum of incident radiation. In our case, there was only one climate station in a pixel that holds a 30x30 meters resolution, hereby questioning the actual authentication of the testing of modeled PRI. The quality of testing could have been increased, if more stations for in-situ validation were present, and if the measuring sensors were of the same type that would allow a genuine comparison.

So far, this is best possible method that we have, for developing a regional PRI for Disko Island. The model setup could consequently have been refined by improving the elevation data, e.g. by including new and enhanced drone derived data..

Precautions should always be made with regards to the climate station data, which may have been malfunctioning. In our case, the underestimation of PRI is too great to neglect the estimations of logged climate data and argue for malfunctioning.

Bibliography

Allen, R. G., Trezza, R., & Tasumi, M. (2006). Analytical integrated functions for daily solar radioation on slopes. (Elsevier, Red.) *Agricultural and Forest Meteorology*, 1-19.

Auslander, M., Nevo, E., & Inbar, M. (26. August 2002). The effects of slope orientation on plant growth,. (E. Science, Red.) *Journal of Arid Environments*, 405-416.

ESRI. (10. 4 2014). *ArcGIS Resources*. Hentede 30. 09 2014 fra An overview of the Solar Radiation tools: http://resources.arcgis.com/en/help/main/10.2/index.html#/An_overview_of_the_Solar_Radiation_tools/009z000000t4000000/

Gastli, A., & Charabi, Y. (2010). Solar electricity prospects in Oman using GIS-based solar radiation maps. *Renewable and Sustainable Energy Reviews*(14), 790-797.

Huang, S. (Spring 2009). *Modeling Small Areas Is a Big Challenge.* Hentede 22. October 2014 fra Esri: http://www.esri.com/news/arcuser/0309/files/solar.pdf

Iqbal, M. (1983). *An Introduction to Solar Radiation.* Academic Press.

Nelson, F. E., & Spies, T. E. (1991). Influence of slope and aspect on active-layer development northern Alaska. *Abstracts of the Association of American Geographers 1991 Annual Meeting*, 146.

Nelson, F. E., Shiklomanov, N. I., Mueller, G. R., Hinkel, K. M., Walker, D. A., & Bockheim, J. G. (1997, November). Estimating Active-Layer Thickness over a Large Region: Kuparuk River Basin, Alaska, U.S.A. *Arctic and Alpine Research, 29*(4), 367-378.

Rich, P. M., & Dubayah, R. (1995). Topographic solar radiation models for GIS. *International Journal of Geographical Information, 9*(4), 405-419.

Modelling the active layer at Disko Island

Andreas Elmelund Hass[1], Andreas Hvam Hoffmann[1], Ellen Lindholdt Nissen[1], Paulina Karkauskaite[1], Tue Mariager[1]

Cand.Scient Stud, Geography and Geoinformatics, Department of Geosciences and Natural Resource Management, University of Copenhagen

Abstract

Based on Stefans solution, this study aims to model the active layer thickness for the entire area of Disko Island, West Greenland. The method of Stefan Solution was chosen for this investigation, since it is widely applied in predicting the depth of thaw/freeze in soils, when little site specific information is available (Nelson et al., 1997; Shiklomanov and Nelson, 2003; Zhang T. et al., 2005). The parameters deployed in Stefan Solution incorporate the factors that influence the ground thermal regime. These parameters comprise of edaphic characteristics, n-factor of vegetation, potential solar radiation and degree-days of thaw. Each parameter (except the edaphic factor) has been derived from remotely sensed data through GIS analysis. In order to support and validate the GIS modeling, in-situ measurements were collected at the study site during August, 2014. Field procedures included probing into the ground, measuring abiotic factors of the soil, measuring NDVI values and recording of climatic data. The investigation has shown that the model based active layer thickness estimations exceeded the ones measured in-situ. This however, may be explained by the time of the probing (in the middle of the growing season) and by uncertainties related to the processing of the remotely sensed data.

Key words: *Active layer modelling, Stefans solution, Potential Radiation Index, Degree-days of thaw, Disko Island*

Introduction

Climatic changes related to increased temperatures are showing an accelerated trend in the Arctic region (IPCC 2013). A major part of these changes is related to the processes occurring between the polar soil and atmosphere in terms of the exchange of greenhouse gasses (Zhang, Osterkamp and Stamnes 1997). Permafrost, a perennially frozen ground that has remained at temperatures below 0°C for at least two consecutive years, is a significant component of the polar soils that exhibits a strong response to increasing temperatures and is therefore considered to be an important indicator of climate change in the Arctic region. These responses are mainly seen in the active layer, which is an annual freezing and thawing layer above the permafrost (Anisimov and Nelson 1995). The responses to the increased temperatures enacted in the active layer occur through thawing of the frozen ground that contains large amount of organic material owing to release of carbon and methane gases (CH_4), which is a potent greenhouse gas that significantly enhance the warming of the climate (Christiansen 1999). According to observations, a particular increase of summer temperatures is evident in the Arctic region and it is projected to continue at the same rate (Raynolds, et al. 2008). Summer air temperatures have a close relationship to the active layer thickness (Hollesen et al., 2010) that is characterized by the length of the growing season, thermal soil regime and days of thawing.

Due to the significant role of permafrost in the Arctic region, it is important to investigate the different factors that are characterizing and influencing the thickness of the active layer. This article aims to link the above four articles on edaphic parameters, the nt-factor (ratio between surface- and air temperatures), Degree-Days of Thaw and the Potential Radiation Index into a spatial representation of the active layer thickness over Disko Island using Stefan's solution. In this context it will also be studied which influence the different parameters have on the active layer.
The study area of Disko Island, West Greenland is a favorable area for our investigation, since it is located within the transition zone of continuous and discontinuous permafrost and is furthermore a

part of the active layer thickness monitoring program by CALM (Circumpolar Active layer Monitoring) operated since 1991. Moreover, the area possesses a diverse availability of climatic observations that are being recorded continuously at the Arctic research station, Qeqertarsuaq. This was considered an advantage as it serves for validation purposes.

Methods

Estimations of the active layer has been performed according to the Stefan solution that offers a reasonable approximation of the thaw depth in soils, even though only a limited amount of site specific information is available (Nelson, et al. 1997). This feature makes thaw depth analysis applicable at vast scales. Stefan solution incorporates the parameters of an edaphic factor, nt-factor, Potential Radiation Index and Degree-days of Thaw that are embodied in the following equation:

Equation 1.1

$$Z = E * \sqrt{nt * PRI * DDT}$$

Where E is Edaphic factor, nt is the n factor (Ts/Ta), PRI stands for Potential Radiation Index and DDT is degree days of thaw.

Edaphic factor was calculated based on in-situ measurements from six different sites in Blæsedalen, [1], using the following equation:

$$E = \sqrt{\frac{2K_t}{P_b w L}}$$

E is the edaphic factor, K_t is the thermal conductivity, P_b is the bulk density, w is the water content and L is the latent heat of fusion (Zhang, McCreight and Barry 2012). A detailed description on the calculation of edaphic factors can be found in: *Edaphic factor of soils in Blæsedalen, Disko Island.*

A relation between Normalized Difference Vegetation Index (NDVI) and the nt-factor recognized by Westerman et.al (2014) superseded the need of temperature input when determining nt-factors. Using satellite imagery nt-factors the entire Disko Island can be estimated. The relation is given by:

$$nt = 2.42\,x\,NDVI^2 - 3.01\,x\,NDVI + 1.54$$

For further information on the calculation of nt, see: *Nt-factor for Disko Island based on NDVI*.

PRI was calculated for Disko Island using ArcGIS to create a complete solar radiation model for a raster surface containing elevation data. Further information on the calculation of PRI see *Potential Radiation Index for Disko Island.*

DDT, cumulative T_a was estimated from the equation of nt, which is calculated by this equation:

$$nt = \frac{T_s}{T_a}$$

Where both nt and T_s (surface temperature) are known variables. T_a, air temperatures were isolated and used to calculate DDT.

Further information on the calculation of DDT can be found in *Estimating Degrees Days of Thaw for Disko Island using satellite imagery.*

The estimations of these parameters were incorporated into the Stefan's Solution equation in order to produce a map of active layer thickness for Disko Island. The procedure in Appendix 1 shows the modeling steps taken in order to provide an estimation of active layer thickness.

In-situ data collection

In order to validate and support the modeled data, various field work procedures were conducted. Thaw depths were measured by pushing an incremented metal probe into the ground at the CALM site and other selected areas. The areas were chosen in relation to slope orientation, biome and soil moisture content to ascertain the relation between these parameters and permafrost depth.

[1] Blæsedalen is presented in the study area description (Figure 4) in the introduction of the report.

Results and discussion

Edaphic factor

As seen in Figure 1 the active layer decreases correspondingly to a declining edaphic factor. In the article *Edaphic factor of Soil in Blæsedalen, Disko Island,* it was observed that low edaphic factors are linked to high soil moisture content, high thermal conductivity rates and highly organic-rich matter. Conversely, high edaphic factors were observed when the bulk density was low. The correlations are summarized in table 1

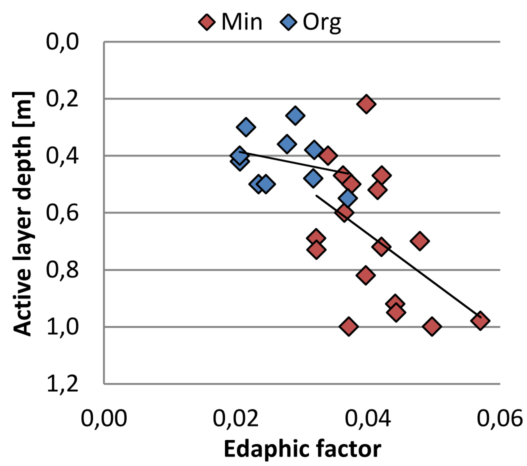

Figure 1 – Measured active layer depths plotted against edaphic factors.

	Low edaphic factor	High Edaphic factor
Soil moisture	High	low
Bulk density	Low	High
)rganic matter	High	Low
rmal conductivity	High	Low

Table 1 –Abiotic factors and their effect on edaphic factors

Nt

The spatial variation of nt over Disko Island is shown in Figure 2. In the article on *Estimating Degrees Days of Thaw for Disko Island using satellite imagery*, it was argued that nt in the final phase of active layer estimation can be excluded from Stefan's Solution, as it already has been incorporated in the process of deriving air temperatures. Therefore the inclusion of nt, would only equalize the air temperature input. Further, the *nt* variable with an average of 1.23 would increase the average energy input but obviously also lower the energy input in areas of low *nt* input (valleys, depressions etc.). Also, high *nt* values associated with non-vegetated areas are likely to increase the energy input (DDT) to these, which is not necessarily meaningful when seen in relation to slope and high altitudes.

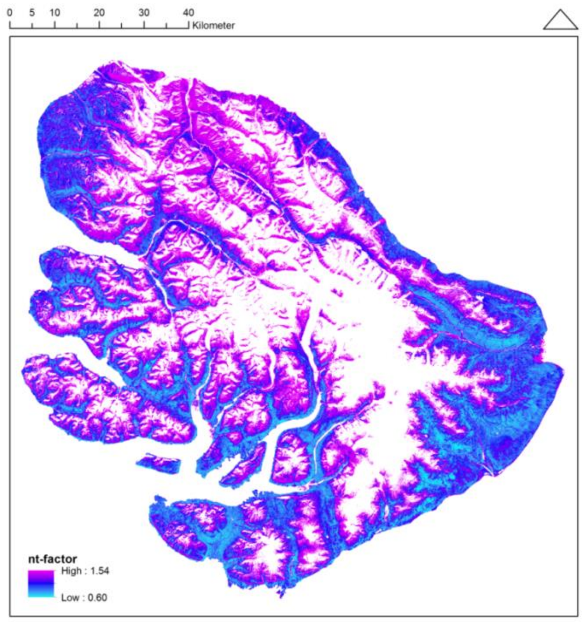

Figure 2 – Nt map of Disko Island.

Potential Radiation Index (PRI)

The analysis of PRI provides topo-climatic adjustments in terms of solar radiation that will work as a correcting factor on all other energy inputs. It accounts for varying radiation due to slope, aspect and even site shading. These are the variables significantly affecting thaw depths (Nelson, 1997). Further information on the results of PRI can be read in: *Potential Radiation Index for Disko Island.*

Degree Days of Thaw (DDT)

DDT calculated in the active layer model produced values that had an average of 1379 degree-days, which is too high to correspond to reality. The reason for this high value is that the input of T_a is derived from the equation of nt. Theoretically T_a should be the air temperature, but in the used method T_a have not represented an ideal air temperature that would account for influencing factors such as wind and soil fluxes. Even though the calculation resulted in unlikely values, the actual active layer depth was still showing trends that could guide to a better setup.

The active layer

The produced map of the active layer of Disko Island, 2014 is shown in Figure 4. The active layer depth has been calculated for three different wetness classes, representing three different edaphic factors[2] for Blæsedalen. As shown in the larger scale maps of Blæsedalen a higher edaphic factor leads to a deeper active layer. The best fitting active layer map in accordance to in-situ measurements is represented by an edaphic factor of 0.029 which is the main product of the modelling of this study.

The areas with the thinnest active layer are situated in the north part of Disko Island and areas with a thick active layer is seen in fjords, valleys and in the South western part of Disko Island. These trends can be explained by latitudinal and aspect related variations of PRI. South facing slopes receive more solar radiation than north facing slopes that results in energy in the soils that raise the temperature and heat the ground. Solar radiation influences can further be observed in the vegetation cover at the south facing slopes and in the fjords and valleys. Regarding permafrost, vegetation is considered to be an isolating factor, but this is not entirely represented in the nt values, that shows a dense cover of vegetation in areas with a thick active layer. However, the nt factor has been excluded in the active layer modelling as mentioned earlier in the result of nt.

An Active layer profile is illustrated from west to east across Blæsedalen, see Figure 4, with the respective edaphic factor. The profile shows an active layer thickness that ranges from 1 to 2.4 meter; this is a bit higher than found in-situ. The in-situ measurement ranged from 22 cm to above 1 meter. The measurement at 22 cm was found in a very wet area and is shown in Image 1. The surface was dominated with cotton grass and horse tail. Horsetail was also dominating areas where the active layer was found to be 0.50 m (See Image 2).

In general the in-situ measurements of the active layer are found to be smaller than calculated in the active layer map, see Figure 3. The mean error (RMSE[3]) was returned as 0.67 meters, which make room for improvements to the model. There are several reasons to this; one is that the field work aimed to measure soil properties in places where permafrost was present. In that context the soil samples took place where the soil moist was high and herby the active layer thin. This is not a representative sampling strategy for the whole Blæsedalen or Disko, which is critical in a validation process of the active layer map. Furthermore, it was challenging to determine the

Image 1 – Permafrost found in 22 cm depth.

Image 2 – Permafrost found in 50 cm

[3] Description of RMSE value - http://gisgeography.com/root-mean-square-error-rmse-gis/

[2] Classified in the article: *Edaphic factor at Disko Island*

active layer depth when it was deeper than one meter.

Another reason for the irregularity can be found in the energy input which is too high as mentioned earlier in the article on PRI.

Finally, the in-situ measurement of the active layer depth were not measured at their maximum, see figure 3 in the introduction chapter, whereas the active layer map was produced to show the maximum active layer. At the time of year it was assumed that the active layer had thawed to its maximum, but it is now known that the maximum active layer depth was reached in the end of September see figure 3 in the introduction. However, it should be noted that this is a model of active layer thickness and it will never completely fit reality.

Conclusion

The aim of the study was to use the Stefan solution to estimate active layer thickness of Disko Island, using both remotely sensed data and in-situ measurements.
The investigation of active layer thickness has shown that Stefan's solution is a reliable method of estimating the active layer thickness; however it is difficult to model. The difficult part was to produce accurate, representative and trustworthy input variables. The energy inputs were estimated generally too high, which resulted in deeper thawing depths than our in-situ measurements. One of the more significant findings that emerged from this study was that the RMSE value was found to be 0.67 m. This indicates that the spatial resolution has been too coarse with regards to the features that we wanted to show. The relevance of active layer thickness modelling is clearly supported by the current findings on amplified warming in the Arctic region that is expected to continue at the same rates. Incorporating of more spectrally and spatially detailed images should be investigated in order to optimize the model and apply it for future studies.

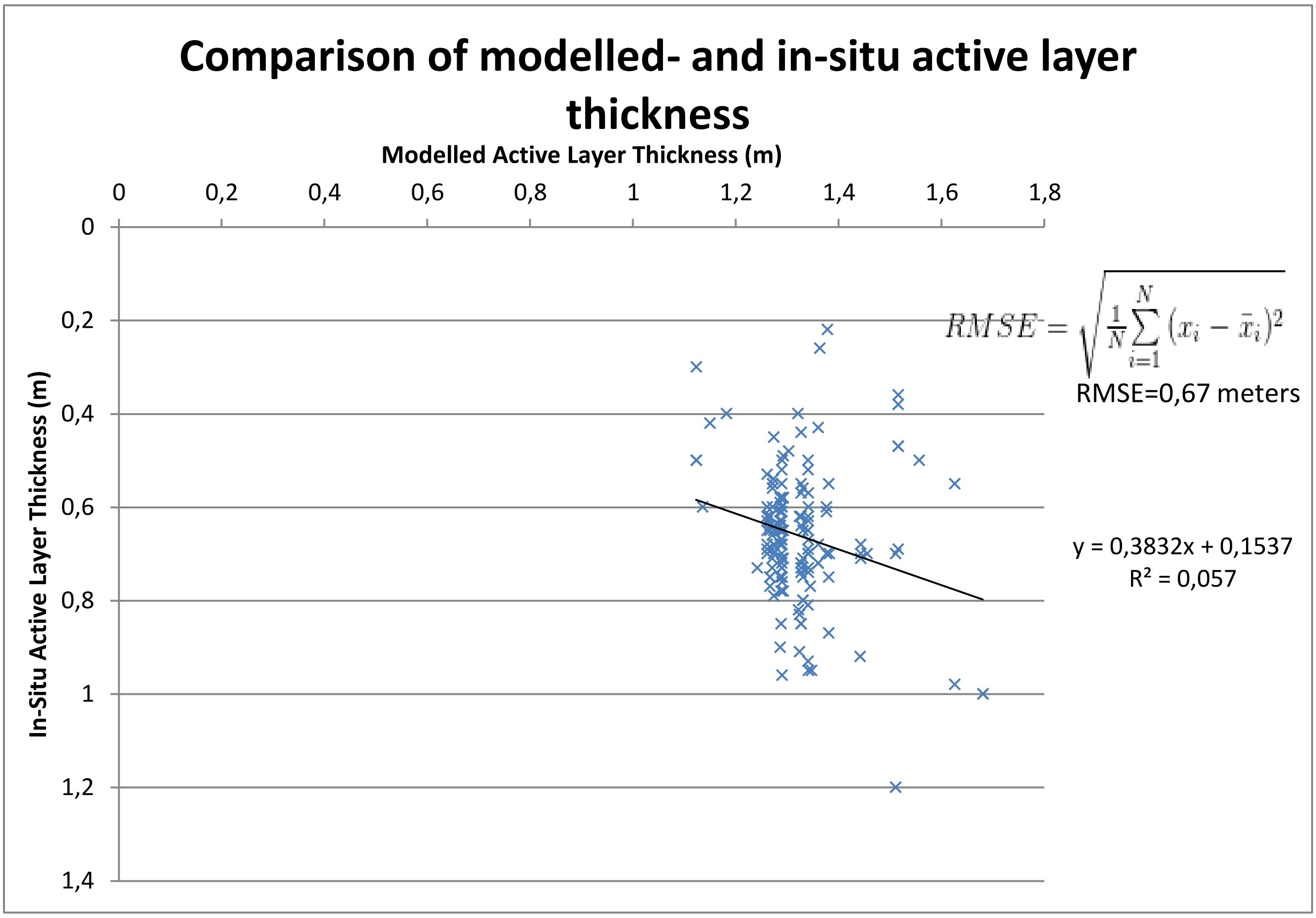

Figure 3 comparison of modelled and in-situ active layer thickness

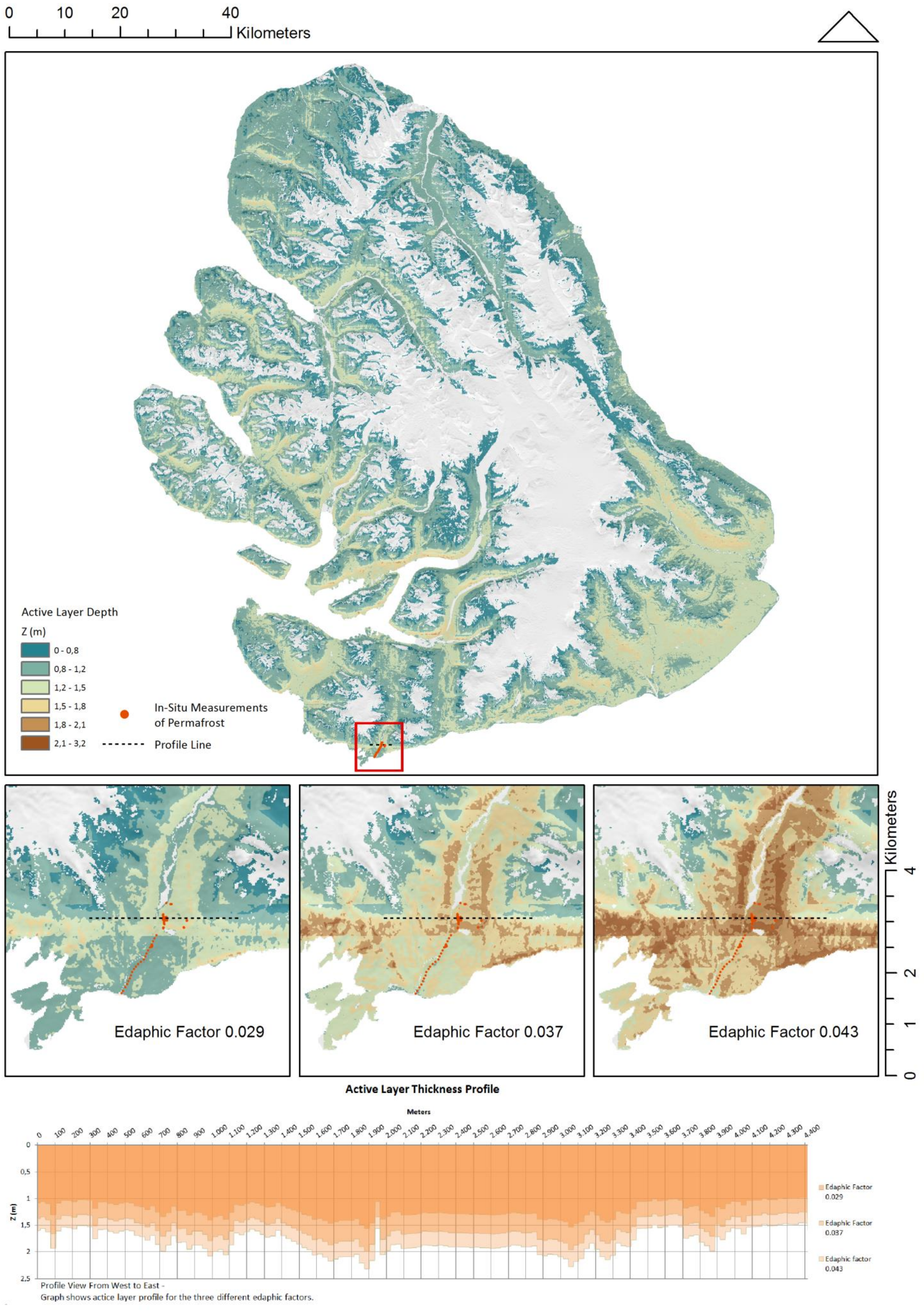

Figure 4 - Active layer map of Disko Island, 2014

Bibliography

Anisimov, Oleg A., and Frederick E. Nelson. "Permafrost distribution in the Northern Hemisphere under scenarios of climatic change." *Global and Planetary Change* 14 (1995): 59-72.

Auslander, M., E. Nevo, and M. Inbar. "The effects of slope orientation on plant growth, developmental instability and susceptibility to herbivores." *Journal of Arid Environments* 55, no. 3 (November 2003): 405-416.

Christiansen, Hanne H. "Active layer monitoring in two Greenlandic permafrost areas: Zackenberg and Disko." *Geografisk Tidsskrift*, 1999: 117.

Hollesen, J., B. Elberling, and P. E. Jansson. "Future active layer dynamics and carbon dioxide production from thawing permafrost layers in Northeast Greenland." *Global Change Biology* 17, no. 2 (2011): 911-926.

IPCC. *Introduction in Climate Change 2013, The Physical Science Basis. Contribution of Working Group I to the Fifth Assessment Report of the Intergovernmental Panel on Climate Change.* Cambridge: Cambridge University Press, 2013.

Lawrence, David M., Andrew G. Slater, Vladimir E. Romanovsky, and Dmitry J. Nicolsky. "Sensitivity of a model projection of near-surface permafrost degradation to soil column depth and representation of soil organic matter." *Journal of Geophysical Research: Earth Surface* 113, no. F2 (2008): 50-62.

Nelson, F. E., N. I. Shiklomanov, G. R. Mueller, K. M. Hinkel, D. A. Walker, and J. G.Bockheim. "Estimating Active-Layer thickness over a large region: Kupurik River Basin, Alaska, U.S.A." *Arctic and Alpine Research* 29, no. 4 (1997): 367-378.

Raynolds, Martha K., Josefino C. Comiso, Donald A. Walker, and David Verbyla. "Relationship between satellite-derived land surface temperatures, arctic vegetation types and NDVI." *Remote Sensing of Environment* 112 (2008): 1884-1894.

Riseborough, Daniel, Nikolay Shiklomanov, Bernd Etzelmüller, Stephan Grube, and Sergei Marchenko. "Recent Advances in Permafrost Modelling." *Permafrost and Periglacial Processes* 19 (2008): 137-156.

Zhang, T., J. McCreight, and R. G. Barry. "Arctic EASE Grid Freeze and Thaw Depth, 1901-2002." (National Snow and Ice Data Center) 2012.

Zhang, T., T. E. Osterkamp, and K. Stamnes. "Effects of Climate on the Active Layer and Permafrost on the North Slope of Alaska, U.S.A." *Permafrost and Periglacial Processes* 8, no. 1 (1997): 45-67.